Geodätisch-geophysikalische Arbeiten in der Schweiz

(Fortsetzung der Publikationsreihe
«Astronomisch-geodätische Arbeiten in der Schweiz»)

herausgegeben von der

Schweizerischen Geodätischen Kommission
(Organ der Schweizerischen Akademie der Naturwissenschaften)

Zweiundfünfzigster Band
Volume 52

HIGH PRECISION GPS PROCESSING IN KINEMATIC MODE

Marc Cocard

1995

Geodätisch-geophysikalische Arbeiten in der Schweiz

(Fortsetzung der Publikationsreihe
«Astronomisch-geodätische Arbeiten in der Schweiz»)

herausgegeben von der

Schweizerischen Geodätischen Kommission
(Organ der Schweizerischen Akademie der Naturwissenschaften)

Zweiundfünfzigster Band
Volume 52

HIGH PRECISION GPS PROCESSING IN KINEMATIC MODE

Marc Cocard

1995

Adresse der Schweizerischen Geodätischen Kommission:

Institut für Geodäsie und Photogrammetrie
Eidg. Technische Hochschule Zürich
ETH-Hönggerberg
CH-8093 Zürich
Switzerland

Redaktion des 52. Bandes:
Dr. M. Cocard
Dr. B. Bürki

Druck: Print-Atelier E. Zingg, Zürich

VORWORT

Ursprüngliches Konzept des Satelliten-Navigationssystems GPS war die Verwendung der Laufzeiten von Codes, welche den Trägerwellen aufmoduliert sind. Hochpräzise geodätische Anwendungen im kinematischen Modus, mit Anforderungen im cm-Genauigkeitsbereich, sind damit aber nicht erreichbar gewesen. Erst die Verwendung der Trägerwellen selbst, durch Messung der Phasenlaufzeitänderungen, hat der GPS-Technologie zu dem enormen Aufschwung verholfen, welcher in den letzten Jahren beobachtet werden kann. Ein zentrales Problem ist dabei die Berechnung der unbekannten Anzahl von ganzen Wellenlängen (sogenannte Ambiguities), welche den gesamten Wellenzug der Trägerwelle, zusätzlich zu den Phasenmessungen, ausmachen.

In der vorliegenden Publikation beschreibt Herr Dr. M. Cocard ein Softwarepaket, mit dem aus differentiellen GPS Messungen cm-genaue Trajektorien von Flugzeugbewegungen bestimmt werden können. Die Software wurde bei realen Flügen getestet. Der Bericht kann in zwei Teile unterteilt werden, einem ersten, die Entwicklung der Software, und einem zweiten, die Anwendungen. Ein wichtiger Aspekt war aber nicht nur die Erstellung der Software, die bei Testflügen funktionierte, sondern vor allem auch die wissenschaftliche Analyse zum Einfluss der Parameter des Messsystems und der Messanordnung auf Güte und Zuverlässigkeit der Ergebnisse. Herr Cocard hat herausgearbeitet, in welchem Mass die erreichbaren Genauigkeiten

- von der Distanz zwischen Referenzstation und Flugzeug,
- von Ein- oder Zweifrequenzmessungen,
- von der Satellitenkonstellation,
- der Integrationszeit,
- der Qualität der Codemessungen und
- der stochastischen Modellierung der Ionosphäre abhängen.

Die real durchgeführten Experimente umfassten

- Laser-Profiler Flüge,
- SAR Flüge mit der Deutschen Versuchsanstalt für Luft- und Raumfahrt und
- GPS gestützte Aerotriangulationsflüge in Zusammenarbeit mit der Professur für Photogrammetrie und Fernerkundung.

Herr Cocard hat zusätzlich ein Kapitel über Anwendungen bei "Airborne" Verfahren in der Geophysik, insbesondere bei der Aerogravimetrie, ergänzt. In einem internationalen Forschungsprojekt, bei dem die Schweiz aerogravimetrisch beflogen worden ist, konnte Herr Cocard die Güte seiner hochpräzisen Positionierung, angewandt auf Beschleunigungen, demonstrieren. Durch Korrektur der aus GPS ermittelten Störbeschleunigungen war es möglich, die unterschiedlichen Anziehungskräfte des Alpenkörpers und der Erdkrustenstruktur vom Flugzeug aus zu detektieren. Nachbarländer haben inzwischen Interesse bekundet, die Aerogravimetrische Schwerekarte der Schweiz auf ihr Gebiet auszudehnen. Zudem bestehen konkrete Pläne für die Weiterentwicklung in der Anwendung bei Landeanflügen in der Schweiz. Ein gemeinsames Pilotprojekt mit dem Bundesamt für Zivilluftfahrt (BAZL), der Swisscontrol und der Crossair ist in Bearbeitung (Projekt ALFASTAR).

Die Schweizerische Geodätische Kommission (SGK) der Schweizerischen Akademie für Naturwissenschaften (SANW) dankt Herrn Dr. Cocard für seinen wertvollen Beitrag zur satellitengestützten Präzisions-Navigation in der Schweiz. Herr Prof. Dr. G. Beutler, Astronomisches Institut der Universität Bern, hat diese Arbeit mit vielen wertvollen Anregungen bereichert. Ihm sei an dieser Stelle in aller Form für seine Kooperation und seine Beiträge gedankt. Herr Prof. Dr. E. Klingelé, Institut für Geodäsie und Photogrammetrie der ETH Zürich, hat den aerogravimetrischen Teil geleitet. Von der SANW wurden die Druckkosten für diesen Band übernommen, wofür die SGK ihren Dank ausspricht.

Direktor F. Jeanrichard
Bundesamt für Landestopographie
Vizepräsident der SGK

Prof. Dr. H.-G. Kahle
ETH Zürich
Präsident der SGK

PRÉFACE

Le concept du système de navigation GPS était basé à l'origine sur les mesures de temps de parcours du signal émis par les satellites. Ces mesures, appelées „pseudo-distances" sont effectuées à l'aide de codes, modulés sur les ondes porteuses. Toutefois pour les applications géodésiques à hautes précisions la qualité des mesures de pseudo-distances est insuffisante. Grâce à l'intégration des mesures de phase on a pu constater ces dernières années un essor important de la technologie GPS. Le problème central pour obtenir une précision de quelques centimètres est de déterminer les nombres entiers de cycles inhérents aux mesures de phase.

Dans le rapport présenté ici, Dr. M. Marc Cocard a développé une série de logiciels permettant de déterminer les trajectoires d'avions à l'aide de mesures différentielles GPS avec la précision du cm. Ces logiciels ont été testés avec succès lors de vols réels. Le travail comprend deux parties: la première est consacrée au développement des logiciels et la seconde aux applications. Non seulement le développement des logiciels mais surtout l'analyse scientifique de l'influence des paramètres du système de mesure et de l'agencement des mesures sur la qualité et la fiabilité des résultats représente un aspect important du travail. M. Cocard a déterminé dans quelle mesure les précisions obtenues dépendent:

- de la distance entre la station de référence et l'avion
- de mesures à une ou deux fréquences
- de la constellation des satellites
- du temps d'intégration
- de la qualité des mesures des pseudo-distances
- de la modélisation stochastique de l'ionosphère.

Les expériences effectuées comprennent:

- des vols avec levés de profils au LASER
- des vols SAR en collaboration avec le "Deutsche Versuchsanstalt für Luft- und Raumfahrt"
- des vols d'aérotriangulation, assistés par GPS en collaboration avec la chaire de photogrammétrie et de télédétection de l'EPF Zurich

Le travail de M. Cocard est complété par un chapitre consacré aux applications géophysiques aéroportées, en particulier à l'aérogravimétrie. M. Cocard a pu démontrer la qualité de son procédé de positionnement de haute précision pour déterminer les accélérations de l'avion dans le cadre d'un projet international de recherche pour lequel un survol aérogravimétrique de la Suisse a eu lieu. La Direction fédérale des mensurations cadastrales a mis aimablement son avion à disposition. Que M. Hübscher, du Service de vol de cette organisation, trouve ici l'expression de notre reconnaissance. Dans le cadre d'un projet-pilote commun à l'Office fédéral de l'aviation civile, Swisscontrol et Crossair, on étudie l'application de ces méthodes aux vols d'approches en Suisse.

La Commission géodésique suisse de l'Académie suisse des sciences naturelles remercie Monsieur Cocard de sa précieuse contribution à la navigation de précision assistée par satellites. Le professseur G. Beutler de l'Institut d'astronomie de l'Université de Berne a enrichi ces travaux de ses précieuses suggestions. Qu'il trouve ici l'expresssion de notre vive reconnaissance. Enfin, la Commission géodésique suisse remercie l'Académie suisse des sciences naturelles pour la prise en charge des coûts d'impression de ce volume.

F. Jeanrichard, directeur
Office fédéral de topographie
Vice-président de la CGS

Prof. Dr. H.-G. Kahle
EPF Zurich
Président de la CGS

FOREWORD

Originally, the concept of the satellite navigation system was to use the travel time of codes that were modulated onto carrier waves. High-precision geodetic applications in the kinematic mode requesting accuracy in the range of cm were not attainable. It was not until the actual carrier phases themselves were used, by measuring the differences of the travel time phases, that GPS-Technology was able to experience the boom we have seen in recent years. A central problem, however, is how to calculate the unknown number of whole wave lengths (so-called ambiguities) that make up the wave, in addition to the phase measurements.

The following publication by Dr. Marc Cocard presents the development of a software package with which, by the use of differential GPS-measurements, trajectories of aircraft movements at the cm-level of accuracy can be pin-pointed. The software has successfully been tested on real flights. The publication is divided into two parts, the first being the development of the software and the latter its application. An important aspect of the work was not only the creation of the software itself, but also the scientific analysis of the influence of various parameters on the measurement system, and the order of measurements on the quality and reliability of the results. Dr. Cocard worked out to what extent the accuracy is dependent on the following

- the distance between the reference stations and the aircraft
- the single or double frequency measurements
- the satellite constellation
- the integration period
- the quality of the code measurements and
- the stochastic modelling of the ionosphere

The experiments that were carried out included

- Laser profiling flights
- SAR flights with the "Deutsche Versuchsanstalt für Luft- und Raumfahrt"
- GPS aided aerotriangulations flights in collaboration with the ETH professorship for Photogrammetry and Remote Sensing

Dr. Cocard has also supplemented a chapter on "airborne"-methods in geophysical applications, particularly as applied in aerogravimetry. During an international research project in which Switzerland was flown over aerogravimetrically, Dr. Cocard was given the opportunity to demonstrate the quality of high precision positioning for the measurement of the accelerations of the aircraft. By correcting the disturbancy accelerations which were determined by GPS, it was possible to detect the gravity anomalies of the Alps and the structure of the earth's crust from the aircraft. In the meantime, bordering countries have stated their interest for the aerogravimetric map to be extended into their region. In addition, there exist concrete plans for the further development of the application for landing approaches in Switzerland. A combined project between the "Bundesamt für Zivilluftfahrt (BAZL)", Swisscontrol, Crossair and the ETH Zurich has commenced.

The Swiss Geodetic Commission (SGC) of the Swiss Academy of Natural Sciences (SANW) would like to thank Dr. Cocard for his valuable contribution to satellite aided precision navigation in Switzerland. Prof. Dr. G. Beutler of the Institute of Astronomy of the University of Bern enriched the paper with many valuable suggestions. At this point, we would like to express our gratitude to him for his co-operation and contribution. We are equally grateful to Prof. Dr. E. Klingelé of the Institute for Geodesy and Photogrammetry of the ETH Zurich, who was in charge of the aerogravimetric part. The SGC's thanks also go to the SANW who kindly took on the costs for the printing of this edition.

Director F. Jeanrichard
Federal Office of Topography
Vice President SGC

Prof. Dr. H.-G. Kahle
ETH Zurich
President SGC

Abstract

This report deals with the calculation of highly accurate trajectories of moving vehicles, and of airplanes in particular, from differential GPS measurements processed in the off-line mode.

In the last few years the Global Positioning System (GPS) has become the most powerful navigation system world-wide. Although it was developed by the American Department of Defense (DoD) and is, therefore, primarily designated for military use, the number of civilian users is rapidly increasing from day to day. Based on satellite measurements, GPS allows instantaneous positioning accurate to within 100-200 meters. [Remondi, 1984] has shown that differential processing of phase measurements allows improvement of position accuracy to few centimeters. There are numerous applications for spatial trajectories calculated with such high quality accuracy: e.g. their integration in photogrammetric aerotriangulation allows considerable reduction of the number of control points on the ground. Also in airborne gravimetry new horizons are being opened by using GPS.

A software system for processing kinematic data in the off-line mode has been developed. Its key features are presented first. A robust and flexible approach using simultaneously phase- and code-measurements in a differential way is used. For the computation the differences between the code and phase information, measured by the roving receiver as well as by a fixed reference receiver, are used in order to reduce the systematic errors, which affect both receivers in a similar way. The main differences between the phase and the code data are (a) noise (decimeters to meters for the code, millimeters for the phase) and (b) the unknown ambiguities in the phase measurements, which are known to be integer values. Processing is carried out in two steps: firstly a least squares adjustment is applied in order to determine the time-invariant parameters, using the entire data set. Parameters which are considered as invariant are the ambiguities and the coordinates of the roving receiver during stationary periods. Next, the integer values of the ambiguities are determined. In a second step the trajectory is re-processed by introducing the known ambiguities.

The key problem in obtaining high-accuracy trajectories consists in making reliable identification of the integer-valued ambiguities. It is demonstrated that a conventional sigma dependent rounding strategy, commonly used in static applications, is still a useful tool in off-line kinematic processing. In addition, a more powerful search strategy has been analyzed and simulations show that under ideal conditions the integer values of the ambiguities can be retrieved within one epoch worth of dual-frequency measurements. These simulated results have been validated by real data. With increasing distance between the roving and the reference receiver a stochastic modeling of the ionospheric path delay gave good results but also showed the limitation of instantaneous ambiguity resolution.

Using GPS data of good quality trajectories with an accuracy of a few centimeters were recovered. With increasing distance between rover and reference station (up to 100 kilometers), however, all ambiguities could not always be resolved and the quality of the resulting trajectories deteriorates to some decimeters. But even in this case it was possible to derive the velocity and acceleration of the aircraft with high accuracy from the coordinates.

Zusammenfassung

Thema des vorliegenden Berichts ist die Bestimmung von hochpräzisen Trajektorien von bewegten Trägern vorallem Flugzeugen mit Hilfe von differentiellen GPS-Messungen im Off-line Modus.

Das Global Positioning System (GPS) hat sich in den letzten Jahren zu einem der besten und verbreitesten Navigationssysteme weltweit entwickelt. Obwohl es vom DoD (Department of Defence) der Vereinigten Staaten betrieben wird und somit vorallem für militärische Zwecke bestimmt ist, wächst die Zahl der zivilen Benutzer tagtäglich. Messungen zu Satelliten ermöglichen eine momentane Positionsbestimmung mit einer Genauigkeit von 100-200 Metern. Durch das Einbeziehen von Phasenmessungen im differentiellen Modus kann aber eine Genauigkeit von einigen Zentimeter erreicht werden [Remondi, 1984]. Die Anwendungen für solche hochgenauen Trajektorien sind mannigfaltig. So führt z.B. die Integration von GPS in die photogrammetrische Aerotriangulation zu einer erheblichen Reduktion der benötigten Passpunkte am Boden. Auch in der Aerogravimetrie öffnen sich durch den Einsatz von GPS neue Horizonte.

Programme zur Auswertung von GPS-Messungen im Off-line Modus wurden erstellt. Ein robuster und flexibler Ansatz unter gleichzeitiger Verwendung von differentiellen Code- und Phasenmessungen wurde benutzt. Durch die Differenzbildung der Messungen des bewegten Empfängers und des statischen Referenzempfängers können eine Reihe von systematischen Fehlern grösstenteils eliminiert werden. Die Hauptunterschiede zwischen Code- und Phasenmessung sind (a) die Messauflösung (Dezimeter bis Meter für den Code, Millimeter für die Phase) und (b) die zusätzlichen unbekannten, aber ganzzahligen Mehrdeutigkeiten der Phasenmessungen. Für die Auswertung wurde folgendes zweistufiges Vorgehen verwendet. In einem ersten Schritt werden aus allen Messungen die zeitunabhängigen Parameter mit der Methode der kleinsten Quadrate ausgeglichen. Als zeitunabhängige Parameter gelten die Mehrdeutigkeiten der Phasenmessungen und die Koordinaten des bewegten Empfänger während statischen Perioden. Anschliessend werden die ganzzahligen Werte der Mehrdeutigkeiten bestimmt. In einem zweiten Schritt wird die Trajektorie unter Verwendung der im ersten Schritt bestimmten Mehrdeutigkeiten berechnet.

Das zentrale Problem um eine hoche Genauigkeit der Trajektorien zu gewährleisten, ist die zuverlässige Identifizierung der ganzzahligen Werte der Mehrdeutigkeiten. Es konnte gezeigt werden, dass die bei statischen Auswertungen oft verwendete statistische Rundungs-Methode (sigma dependent rounding strategy) auch in kinematischen Anwendungen benutzt werden kann. Daneben aber wurde ein effizienterer Surchalgorithmus analysiert. Simulationsrechnungen zeigten, dass es unter idealen Bedingungen möglich ist, die Mehrdeutigkeiten aus Zweifrequenz-Messungen einer einzigen Epoche auf ihre Integer-Werte zu fixieren. Dieses Simulationsresultat bestätigte sich im Fall von reellen Messdaten. Mit zunehmender Distanz zwischen bewegten und Referenzemfänger zeigte ein stochastisches Modellieren des Ionosphäreneinflusses gute Resultate aber auch die Grenzen der schnellen Auflösung der Mehrdeutigkeiten.

Unter Verwendung von qualitativ guten GPS-Messungen konnten Flugtrajektorien mit einer Genauigkeit von einigen Zentimetern bestimmt werden. Mit zunehmender Distanz zwischen bewegtem und Referenzempfänger (bis zu 100 km) konnten nicht mehr alle Mehrdeutigkeiten gelöst werden und die Qualität der Koordinaten verschlechterte sich zu einigen Dezimetern. Aber auch in diesem Fall konnten Geschwindigkeit und Beschleunigung mit hoher Genauigkeit aus den Koordinaten abgeleitet werden.

1 Introduction

The Global Positioning System (GPS) has made a tremendous impact on geodesy. It allows the measurements of networks on a global scale with an accuracy comparable to the accuracy achieved by Very Long Baseline Interferometry (VLBI). The methods used for static positioning are based on highly accurate measurement of the carrier phase of the signals emitted by GPS satellites, whereas the conventional navigation approach uses less accurate code measurements. Efforts have been made to use phase measurement for kinematic purposes as well, to obtain trajectories of vehicles of all kind with the highest precision.

The applications for highly precise GPS trajectories cover a wide range. The determination of terrain elevation by measuring the height above ground with a laser ranging system is only possible if the position and the flight level of the aircraft are known accurately; GPS may be used for this purpose. The accurate determination of photogrammetric projection centers of an aerophotogrammetric block with GPS allows significant reduction of the number of terrestrial control points. For geophysical airborne surveys positioning is essential (aeromagnetism, aeroradiometry etc.). For the determination of the earth's gravity field with an airborne gravimeter the information of the GPS trajectory is necessary for the determination of the location, the velocity and the acceleration of the aircraft. It is characteristic of all these applications that the positions need not be determined on-line during the flight, but may be calculated in the post processing mode (off-line mode).

When starting the project 'GPS-supported aerotriangulation' in 1990 it soon became obvious that the approaches used in commercial software at that time were not robust enough to reliably deal with kinematic flight data. With the poorer satellite constellation in 1990 the requirement of continuous phase data without major losses of lock to the satellites during the entire flight was difficult to meet. Software for the processing of absolute and differential code measurements had already been developed at our institute at an earlier stage. In order to be able to produce our own solutions, we therefore decided to extend the existing software by integrating the phase measurements. The goal was to have a robust and flexible tool at our disposal to process kinematic GPS data in the off-line mode. This also allowed us to study different aspects of kinematic GPS, such as the fast 'on the fly' ambiguity resolution in the dual frequency mode. 'On the fly' ambiguity resolution is commonly understood as the mode where only measurements during the moving phase of the vehicle are used to fix ambiguities.

The key features of the software system are presented in chapters 2 to 4.

- In ***chapter 2*** a two-step strategy for the off-line mode, simultaneously using code and phase measurements in the differential mode, is presented.

- ***Chapter 3*** deals with the problem of screening phase measurements, in a kinematic environment in particular.

- The main challenge when processing kinematic GPS data is the reliable fixing of the double difference ambiguities to integer values. Different strategies are discussed in ***chapter 4*** and the details of the implemented search algorithm are given. Special em-

phasis is put on the discrimination potential of single and dual frequency measurements. These are studied in a theoretical way by using simulation techniques.

Results from real GPS data are presented in chapters 5 to 8. The data sets were selected by their characteristics to show specific aspects and problems in the processing of kinematic GPS data, based on the performance and limits of our approach. Special emphasis is put on the problem of ambiguity resolution and the validation of the obtained trajectories.

- The main topic of ***chapter 5*** is instantaneous ambiguity resolution in the dual frequency mode. The results of the simulations from chapter 4 are first validated in the ideal case of a static 10 m baseline. We analyze the instantaneous discrimination potential on high-quality flight data. Using two reference stations at different locations we focus on the impact of the distance between the reference and roving receiver on ambiguity fixing and coordinate determination.

- Results from the first kinematic data sets collected at our institute in 1989 show the low capacity for retrieval of the ambiguities from single frequency measurements under the satellite constellation available in 1989. The main topic of ***chapter 6***, however, consists of the comparison of two heterogeneous unsynchronized data sets, i.e. the trajectories obtained by GPS and by a simultaneously operating Laser-tracker.

- ***Chapter 7*** deals with the use of GPS in aerophotogrammetry. Photogrammetric aerotriangulation is one of the few examples allowing an accurate external validation of the GPS trajectory. After a general discussion of the question as to how to include the GPS-derived coordinates of the projection centers in the photogrammetric bundle block adjustment, data from a test flight is analyzed.

- The interesting characteristics of the data set, presented in ***chapter 8***, are comprised in the fact that it has been collected simultaneously with airborne gravity meter data. Different reference stations, located at distances of some 100 kilometers apart, were occupied during the survey. This allowed comparison of the coordinates. In addition, velocity and acceleration of the airplane, as derived from GPS, are of interest for the reduction of the gravity meter measurements.

2 Processing of kinematic GPS data

2.1 Observation equations

Two different types of observation are carried out by GPS receivers: phase measurements, which correspond to the difference between the carrier signal generated by the internal oscillator of the receiver and the carrier signal coming in from the satellite, and code measurements. The code measurements (pseudo-range measurements) are obtained by correlation technique using known pseudo-random sequences, which are modulated on the carrier wave. Basically both types of observations can be thought of as range measurements corrupted by some biases.

2.1.1 Zero-difference observations

The basic observation equation related to the code measurement is given e.g. by [Bauersima, 1983]:

$$\begin{aligned}\rho_j^i(t_R) &= d_j^i + c\cdot cl_j - c\cdot cl^i + Ion_j^i + Trp_j^i \\ &= \left|\vec{X}^i(t_T) - \vec{x}_j(t_R)\right| + clBias_j - clBias^i + Ion_j^i + Trp_j^i\end{aligned} \tag{2.1}$$

and for the phase measurement by :

$$\begin{aligned}\varphi_j^i(t_R) &= d_j^i + c\cdot cl_j - c\cdot cl^i - Ion_j^i + Trp_j^i \\ &= \left|\vec{X}^i(t_T) - \vec{x}_j(t_R)\right| + clBias_j - clBias^i - \lambda\cdot A^i - Ion_j^i + Trp_j^i\end{aligned} \tag{2.2}$$

with

t_R	receiving time in GPS time.
t_T	transmitting time in GPS time.
c	speed of light in the vacuum.
$d_j^i = \left\|\vec{X}^i(t_T) - \vec{x}_j(t_R)\right\|$	slant range between receiver and satellite.
$\vec{X}^i(t_T)$	coordinates of the satellite (i)
$\vec{x}_j(t_R)$	coordinates of the ground station (receiver j)
$clBias^i = c\cdot cl^i$	unknown clock bias of the receiver (in meters).
$clBias_j = c\cdot cl_j$	clock bias of the satellite (in meters).
A^i	ambiguity of the phase measurement.
Ion_j^i	path delay due to the ionosphere.
Trp_j^i	path delay due to the atmosphere.
λ	wavelength of the carrier.

The measurements are actually related to the nominal time of the receiver clock t_{Nom}. The corresponding 'true' GPS time of reception t_R is :

$$t_R = t_{Nom} - cl_j \tag{2.3}$$

This means that the coordinates of the receiver $\vec{x}_j$ refer to the 'true' GPS time. The coordinates $\vec{X}^i$ and the clock error cl_j of the satellites, however, have to be calculated at the time of transmission t_T :

$$t_T = t_R - \frac{d_j^i}{c} \tag{2.4}$$

The time difference between the transmission and reception time of the signal corresponds to the propagation time of the signal, i.e. the distance from receiver to satellite divided by the speed of light.

It is interesting to note that the transmission time t_T can be directly connected to the nominal time using the pseudo-range measurement.

$$t_T = t_R - \frac{d_j^i}{c} = t_{Nom} - cl_j - \frac{d_j^i}{c} = t_{Nom} - \left(\frac{d_j^i}{c} + cl_j - cl^i \right) - cl^i$$

$$t_T \approx t_{Nom} - \frac{\rho_j^i}{c} + cl^i(t_{Nom}) \tag{2.5}$$

If we assume that the positions $\vec{X}^i$ and the clock errors cl^i of the satellites are calculated using broadcast or precise ephemerides, the unknown parameters to be determined are :

- *the geocentric coordinates of the roving receiver* x_j, y_j, z_j
- *the clock bias of the roving receiver* $clbias_j$
- *the ambiguities of the carrier phase* A^i

For the actual processing the equations (2.1) and (2.2) have to be linearized. Formally the linearized equation can be written as

$$l_j^i = l_j^i\big|_{p0} + \sum_{m=1}^{n} \left(\frac{dl_j^i}{dp_m} \right)\Bigg|_{p0} \cdot dp_m = l_j^i\big|_{p0} + \sum_{m=1}^{n} a_m \cdot dp_m \tag{2.6}$$

where

$l_j^i\big|_{p0}$ is an approximated value for the measurement l_j^i, obtained from the observation equation using the approximation values p_0 for the unknown parameters.

dp_m are the linearized unknown parameters.

$a_m = \frac{dl_j^i}{dp_m}$ are the coefficients of the linearization.

The coefficients a_m of the linearisation for the code and the phase measurements are then :

$a_m =$	x	y	z	$clBias$	A^i
$code$	e_x	e_y	e_z	1	0
$phase$	e_x	e_y	e_z	1	λ

(2.7-a)

with

$$e_x = \frac{X^i(t_T) - x_j(t_R)}{\left|\vec{X}^i(t_T) - \vec{x}_j(t_R)\right|} \qquad e_y = \frac{Y^i(t_T) - y_j(t_R)}{\left|\vec{X}^i(t_T) - \vec{x}_j(t_R)\right|} \qquad e_z = \frac{Z^i(t_T) - z_j(t_R)}{\left|\vec{X}^i(t_T) - \vec{x}_j(t_R)\right|} \tag{2.7-b}$$

where $e_{x,y,z}$ are the Cartesian coordinates of the unit vector between the receiver (at reception time) and the satellite (at transmission time).

2.1.2 *Single-difference observations*

The so called 'single difference' measurements are obtained by forming the difference between two simultaneous observations from two different stations to the same satellite. This differentiation technique may be applied to code as well as to phase measurements. The simultaneity is in fact defined by the readings of the two receivers. This means that the true GPS times of the two zero difference measurements are not equal, due to the different receiver clock biases. Even in the absence of any receiver clock error, transmission times would slightly differ because the distances to the satellites are different. In the following equations the indices (f) will be used for the fixed station, (m) for the moving receiver and (s) for the satellite.

The observation equation for the single difference code measurements are:

$$\Delta\rho^s_{mf}(t_{Nom}) = \rho^s_m(t_{Nom\ m}) - \rho^s_f(t_{Nom\ f}) \tag{2.8}$$

and for single difference phase measurement :

$$\Delta\varphi^s_{mf}(t_{Nom}) = \varphi^s_m(t_{Nom\ m}) - \varphi^s_f(t_{Nom\ f}) \tag{2.9}$$

They may be formally expressed by :

$$code: \quad \Delta\rho^s_{mf} = \Delta d^s_{mf} + \Delta clBias_{mf} - \Delta clBias^s_{mf} + \Delta Ion^s_{mf} + \Delta Trp^s_{mf} \tag{2.10-a}$$

$$phase: \quad \Delta\varphi^s_{mf} = \Delta d^s_{mf} + \Delta clBias_{mf} - \Delta clBias^s_{mf} - \lambda\cdot\Delta A^s_{mf} - \Delta Ion^s_{mf} + \Delta Trp^s_{mf} \tag{2.10-b}$$

with:

$$\Delta d^s_{mf} = \left|\vec{X}^s(t_{Tm}) - \vec{x}_m(t_{Rm})\right| - \left|\vec{X}^s(t_{Tf}) - \vec{x}_f(t_{Rf})\right| \qquad (2.10\text{-c})$$

$$\Delta clBias_{mf} = clBias_m(t_{Rm}) - clBias_f(t_{Rf}) = c\cdot(cl_m(t_{Rm}) - cl_f(t_{Rf})) \qquad (2.10\text{-d})$$

$$\begin{aligned}\Delta clBias^s_{mf} &= clBias^s_m(t_{Rm}) - clBias^s_f(t_{Rf}) \\ &= c\cdot(cl^s_m(t_{Rm}) - cl^s_f(t_{Rf})) \\ &\approx c\cdot(\tfrac{d}{dt}cl^s\cdot(t_{Rm} - t_{Rf})) \qquad \approx 0\end{aligned} \qquad (2.10\text{-e})$$

From the point of view of system performance this term may be neglected, since typical values for $\frac{d}{dt}cl^s$ are on the order of 10^{-10} or better. A differential synchronization error $(t_{Rm} - t_{Rf})$ of 1 second would provoke an error of 3 mm in $\Delta clBias^s_{mf}$, This assumption, however, is no longer correct under Selective availability (SA), where an artificial degradation of the satellite clocks is introduced.

$\Delta Ion^s_{mf} = Ion^s_m - Ion^s_f$ differential ionospheric delay.

$\Delta Trp^s_{mf} = Trp^s_m - Trp^s_f$ differential tropospheric delay.

ΔA^s_{mf} single-difference ambiguity of the phase measurements.

If we assume that the positions $\vec{X}^s$ of the satellites are calculated using broadcast or precise ephemerides and that the coordinates of the reference station $\vec{x}_f$ are known, the unknown parameters to be determined are :

- *the geocentric coordinates of the roving receiver* x_j, y_j, z_j
- *the differential clock bias of the roving receiver* $\Delta clBias_{mf}$
- *the 'single-difference' ambiguities of the carrier-phase* ΔA^s_{mf}

The coefficients of the linearisation for the code and the phase measurements are then :

$a_m =$	x_m	y_m	z_m	$\Delta clBias_{mf}$	ΔA^s
code	e_x	e_y	e_z	1	0
phase	e_x	e_y	e_z	1	λ

(2.11-a)

with

$$e_x = \frac{X^i(t_{Tm}) - x_m(t_{Rm})}{\left|\vec{X}^i(t_{Tm}) - \vec{x}_m(t_{Rm})\right|} \quad e_y = \frac{Y^i(t_{Tm}) - y_m(t_{Rm})}{\left|\vec{X}^i(t_{Tm}) - \vec{x}_m(t_{Rm})\right|} \quad e_z = \frac{Z^i(t_{Tm}) - z_m(t_{Rm})}{\left|\vec{X}^i(t_{Tm}) - \vec{x}_m(t_{Rm})\right|} \qquad (2.11\text{-b})$$

where $e_{x,y,z}$ are the Cartesian coordinates of the unit vector between the receiver (at reception time) and the satellite (at transmission time).

2.2 Computational approach

The strategy used here to deal with kinematic GPS data is to process code and phase measurements simultaneously. The unknown parameters are subdivided into two groups : the time dependent and the time independent parameters.

The time dependent parameters refer to one epoch only

- *clock biases*
- *coordinates of the moving receiver*

The time independent parameters are common to two or more epochs

- *coordinates of the moving receiver if at rest*
- *ambiguities of the phase measurements*

The processing involves the following steps.

- *Screening of the phase measurements for cycle slips*
- *Definition of a site allocation table*
- *Initialization of the ambiguities*
- *Determination of the time independent parameters (floating point solution of the ambiguities)*
- *Fixing of the double difference-ambiguities to integers (if possible)*
- *Determination of the time dependent parameters.*

The different steps will be discussed in more detail below. The screening of phase measurements for cycle slips is dealt with in chapter 3. The problem of fixing the double-difference ambiguities to integers is discussed in chapter 4.

The basic idea is to perform a least square estimation in two steps. In the first step the time-independent parameters are estimated. For each epoch all time-dependent parameters are eliminated from the normal equation system (NEQ). The reduced NEQ systems are then accumulated over the total time span. By inversion the time independent parameters are obtained. In the second step the values of the ambiguities, obtained from the first step, are used to determine the time dependent parameters, i.e. the coordinates of the moving receiver. The advantage of this procedure is that it allows the implementation of the total amount of measurements in estimating the ambiguities, and that it is best suited for the off-line mode.

2.2.1 Site allocation table

For the moving receiver a site allocation table is defined with the temporal information of the stationary site occupations.

Two examples are given in illustration :

Example 1 :

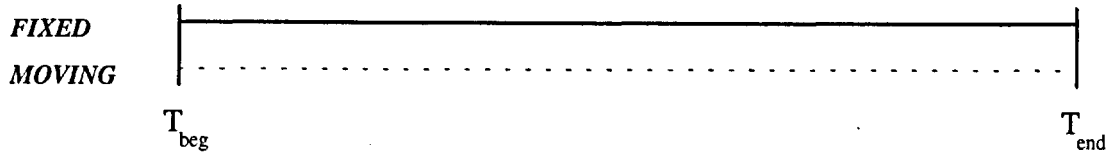

The Moving Receiver does not include any stationary site occupation.

Example 2 :

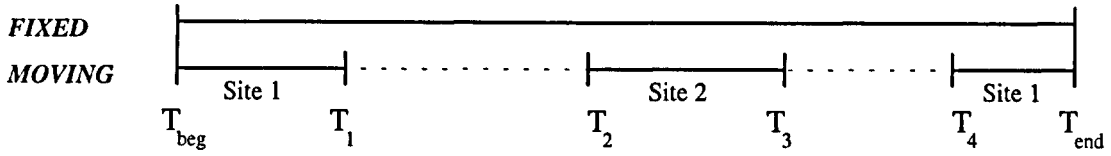

In this configuration there are three stationary periods and site 1 was occupied during two periods (period 1 and 3).

2.2.2 Initialization of ambiguities

Initialization of phase ambiguities is carried out by using code measurements, and a mapping file containing the value and a corresponding period of validity for the ambiguities is created.

For every satellite a value for the ambiguity is calculated from the difference between the single-difference of the code observation and the single-difference of the phase observations. By subtracting equation (2.10-a) from equation (2.10-b) and neglecting ionospheric refraction, one obtains :

$$\Delta A^s_{mf}(t_i) = \frac{1}{\lambda} \cdot (\Delta\rho^s_{mf}(t_i) - \Delta\varphi^s_{mf}(t_i)) \tag{2.12}$$

If an interruption in the phase measurements occurs, a new ambiguity is set up. This means that a specific value for an ambiguity is only valid for a certain time span, from epoch i_1 to epoch i_2, and over this time span the initial value for the ambiguity is defined as the mean value from all individual epoch values:

$$\Delta A^s_{mf}(i_1, i_2) = \sum_{i=i_1}^{i_2} \frac{1}{\lambda}(\Delta\rho^s_{mf}(t_i) - \Delta\varphi^s_{mf}(t_i)) \tag{2.13}$$

The following diagram illustrates graphically a mapping file of the ambiguities for 7 satellites (S1 to S7) as a function of time.

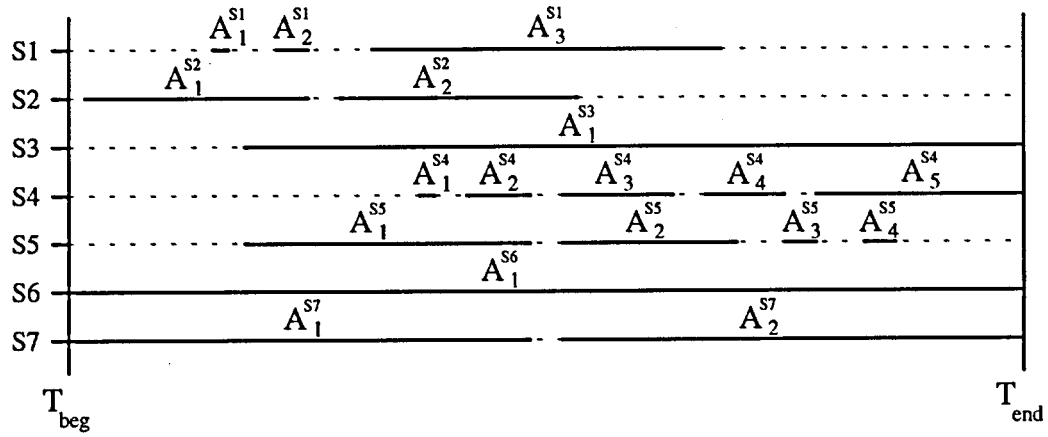

Figure 2.1 : Illustration of a mapping file of ambiguities.

The quality of these values depends on the quality of the code measurements and on the amount of uninterrupted phase data used for the averaging. These values are only used as starting values in the next step.

2.2.3 *Evaluation of time independent parameters*

To deal with kinematic GPS data we introduce two different normal equation systems, the first referring to the unknowns of one single epoch, the second covering all unknowns, which are common to several epochs.

Let us remind ourselves that the time independent parameters are :

- *The coordinates of the stationary sites (given in the site allocation table).*
- *All phase ambiguities (given by the mapping file for ambiguities).*

For each satellite i at every epoch j up to 4 independent measurements (phase and code on L1 resp. L2) are available. Using equation (2.6) the linearized observation equations may be written as:

$$n_j^i = \sum_{m=1}^{n} a_m \cdot dp_m - (l_j^i - l_j^i\big|_{p0}) \qquad \text{with the associated weight} \quad p_i^j \qquad (2.14)$$

Using matrix notation the previous formula may be written as :

$$v = A \cdot x - f \qquad \text{with the associated weight matrix} \quad P \qquad (2.15)$$

A least squares estimation using the optimization criteria $v^T Pv = minimum$ leads to the corresponding normal equation system (NEQ) :

$$(A^T PA)\cdot x = A^T Pf \quad \text{or} \quad N\cdot x = n \qquad \text{with } N = A^T PA \quad \text{and} \quad n = A^T Pf \qquad (2.16)$$

The coefficient matrix A (design matrix per epoch) for n satellites is given in figure 2.2.

$A-matrix$	x	y	z	Δcl	A^1_{L1}	A^1_{L2}	A^2_{L1}	A^2_{L2}	....	A^i_{L1}	A^i_{L2}	....	A^n_{L1}	A^n_{L2}
Sat 1 : *Code* L_1	e^1_x	e^1_y	e^1_z	1	0	0								
Sat 1 : *Code* L_2	e^1_x	e^1_y	e^1_z	1	0	0								
Sat 1 : *Phase* L_1	e^1_x	e^1_y	e^1_z	1	λ_{L1}	0	0		....	0		....	0	
Sat 1 : *Phase* L_2	e^1_x	e^1_y	e^1_z	1	0	λ_{L2}								
Sat 2 : *Code* L_1	e^2_x	e^2_y	e^2_z	1			0	0						
Sat 2 : *Code* L_2	e^2_x	e^2_y	e^2_z	1			0	0						
Sat 2 : *Phase* L_1	e^2_x	e^2_y	e^2_z	1	0		λ_{L1}	0	....	0		....	0	
Sat 2 : *Phase* L_2	e^2_x	e^2_y	e^2_z	1			0	λ_{L2}						
⋮		⋮			⋮		⋮		⋮⋮⋮⋮	⋮		⋮⋮⋮⋮	⋮	
Sat i : *Code* L_1	e^i_x	e^i_y	e^i_z	1						0	0			
Sat i : *Code* L_2	e^i_x	e^i_y	e^i_z	1						0	0			
Sat i : *Phase* L_1	e^i_x	e^i_y	e^i_z	1	0		0		....	λ_{L1}	0	....	0	
Sat i : *Phase* L_2	e^i_x	e^i_y	e^i_z	1						0	λ_{L2}			
⋮		⋮			⋮		⋮		⋮⋮⋮⋮	⋮		⋮⋮⋮⋮	⋮	
Sat n : *Code* L_1	e^n_x	e^n_y	e^n_z	1									0	0
Sat n : *Code* L_2	e^n_x	e^n_y	e^n_z	1									0	0
Sat n : *Phase* L_1	e^n_x	e^n_y	e^n_z	1	0		0		⋮	0		⋮	λ_{L1}	0
Sat n : *Phase* L_2	e^n_x	e^n_y	e^n_z	1									0	λ_{L2}

Figure 2.2 : Design matrix for the measurements of one epoch.

The weight matrix P may be assumed to be diagonal and deduced from a priori values for the different types of observations. Typical values for the a priori rms for the different types of observations are :

phase	2 - 5 mm
C/A-code	1 - 5 m
P-Code	0.1 - 0.8 m

Some refinements can be obtained by introducing weights which are dependent on the baseline distance and/or of the elevation angle.

The NEQ matrix N for one epoch becomes :

x	y	z	Δcl	A_{L1}^1 A_{L2}^1	...	A_{L1}^i A_{L2}^i	...	A_{L1}^n A_{L2}^n
$\sum_{i=1}^{n}(\overline{p}^i e_x^i e_x^i)$	$\sum_{i=1}^{n}(\overline{p}^i e_x^i e_y^i)$	$\sum_{i=1}^{n}(\overline{p}^i e_x^i e_z^i)$	$\sum_{i=1}^{n}(\overline{p}^i e_x^i)$	$p_{L1}^1 e_x^1 \lambda_{L1}$ $p_{L2}^1 e_x^1 \lambda_{L2}$		$p_{L1}^i e_x^i \lambda_{L1}$ $p_{L2}^i e_x^i \lambda_{L2}$		$p_{L1}^n e_x^n \lambda_{L1}$ $p_{L2}^n e_x^n \lambda_{L2}$
	$\sum_{i=1}^{n}(\overline{p}^i e_y^i e_y^i)$	$\sum_{i=1}^{n}(\overline{p}^i e_y^i e_z^i)$	$\sum_{i=1}^{n}(\overline{p}^i e_y^i)$	$p_{L1}^1 e_y^1 \lambda_{L1}$ $p_{L2}^1 e_y^1 \lambda_{L2}$	...	$p_{L1}^i e_y^i \lambda_{L1}$ $p_{L2}^i e_y^i \lambda_{L2}$	...	$p_{L1}^n e_y^n \lambda_{L1}$ $p_{L2}^n e_y^n \lambda_{L2}$
		$\sum_{i=1}^{n}(\overline{p}^i e_z^i e_z^i)$	$\sum_{i=1}^{n}(\overline{p}^i e_z^i)$	$p_{L1}^1 e_z^1 \lambda_{L1}$ $p_{L2}^1 e_z^1 \lambda_{L2}$		$p_{L1}^i e_z^i \lambda_{L1}$ $p_{L2}^i e_z^i \lambda_{L2}$		$p_{L1}^n e_z^n \lambda_{L1}$ $p_{L2}^n e_z^n \lambda_{L2}$
			$\sum_{i=1}^{n}(\overline{p}^i)$	$p_{L1}^1 \lambda_{L1}$ $p_{L2}^1 \lambda_{L2}$		$p_{L1}^i \lambda_{L1}$ $p_{L2}^i \lambda_{L2}$		$p_{L1}^n \lambda_{L1}$ $p_{L2}^n \lambda_{L2}$
				$p_{L1}^1 \lambda_{L1}^2$ 0 0 $p_{L2}^1 \lambda_{L2}^2$	0	0	0	0
					$\ddots$	0	0	0
						$p_{L1}^i \lambda_{L1}^2$ 0 0 $p_{L2}^i \lambda_{L2}^2$	0	0
					$\cdot$		$\ddots$	0
								$p_{L1}^n \lambda_{L1}^2$ 0 0 $p_{L2}^n \lambda_{L2}^2$

Figure 2.3 : NEQ-matrix N for one epoch

where $\overline{p} = \sum_{j=1}^{n} p_j$ is the sum of the weights of the different observation types present.

The constant term $\boldsymbol{n} = \boldsymbol{A}^T \boldsymbol{P} \boldsymbol{f}$ of the normal equation system becomes :

x	y	z	Δcl	A_{L1}^1 A_{L2}^1	...	A_{L1}^i A_{L2}^i	...	A_{L1}^n A_{L2}^n
$\sum_{i=1}^{n} e_x(\overline{pf})^i$	$\sum_{i=1}^{n} e_y(\overline{pf})^i$	$\sum_{i=1}^{n} e_z(\overline{pf})^i$	$\sum_{i=1}^{n}(\overline{pf})^i$	$\lambda_{L1} f_{L1}^1$ $\lambda_{L2} f_{L2}^1$	...	$\lambda_{L1} f_{L1}^i$ $\lambda_{L2} f_{L2}^i$	...	$\lambda_{L1} f_{L1}^n$ $\lambda_{L2} f_{L2}^n$

Figure 2.4 : Constant term n of the NEQ-system for one epoch.

with $(\overline{pf}) = \sum_{j=1}^{n} p_j f_j$

This normal equation system for a single epoch regroups the ITRF-92 coordinates and the synchronization error of the moving receiver as well as the ambiguities of the phase differences. The time dependent elements of this normal equation system are then eliminated using a Gaussian elimination procedure.

As the clock is always time-dependent, it is eliminated. The coordinates of the receiver are only eliminated during a 'moving period'. Whether the receiver is on a fixed site or in motion is determined by the site allocation table.

Example 1 : Moving Receiver on fixed site

(Elimination of the clock bias)

Example 2 : Moving Receiver in motion

(Elimination of the 3 coordinates and the clock bias)

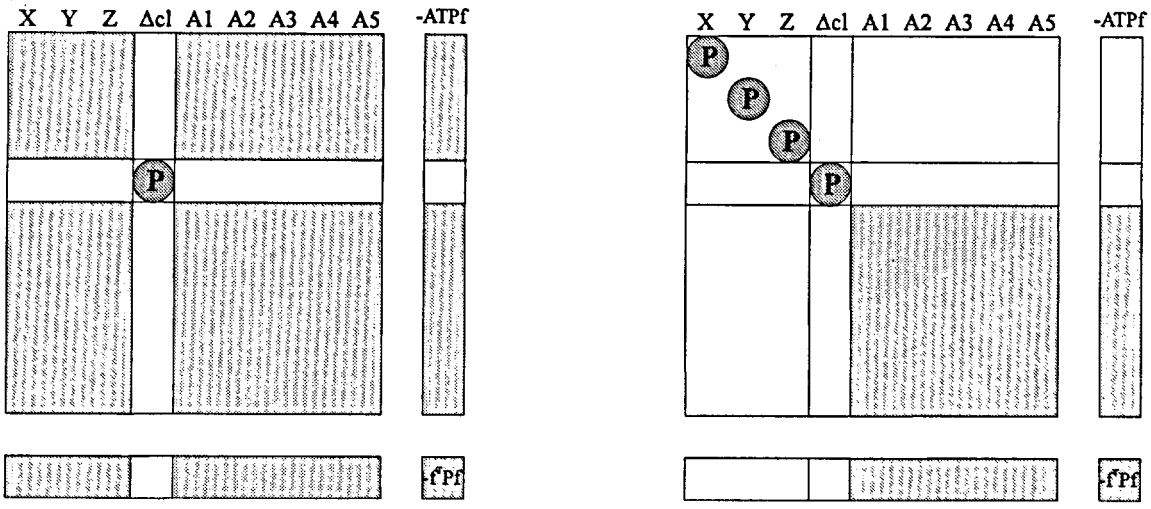

Figure 2.5 : Elimination of the time dependent parameters from the NEQ system.

For every epoch the corresponding NEQ system is reduced and the remaining part added to the second separated NEQ system, which contains only the time independent parameters. After having sequentially added all individual parts from all epochs, one obtains the NEQ system for the independent parameters, containing the coordinates of the stations occupied for 2 or more consecutive epochs and the ambiguities. Solving this system gives the so-called floating point solution for the ambiguities. The NEQ system also contains all information necessary for determining the integer values of the ambiguities. (chapter 4).

2.2.4 Evaluation of time dependent parameters

In a third step, the entire calculation is repeated, where the values for the ambiguities are introduced as known. The same normal equation system for a single epoch as in the previous step is used, but only the ITRF-92 coordinates and the synchronization error of the moving receiver are introduced as unknowns.

2.2.5 *Flow-chart of the computational approach*

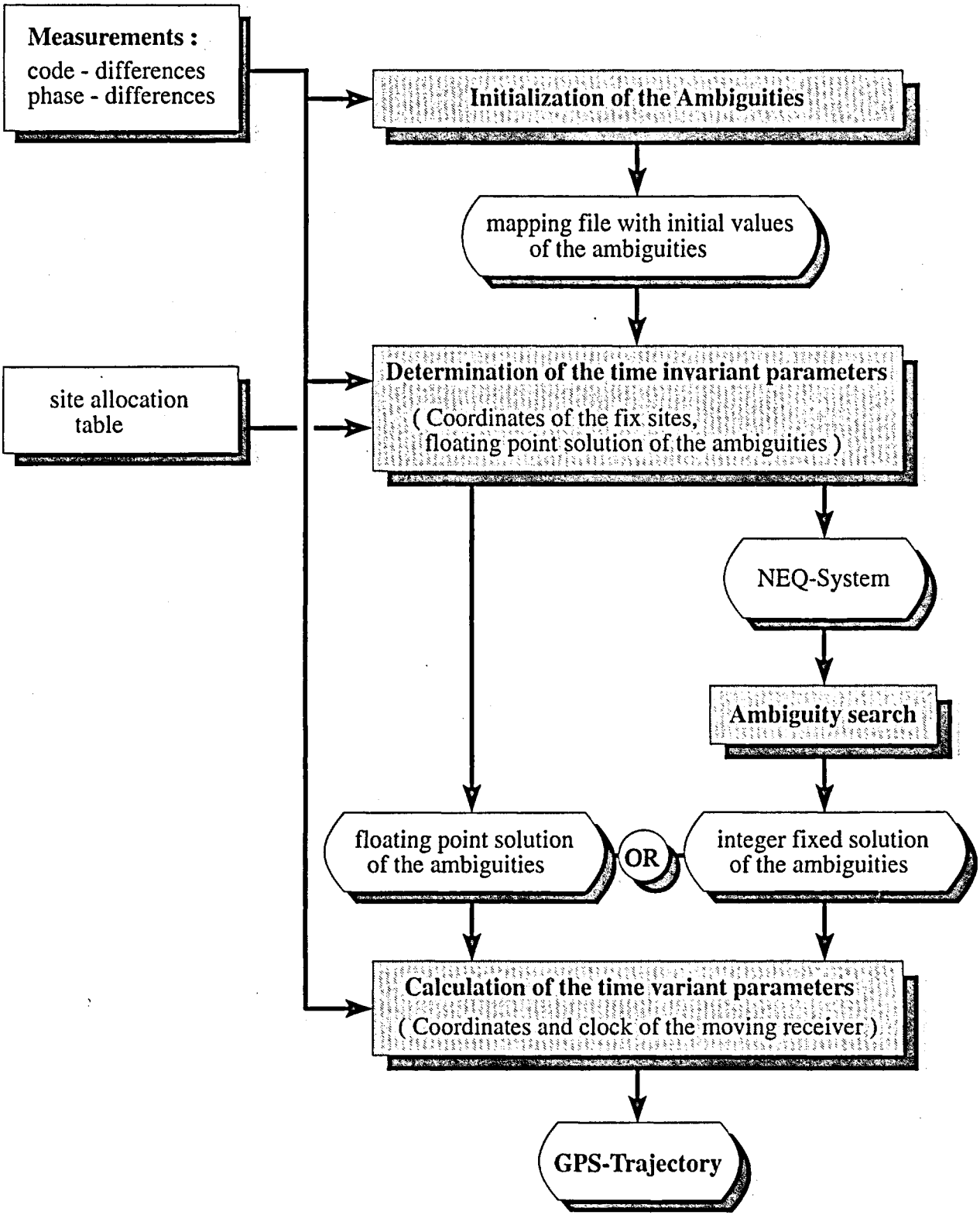

Figure 2.6 : Overview of the different steps in the processing of kinematic GPS data

2.2.6 *Remarks*

When processing dual-frequency measurements it proved to be necessary to introduce two different clock biases for the single differences of the L1 and the L2 phases. The use of a unique clock parameter led to strong constraints in the solution. Theoretically the estimation of two clock biases corresponds to the double differencing of the L1 and L2 phase observations.

To account for the tropospheric path delay the model given by [Saastamoinen, 1973] was implemented, and surface meteorological data derived from a standard model of the troposphere were used. This a priori model was adopted for all examples presented here. If not explicitly specified only measurements above a minimum elevation angle of 15° were used in the computation.

Ionosphere refraction was modeled by additional stochastic biases (see chapter 4.4).

For the computation of the satellite coordinates the broadcast ephemerides were used [Van Dierendonck et al, 1980] for all the data sets, except in chapter 8 where precise ephemerides of the CODE analysis center of the IGS (Beutler, 1994) were used.

3 Detection and repair of cycle slips

A well known problem in the processing of GPS phase measurements are jumps of a full number of cycles in the phase measurements, so called cycle slips. The presence and the frequency of cycle slips are good indicators of the quality of GPS receivers. In the new generation of receivers cycle slips are becoming less and less frequent. Nevertheless their presence can never be totally excluded.

The most common procedure for screening GPS data is to look for outliers in the triple differences using L1, L2 measurements or some linear combination of the two basic frequencies. This method works very well in the case of static data, but cannot easily be applied to kinematic data. A further particularity of triple-difference screening has to be seen in the fact that detected cycle slips cannot unambiguously be assigned to a station and a satellite.

3.1 Screening of kinematic data

In the following sections some different methods for screening kinematic GPS data are presented. Common to all methods is that they may fail under severe ionospheric conditions with large short-time fluctuations.

3.1.1 Integrated Screening

A strategy often used to detect cycle slips is a sequential search during the adjustment process itself. If we assume e.g. that the processing is done using a Kalman filter, the following steps must be executed:

1. *Propagation of the state vector and its covariance matrix.*
2. *After linearization of the measurement model the reduced measurements (i.e. the terms 'observed-computed') may be calculated :* $z_R = Z - f(x_E) + Noise$ *(* z_R *= reduced measurement,* Z *= observed,* $f(x_E)$ *= computed). reliably*
3. *Checking the reduced measurements* z_R *for possible cycle slips. reliably*
4. *Update step with the checked measurements. reliably*

The basic idea is to extrapolate the state vector and its covariance matrix and to make an estimate for the value of the measurements for the new epoch without actually using the new measurements. Comparing this estimate with the measurements allows the detection of cycle slips. The only problem is obtaining an estimate for the state vector, i.e. the coordinates, from the propagation which is accurate enough to detect for cycle slips at the 1-cycle level. This means, in the case of L1 measurements, because an L1-cycle corresponds to 19 cm, that the quality of the extrapolation should be on the order of one centimeter. Whether this is possible or not depends on the dynamic of the movement and on the time span over which one has to propagate.

If we consider e.g. a photogrammetric flight with a data rate of 1 Hz, the movement during the photogrammetric lines is smooth enough to allow a reliable screening (see also chapter 7.3.4 Interpolation to the time of exposure), but during the curves things often become criti-

cal due to higher dynamics and to the fact that often the quality of the GPS data is poorer. Unfortunately loss of lock to the satellites often occurs during curves: practical experience shows that often different parts of the data can not be screened reliably.

3.1.2 *Screening using phase rate measurements*

A different approach is to use the phase rate to screen the phase measurements. A necessary condition is that physically the phase rate measurements must be actually available to the analyst. The advantage of this method is that the raw data of every satellite may be screened separately and that therefore the screening must not skip parts of the data where only three satellites have been measured. Another advantage of the method is that it can also be used if only L1 data have been collected. The procedure consists of the following steps :

$$\Delta\varphi_A = \varphi(t_{i+1}) - \varphi(t_i) \tag{3.1}$$

$$\Delta\varphi_B = \dot{\varphi} \cdot (t_{i+1} - t_i) \qquad \text{with} \qquad \dot{\varphi} = \frac{\dot{\varphi}(t_i) + \dot{\varphi}(t_{i+1})}{2} \tag{3.2}$$

$$\varepsilon = \Delta\varphi_A - \Delta\varphi_B = \Delta\varphi - \dot{\varphi} \cdot \Delta t \tag{3.3}$$

where

$\varphi(t_i)$, $\varphi(t_{i+1})$ are the phase measurements at the epochs t_i and t_{i+1}

$\dot{\varphi} = \frac{\dot{\varphi}(t_i) + \dot{\varphi}(t_{i+1})}{2}$ is the average of the phase rates over the 2 epochs.

ε is the cycle slip indicator and the integer part of ε gives the size of the cycle slip directly.

The ability to detect cycle slips depends on the noise level of the cycle slip indicator ε. On the one hand the dynamics of the roving receiver and the measuring frequency have a strong impact on the quality of the linear approximation of the phase differences by the phase rate and on the other hand the measuring noise of the phase rates is a limiting factor in this method.

3.1.3 *Screening the difference between L1 and L2 phase measurements*

If L1 and L2 phase measurements are both available, the geometry-free linear combination L4 may be used to detect cycle slips.

$$\begin{aligned}\varphi_4[m] &= \varphi_1[m] - \varphi_2[m] \\ &= \lambda_1 \cdot \varphi_1[cy] - \lambda_2 \cdot \varphi_2[cy] \\ &= (d + \Delta cl + \lambda_1 \cdot A_1 + \Delta Ion_1) - (d + \Delta cl + \lambda_2 \cdot A_2 + \Delta Ion_2) \\ &= (\lambda_1 \cdot A_1 - \lambda_2 \cdot A_2) + (\Delta Ion_1 - \Delta Ion_2)\end{aligned} \tag{3.4}$$

So

$$\varphi_4[m] = const + \alpha \cdot \Delta Ion_1 .$$

By looking at the time differences of subsequent φ_4 measurements one obtains the following cycle slip indicator :

$$\begin{aligned} \Delta\varphi_4 &= \varphi_4(t_{i+1}) - \varphi_4(t_i) \\ &= \alpha(\Delta Ion(t_{i+1}) - \Delta Ion(t_i)) \\ &\qquad + \lambda_1 \cdot (A_1(t_{i+1}) - A_1(t_i)) - \lambda_2 \cdot (A_2(t_{i+1}) - A_2(t_i)) \\ &\approx \alpha \cdot \tfrac{d}{dt}\Delta Ion \cdot \Delta t + \lambda_1 \cdot \Delta A_1 - \lambda_2 \cdot \Delta A_2 \end{aligned} \tag{3.5}$$

Kinematic data are usually collected at a high frequency, typically from 0.2 to 10 Hz. For such small values of Δt the term $\alpha \cdot \frac{d}{dt}\Delta Ion_1$ may often be neglected. The expectation value for $\Delta\phi_4$ may be written as :

$$\Delta\phi_4 \approx \lambda_1 \cdot \Delta A_1 - \lambda_2 \cdot \Delta A_2 \tag{3.6}$$

where

$\Delta A_1 = A_1(t_{i+1}) - A_1(t_i)$ is a cycle slip in the L1 phase measurement.

$\Delta A_2 = A_2(t_{i+1}) - A_2(t_i)$ is a cycle slip in the L2 phase measurement.

So the indicator allows the determination of a combination of cycle slips in L1 and L2. Theoretically it is possible to have cycle slips in the L1 and L2 which almost compensate for each other. If we assume, however, that the cycle slips in the L2 measurements are independent of the cycle slips in the L1 measurements and that cycle slips are rare events, the probability of a 'double'-cycle slip (simultaneously in L1 and L2) is very small. If, in addition, this method is combined with a screening using the phase rate measurements the separation of combined L1 and L2 cycle slips becomes possible.

If the data frequency is not high enough or the variation in the ionospheric path delay too big to neglect the ionospheric term $\alpha \cdot \frac{d}{dt}\Delta Ion_1$, a simple Kalman filter, introducing this ionospheric term as a state, might be used. This requires a certain regularity in the ionospheric path delay and may be inefficient for data corrupted by 'pathological' ionospheric behavior.

3.2 Screening the raw phase measurements of a stationary site

If the data was taken by a stationnary receiver one may take advantage of this fact to directly screen the between-satellite differences of the raw phase measurements.

Let the term 'observed - computed' be expressed as :

$$\overline{\varphi}_i = \varphi_i - \rho_i^0 \tag{3.7}$$

where:

φ_i is the measured phase value to satellite *i* in [meter].

ρ_i^0 is the approximated pseudo range to the satellite *i*, calculated using the satellite broadcast message (ephemerides and clock correction) and approximate coordinates of the station.

$\overline{\varphi}_i$ is the reduced observation.

This reduced observation may be expressed as :

$$\overline{\varphi}_i = b_i + cl \tag{3.8}$$

where

b_i is a satellite and station specific bias, collecting the ambiguity, orbit errors, errors in the station coordinates etc.

cl is the clock bias of the receiver and is identical for all satellites.

In a Kalman filter approach the satellite bias b_i and its first time derivative may be introduced as the state vector $\vec{x}_i^T = \left[b_i, \dot{b}_i\right]$.

The cycle slip detection is given through the following steps :

1. *The extrapolation of the state vector from time t_{i-1} to time t_i gives the satellite bias for all satellites $\hat{b}_i$*
2. *'Reduction' of the observation by subtracting the approximation : $\overline{\varphi}_i = \varphi_i - \rho_i^0$*
3. *Calculation of the receiver clock cl_i for every satellite i separately : $cl_i = \overline{\varphi}_i - \hat{b}_i$*
4. *Taking the receiver clock bias cl as the median of the individual cl_i : $cl = Median(cl_i)$ (The median is more robust against cycle slips than averaging).*

5. *Search for possible cycle slips :* $|\delta_i| = |\overline{\varphi}_i - \hat{b}_i - cl| = |cl_i - cl| < \varepsilon$ *with a fixed value for* ε *or with a statistically-derived value from the covariance matrix of the filter.*
6. *Correction of the detected cycle slips*
7. *Update of the filters*

Example:

Receiver	TRIMBLE 4000 SST (dual band receiver)
Site	Zurich
Date	25. July. 1991
Time	8:00 - 18:00 UT (10 hours of data)
Elevation mask	10 degrees
Measuring Rate	0.5 Hz

Table 3.1 : System information

SatId	2	3	11	14	15	16	17	19	20	21	23
# L1 obs.	2227	10519	7769	581	4135	1684	9599	2210	8892	7404	7163
# L2 obs.	2222	10428	7760	581	4135	1623	9562	2208	8892	7369	7154

Table 3.2 : Satellite Configuration

The capability of detecting cycle slips depends on the noise $rmsqr(\delta_i)$ of the difference δ_i between the extrapolated value and the measured value of the raw phase : $\delta_i = \overline{\varphi}_i - \hat{b}_i - cl$. The $rmsqr(\delta_i)$ mainly depends on the frequency of the measurement. In the following table the results for the $rmsqr(\delta_i)$ and the maximum absolute value of δ_i are given for 3 different data rates. The 4-sec and 10-sec data set was generated from the original 2-sec data set by decimating the original set.

L1 [cy]	2-SEC DATA SET		4-SEC DATA SET		10-SEC DATA SET	
SatId	*rmsqr* (δ_i)	*Max* ($\|\delta_i\|$)	*rmsqr* (δ_i)	*Max* ($\|\delta_i\|$)	*rmsqr* (δ_i)	*Max* ($\|\delta_i\|$)
2	0.008	0.028	0.013	0.042	0.038	0.178
3	0.018	0.076	0.028	0.109	0.063	0.262
11	0.007	0.036	0.012	0.051	0.032	0.179
14	0.013	0.059	0.021	0.056	0.054	0.164
15	0.010	0.042	0.016	0.060	0.047	0.193
16	0.014	0.056	0.023	0.077	0.067	0.203
17	0.012	0.043	0.020	0.070	0.056	0.231
19	0.009	0.035	0.014	0.048	0.037	0.116
20	0.012	0.044	0.019	0.057	0.049	0.164
21	0.007	0.032	0.012	0.051	0.033	0.222
23	0.010	0.043	0.017	0.062	0.047	0.176
all	**0.010**	**0.076**	**0.017**	**0.109**	**0.048**	**0.262**

Table 3.3 : Residuals in cycles of L1 of screening the L1 phase for different measurement rates.

The detected cycle slips in the L1 phase measurements are :

Epoch	SatId	Timegap	Estimated	cycle slip
3336	16	4.0 sec	883969.031	883969.
3351	16	12.0 sec	33704.048	33704.
11719	2	4.0 sec	-265915.985	-265916.

Table 3.4 : Detected cycle slips in the L1-phase measurements.

It is interesting to note that over 10 hours of data only 3 cycle slips occurred and that all 3 cycle slips occurred after a time gap in the data. This means that if the phase measurement is missing for at least one epoch, a probable loss of lock to the satellite is indicated.

Note that in our processing these cycle slips would not be interpreted as such, because during the initialization of the ambiguities a new ambiguity is automatically set up after a time gap in the data (see section 2.2.2).

Epoch	SatId	Timegap	Estimated	cycle slip
6857	3	36.0 sec	14292106.947	14292107.
6906	3	48.0 sec	311129.989	311130.
6960	3	44.0 sec	-265915.985	-265916.
7031	3	2.0 sec	454092.498	454092.5
7173	3	48.0 sec	912714.911	912715.
7216	3	84.0 sec	277645.998	277646.
7226	3	2.0 sec	64654.500	64654.5
9496	17	2.0 sec	16818883.463	16818883.5
9540	17	88.0 sec	312814.395	312814.5
11734	2	34.0 sec	-200224.117	-200224.

Table 3.5 : Detected cycle slips in the L2 phase measurements.

In the L2 phase half cycle slips were present and detected using the same method as for the L1 cycle slips. This is certainly not the best way to screen the L2 data in the presence of already checked L1 data. By directly looking at the difference between the L2 and L1 measurements one finds the same cycle slips but with an even higher reliability.

A high measurement rate (of the order of 1 Hz) is an absolute requirement for this method. The advantage of the method consists in having complete control of the cycle slips for one station (at the zero-difference level). In the case where the time gap is too big to securely repair the cycle slip, it is still possible to flag the data set to indicate the possible presence of a cycle slip.

It would be interesting to use this method at permanent sites (e.g. at the IGS sites). Measured at a high frequency (for example 1 Hz) the phase data can be reliably checked and then be stored at a lower rate (for example 1/30 Hz). This avoids screening the 30-sec data sets, which is sometimes problematic for long baselines. Screening the data of a reference station of a kinematic survey is another typical application. (a classical 'triple-difference' screening is not possible in such cases).

4 Strategies for the ambiguity resolution 'on the fly'

Coordinate estimation and ambiguity resolution are closely related when processing GPS phase observations. The ambiguities of the double difference phase measurements are integers. The challenge of processing kinematic data consists in securely fixing these integers. For on-line applications this has to be done as rapidly as possible; in off-line applications, however, the entire data set of a kinematic survey may be used for the task.

The approach used here is to build up a normal equation system (NEQ), containing all time-invariant parameters, i.e. the coordinates of the fixed sites and all ambiguities (see chapter 2). The inversion of this NEQ system leads directly to the floating point solution of the ambiguities. This NEQ system also contains all the information necessary to fix the ambiguities.

4.1 Conventional approach : Sigma-dependent rounding

The confidential interval around the real value of the floating point solution is used to decide whether or not an ambiguity may securely be rounded to the nearest integer. As mentioned above the inverted NEQ system gives for every ambiguity a real (floating point) value and its corresponding root mean square error (*rms*). By fixing the confidential level to some reasonable value (2-3 *rms* for example) the following procedure is applied :

If exactly one integer value A_2 lies in the interval $[A_{min}, A_{max}]$, this integer value is selected to be the correct integer valued ambiguity. ($A_{min} = A_{real} - 3 \cdot rms$, $A_{max} = A_{real} + 3 \cdot rms$, A_{real} = real valued estimate of the ambiguity considered).

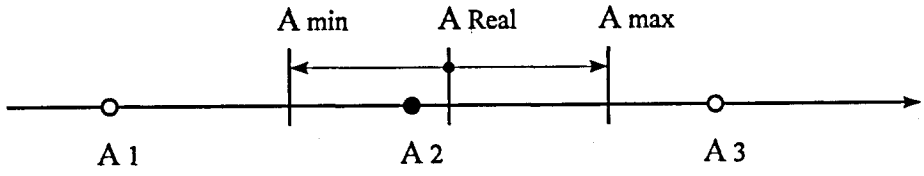

Figure 4.1 : Confidence interval for the fixing of the ambiguities in the conventional approach

This resolution method may be used iteratively. In a first iteration all ambiguities are checked. Those meeting the criterion mentioned are fixed and the NEQ-system is accordingly modified. By introducing these fixed ambiguities as known, the geometry of the NEQ system is stabilized and the values and the *rms* of the remaining, not yet solved, ambiguities are changing. In the next iteration step the remaining ambiguities are checked. This algorithm stops when all ambiguities are resolved or when in the last iteration step no additional ambiguities were resolved. This approach is used e.g. in the Bernese Software [Rothacher, 1993]. It is also possible to fix only a user-defined maximal number of ambiguities per iteration step.

The conventional method has its limitations. It may happen that the *rms* of the individual ambiguity is so large and more than one integers are lying in the confidence interval. For static data over longer periods this hardly happens; this is, however, often the main problem for kinematic data. On the other hand, it may also happen, especially for long baselines, that despite good *rms* values no integer lies in the confidence interval. This is usually due to systematic errors (troposphere, ionosphere, orbit errors).

Additionally, due to the fact that kinematic data is normally taken at a higher frequency (typically 1 Hz), the estimation of the *rms* is often to optimistic, because the assumption of white noise for the measurement errors is not correct. This may easily lead to incorrect fixing of the ambiguities.

Nevertheless for static data this method is robust and works well. For kinematic applications, however, especially in the on-line mode where the resolution of the ambiguities has to be done as quickly as possible, other strategies have to be applied such as search algorithms.

It should be mentioned that recently the method has been generalized to take all possible linear combinations of double-difference ambiguities into account. In this form it is well-suited for long sessions and long baselines [Mervart et al., 1993].

4.2 Searching for combinations

Search strategies are not new in GPS processing and have been widely used in static and kinematic GPS processing (e.g. [Remondi, 1984]). The basic idea of the search strategies is to exploit the fact that all double-difference ambiguities have to be integers. No ambiguity is therefore tested separately if it can be fixed as in the conventional approach. All search algorithms have two key characteristics : the defining of the combinations of interest and the validation of the correct combination.

One commonly-used method consists in defining a search space (derived for example from a code solution) in such a way that with high probability the correct position lies within this volume. From this search space, boundary values (minimum and maximum) for every ambiguities are derived. By taking all possible combinations into account, a list of all ambiguity combinations is created. For the creation of this list [Hatch, 1989, 1990] proposed to restrict to a primary set of 3 double-difference ambiguities. Here a grid of candidates in the 3-dimensional ambiguity space is associated through a linear transformation to a grid of candidates in the 3-dimensional Euclidian space. The remaining ambiguities (secondary set) are then determined from the coordinates associated to the primary set. Validation, is carried out by using the phase measurements from all satellites (primary and secondary sets) and by looking at the resulting *rms* of the phase residuals. More and more candidates are discarded until only one candidate is left.

A different validation method is provided by the so-called ambiguity function, proposed by [Counselman and Gourevitch, 1981] and used e.g. by [Mader, 1992], [Remondi, 1991]. Instead of looking at the *rms* of the phase residuals of the candidates, a function of these residuals is evaluated and maximized. Small values of the resulting ambiguity function allow discarding candidates and again the search is successful if only one candidate is left over. It

has been shown that in the static mode the ambiguity function is not affected by cycle slips, because the position and not the ambiguities are validated. In the kinematic mode, however, this advantage is (at least partially) lost.

A different approach, used by [Euler, 1992], consists of using the information of the normal equation system of the floating point ambiguities to confine the search space for the ambiguities and to perform the search implicitly on the NEQ system without the necessity to actually create a list of possible candidates. Validation is performed by comparing the best candidate to the second best [Euler et al, 1990]. If the ratio of the corresponding *rms* is significant, one concludes that the best candidate set is also the correct one. The use of L1 and L2 phase measurements introduced as separate measurements (no linear combination) in a common adjustment dramatically increases the power of discrimination of the possible candidate even for short observation time spans [Frei 1992].

The approach presented here is based on a strategy similar to [Frei, 1992] for using the information of the NEQ system to retrieve integer ambiguities.

4.2.1 Concept of the search strategy used

Let us assume that we have at our disposition the NEQ system containing the time independent parameters (see section 2.2.5). If stationary sites are still present, they are eliminated now. A resulting NEQ system, containing only ambiguities, is left.

The first step consists of calculating the ***floating point solution*** , where we start from the NEQ system containing ambiguities only :

$$N\vec{x} = \vec{n} \qquad \text{and} \qquad \vec{x} = N^{-1}\vec{n} \tag{4.1}$$

The floating point solution of the ambiguities may then be written as :

$$\vec{A}_{fl} = \vec{A}_0 + \vec{x} \tag{4.2}$$

and the normalized root mean square error (*rms*) a posteriori σ_{fl} of the floating point solution is given by :

$$\sigma_{fl} = \sqrt{\frac{(\vec{v}_{fl}{}^T P v_{fl})}{n_{obs} - u_{fl}}} = \sqrt{\frac{(\vec{v}_{fl}{}^T P v_{fl})}{f_{fl}}} \tag{4.3}$$

(The calculation of σ_{fl} can be performed without having to explicitly compute the residuals)

with

N	normal equation matrix
$\vec{A}_0$	initial values of the ambiguities

$\vec{A}_{fl}$	floating point solution of the ambiguities
$\vec{v}_{fl}$	residuals of the least square adjustment
$\boldsymbol{P}$	weighting matrix
$f_{fl} = n_{obs} - u_{fl}$	degree of freedom = number of measurements - number of unknowns

An ***integer combination*** $\vec{A}$ for all ambiguities is now characterized by :

$$\vec{A} = \vec{A}_{fl} + \Delta\vec{A} \tag{4.4}$$

and by the corresponding normalized root mean square error σ :

$$\sigma = \sqrt{\frac{\vec{v}^T \boldsymbol{P} v}{f_{Fix}}} \qquad \text{with} \qquad f_{Fix} = f_{fl} + n_{Amb} \tag{4.5}$$

where n_{Amb} is the number of ambiguities.

The expression $\vec{v}^T \boldsymbol{P} v$ may be written in the form :

$$\vec{v}^T \boldsymbol{P} v = (\vec{v}^T \boldsymbol{P} v)_{fl} + \Delta(\vec{v}^T \boldsymbol{P} v) \tag{4.6}$$

Note that $\Delta(\vec{v}^T \boldsymbol{P} v)$ has to be positive because the floating point solution is the result of a least square adjustment, which minimizes $\vec{v}^T \boldsymbol{P} v$. It is easy to verify that the increment $\Delta(\vec{v}^T \boldsymbol{P} v)$ is given by the following quadratic form :

$$\Delta(\vec{v}^T \boldsymbol{P} \vec{v}) = \Delta\vec{A}^T \boldsymbol{N} \Delta\vec{A} \tag{4.7}$$

The goal of our search algorithm is to find the solution minimizing $\Delta(\vec{v}^T \boldsymbol{P} \vec{v})$. This procedure, from a certain point of view, still corresponds to a least square adjustment with the additional condition that the unknown parameters (the ambiguities) must be integer numbers.

In a more general way we want to generate a list of the n best sets of integer combinations, where n is a user-defined input parameter. In order to be able to compare the best to the second best solution and to decide whether the discrimination is sufficient for a successful fixing of the ambiguities, a minimal number of 2 sets is necessary ($n = 2$).

$$\Delta(\vec{v}^T \boldsymbol{P} \vec{v}) = min \tag{4.8}$$

By using the Cholesky decomposition the NEQ matrix N may be expressed by :

$$\boldsymbol{N} = \boldsymbol{R}^T \boldsymbol{R} \qquad \text{where} \qquad \boldsymbol{R} \text{ is a lower triangular matrix} \tag{4.9}$$

By introducing expression (4.9) in equation (4.7) one obtains :

$$\begin{aligned}\Delta(\vec{v}^T \boldsymbol{P} \vec{v}) &= \Delta\vec{A}^T \boldsymbol{R}^T \boldsymbol{R} \Delta\vec{A} \\ &= (\boldsymbol{R}\Delta\vec{A})^T (\boldsymbol{R}\Delta\vec{A}) \\ &= \left\| \boldsymbol{R}\Delta\vec{A} \right\|^2\end{aligned} \tag{4.10}$$

This means that $\Delta(\vec{v}^T \boldsymbol{P} \vec{v})$ can be written as a sum of quadratic terms :

$$\Delta(\vec{v}^T \boldsymbol{P} \vec{v}) = \sum_{i=1}^{n} (\sum_{j=1}^{i} r_{ij}\, \delta a_j)^2 = \sum_{i=1}^{n} (\Delta_i)^2 \tag{4.11}$$

where n corresponds to the number of ambiguities and the abbreviation Δ_i are defined as :

$$\Delta_i = (\sum_{j=1}^{n} r_{ij}\, \delta a_j) \tag{4.12}$$

By introducing a second abbreviation as :

$$\Sigma_i = \sum_{j=1}^{i} (\Delta_j)^2 \tag{4.13}$$

the following inequalities hold :

$$\Sigma_1 < \Sigma_2 < \ \ldots\ \Sigma_i\ \ldots < \Sigma_{n-1} < \Sigma_n = \Delta(\vec{v}^T P \vec{v}) \tag{4.14}$$

since

$$\Sigma_i = \Sigma_{i-1} + (\Delta_i)^2 \tag{4.15}$$

The value for Σ_i thus only depends on the integer values for the ambiguities $[A_1, A_2, \ldots, A_i] = [A_1, A_i]$. If Σ_i now already exceeds a certain limit value, then no further combinations for $[A_{i+1}, \ldots, A_{n-1}, A_n] = [A_{i+1}, A_n]$ need be examined, since all combinations including the given combination for $[A_1, A_i]$ must be rejected. With the strategy used this limit value, as will be shown, can be continuously decreased during the search itself and need not to be put to some pre-defined or user-specified constant value.

4.2.2 Details of the search algorithms used

After this more general remarks, the search algorithm is presented below in more detail. The following different key steps are presented first :

i) Initialization level i

ii) Variation at level i

iii) Including a combination in the list and updating the limit value

The overall procedure, based on these key steps, is summed up in:

iv) General procedure

A flow-chart of the search algorithm is drawn in figure 4.4.

i) Initialization of level i

Let us assume that we are at search level i-1, which means that the integer values for the ambiguities $[A_1, A_{i-1}]$ are known, and consequently Σ_{i-1} as well. Let us assume furthermore that Σ_{i-1} is still smaller than some limit value, so that the combination $[A_1, A_{i-1}]$ is at the moment still a valid set of integer ambiguities.

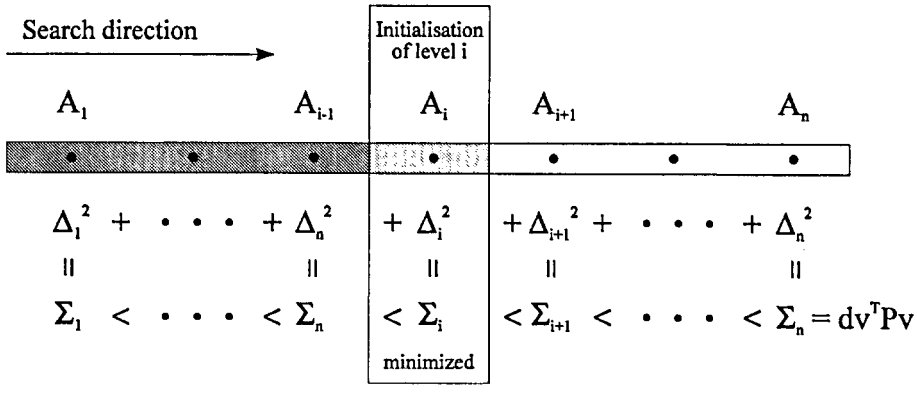

Figure 4.2 : Initialization of level i for a given combination $[A_1, A_{i-1}]$.

We now have to initialize level *i*, by assigning an integer value A_i^0 to the real estimate A_i We choose A_i^0 in such a way, that :

$$\Delta_i^2 = \min \tag{4.16}$$

This leads to :

$$\Delta_i = (\sum_{j=1}^{i-1} r_{ij}\delta a_j) + r_{ii}\delta a_i = 0 \tag{4.17}$$

and

$$\delta a_i^{\min} = -\frac{1}{r_{ii}}(\sum_{j=1}^{i-1} r_{ij}\delta a_j) \tag{4.18}$$

We define the real value $A_i^{\min}$ and the associated integer value A_i^0 as :

$$A_i^{\min} = A_{i\,fl} + \delta a_i^{\min} \qquad \text{and} \qquad A_i^0 = \textit{nearest integer}\ (A_i^{\min}) \tag{4.19}$$

This means that for a given combination $[A_1, A_{i-1}]$ the chosen integer A_i^0 minimizes Δ_i^2 and thus also Σ_i. Note that the real value $A_i^{\min}$ corresponds to the floating point solution for A_i on the assumption that the integer values for ambiguities $[A_1, A_{i-1}]$ are known.

ii) Variation at level i

The variation of A_i around A_i^0 is performed in such a way that :

$$(\Delta_i^0)^2 < (\Delta_i^1)^2 < (\Delta_i^2)^2 < (\Delta_i^3)^2 \ldots\ldots \tag{4.20a}$$

This is equivalent to :

$$\Sigma_i^0 < \Sigma_i^1 < \Sigma_i^2 < \Sigma_i^3 \ldots\ldots \tag{4.20b}$$

This variation is illustrated by figure 4.3. and is denoted by (Next A_i) in the flow-chart (figure 4.4.)

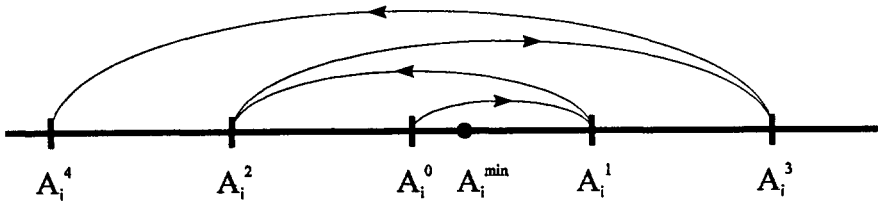

Figure 4.3 : Variation of A_i around A_i^0

Therefore, if $\Sigma_i^j > limit$ the variation in level i can be stopped and the algorithm returns to level i *-1.*

iii) Including a combination in the list and updating the limit value

If the search level n is reached, an interesting combination $[A_1, A_n]$ with an associated $\Delta(\vec{v}^T \boldsymbol{P} \vec{v}) = \Sigma_n < limit$ is found. This combination is put into a list sorted accordingly to increasing $\Delta(\vec{v}^T \boldsymbol{P} \vec{v})$. The list contains a pre-defined number (*maxvariant*) of combinations. The value for the *limit* is now updated and set equal to the value of $\Delta(\vec{v}^T \boldsymbol{P} \vec{v})$ of the last combination in the list, because this value is the threshold for any further combination to enter the list. The combination may again drop out, if better candidates enter the list.

iv) General procedure

Starting at level $i = 0$ we increment and initialize a new level ($i = i + 1$) until level $i = n$ is reached or ($\Sigma_i > limit$)

if level $i = n$ we accept the integer set update our list and the value of *limit*, we vary A_1

if Σ_i is to large we decrement i ($i = i - 1$) and vary A_i.

The procedure stops when we again reach level $i = 0$.

In principle, the only parameter which has to be specified is the number of elements in the list (*maxvariant*) containing the combinations. The algorithm is thus just told to look for the *maxvariant* best integer combinations with no other additional restrictions or information. This only works because the NEQ system not only contains information from the phase but also from the code measurements, which implicitly limits the ambiguity search area.

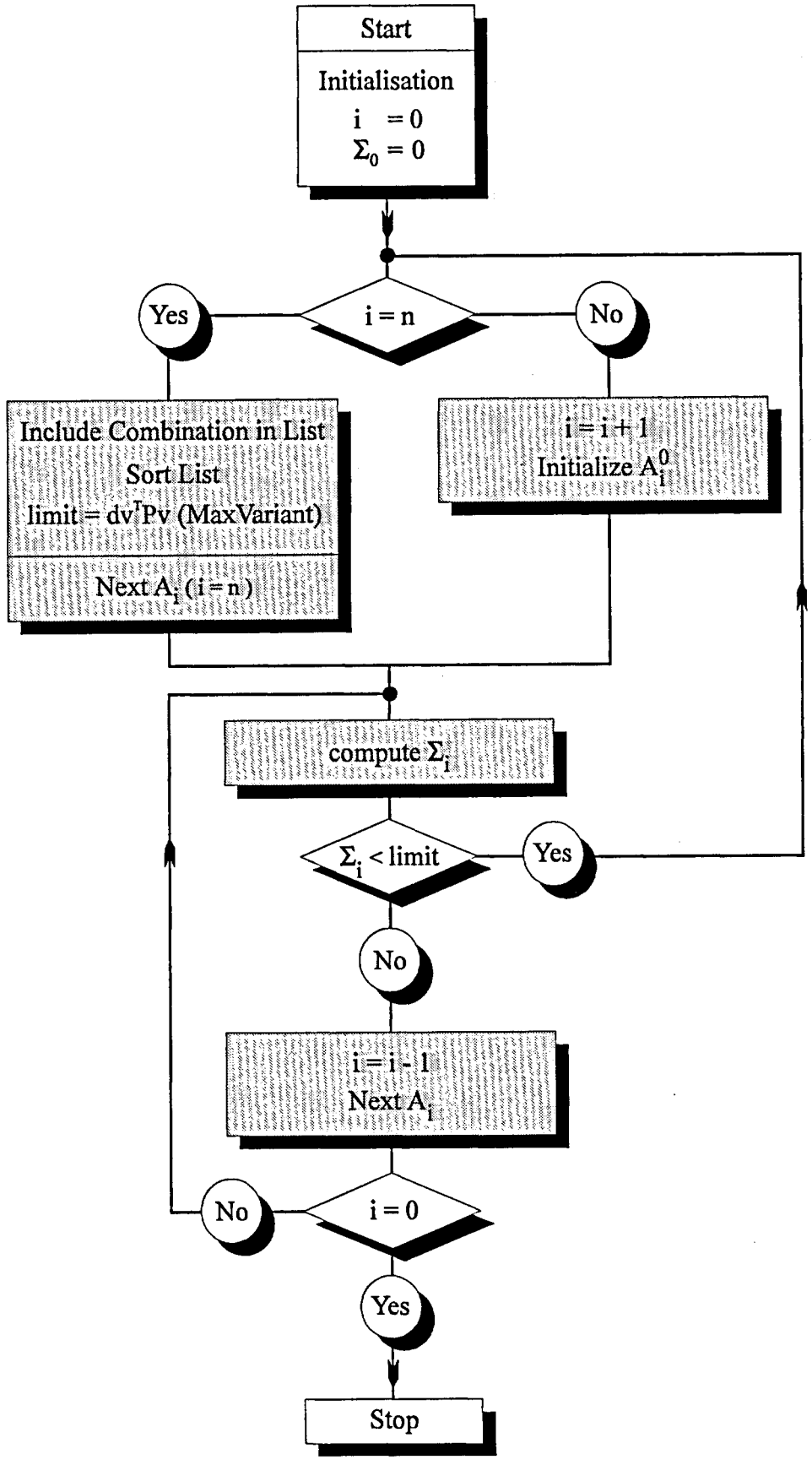

Figure 4.4 : Flow-chart for the core of the search algorithm.

4.2.3 Compatibility of the integer solutions with the floating point solution

The covariance matrix Q_{xx} of the floating point solution $\vec{A}_{fl}$ is given by :

$$Q_{xx} = \sigma_{fl}^2 N^{-1} \tag{4.21}$$

and defines (see for example [Pelzer, 1985]) a n-dimensional hyper-ellipsoid. The probability p that the floating point solution $\vec{A}_{fl}$ and an integer solution $\vec{A}_i$ are compatible is represented by the expression:

$$p\left\{(\vec{A}_i - \vec{A}_{fl})^T Q_{xx}^{-1} (\vec{A}_i - \vec{A}_{fl}) < \chi^2_{u,1-\alpha}\right\} = 1-\alpha \tag{4.22}$$

where

$\chi^2_{u,1-\alpha}$	the quantile based on the chi-square probability density function
u	degree of freedom, corresponding to the number of unknowns (ambiguities).
α	error probability. (1-α corresponds to the confidence level)

By denoting the test variable by t_1, an upper limit for t_1 may be computed using the χ^2_u-density function for a given confidence level 1-α.

$$t_1 = (\vec{A}_i - \vec{A}_{fl})^T Q_{xx}^{-1} (\vec{A}_i - \vec{A}_{fl}) \quad \text{and} \quad t_1 < \chi^2_{u,1-\alpha} \tag{4.23}$$

By denoting $\Delta\vec{A}_i = A_i - \vec{A}_{fl}$, introducing (4.21) in (4.23) and using (4.7) the test variable may be written as :

$$t_1 = \frac{1}{\sigma_0^2}(\Delta\vec{A}_i^T N \Delta\vec{A}_i) = \frac{1}{\sigma_0^2}\Delta(\vec{v}^T \boldsymbol{P} \vec{v}) \tag{4.24}$$

This leads to the following relation :

$$\Delta(\vec{v}^T \boldsymbol{P} \vec{v}) < \sigma_0^2 \ \chi^2_{u,1-\alpha} = limit \tag{4.25}$$

Our criterion for the search $\Delta(\vec{v}^T \boldsymbol{P} \vec{v}) = min$ of the integer solutions is identical to the criterion of looking for the set of integers with the highest probability density to correspond to the floating point solution.

Note that we do not make use of *limit* during the search; the initial value for the limit for $\Delta(\vec{v}^T \boldsymbol{P} \vec{v})$ is formally put to '∞' and during the search subsequently reduced. The value of

t_1 is an indicator for the agreement between the floating point solution and the integer solutions.

The probability statement (4.22) however is based on the hypothesis of uncorrelated normally-distributed measurements without systematic errors in the mathematical model of the adjustment. With real data this assumption almost never holds. In particular, measurements taken at a high sampling rate (1 Hz) are highly correlated in time. Moreover, ionospheric refraction will cause biases. This often leads to an overestimation of the quality of the floating point solution and to a deterioration of the t_1-values.

4.2.4 Speeding up the search algorithm

As the algorithm is primarily designed for off-line applications the processing time for finding all integer combinations of interest is not as critical as in the case of on-line applications. Nevertheless an increase in the efficiency of the algorithm can be obtained by various means:

In the NEQ system the L2 ambiguities may be replaced by the linear wide lane combinations (L5 ambiguities), which correspond to the difference between the L2 and L1 ambiguities. Instead of searching for the L1/L2 ambiguities, we search for the L1/L5 ambiguities. This linear transformation does not influence the result of the search and the original L2 ambiguities may be restored after the search.

A rearrangement of the ambiguities in the NEQ system proved to be very effective: Before entering the search algorithm the floating point solution is computed by inverting the NEQ system (see equation 4.1). During inversion a pivot strategy, taking always the largest element of the not yet inverted elements of the diagonal defines a classification of the ambiguities. This hierarchy is used to rearrange the ambiguities in the NEQ system. In case of a search on the L1/L2 ambiguities this automatically leads to an order where the ambiguities pertaining to the same satellite occupy subsequent places in the re-arranged NEQ system (L1 and L2 ambiguities). In the case of a search on the L1/L5 ambiguities, the L5 ambiguities are normally occupying the 'best' places in the re-arranged NEQ system. This rearrangement of the ambiguities does not influence the result.

4.2.5 Compatibility factor CF and discrimination factor DF

Let us assume that from the result of the ambiguity search we have the following three *rms a posteriori of the unit weight* :

σ_{fl} rms of unit weight of the floating point solution.

σ_1 rms of unit weight of the solution with the best integer ambiguity set.

σ_2 rms of unit weight of the solution with the second best integer ambiguity set.

The following two factors, which allow testing as to whether the best integer solution may be accepted or not as the correct one, are introduced :

i) Compatibility factor *CF* : $CF = \sigma_1/\sigma_{fl} < limit_0$ (4.26)
(σ_1 should not be significantly larger than σ_{fl})

ii) Discrimination factor *DF* : $DF = \sigma_2/\sigma_1 > limit_1$ (4.27)
(σ_2 should be significant larger than σ_1)

In the 'Fast Ambiguity Resolution Algorithm' (FARA) [Frei, 1991] the identical approach is proposed, where the values for $limit_0$ and $limit_1$ are derived using the tool of statistical hypothesis testing. The similar criteria may be found in [Euler, Schaffrin, 1990].

The corresponding probabilities *p* are :

i) $$p\left\{CF^2 = \left(\sigma_1/\sigma_{fl}\right)^2 < F_{f_{Fix},\, f_{fl},\, 1-\alpha}\right\} = 1-\alpha \tag{4.28}$$

and

ii) $$p\left\{DF^2 = \left(\sigma_2/\sigma_1\right)^2 < F_{f_{Fix},\, f_{Fix},\, 1-\alpha}\right\} = 1-\alpha \tag{4.29}$$

where

$F_{f_1,\, f_2,\, 1-\alpha}$ quantile based on Fisher's probability density function with f_1 and f_2 degrees of freedom on the confidence level $1-\alpha$

f_{Fix} degree of freedom of the integer fixed solution

f_{fl} degree of freedom of the floating point solution

α error probability

and for a given confidence level $1-\alpha$ the values for $limit_0$ and $limit_1$ can be written as:

i) $$limit_0 = \sqrt{F_{f_{Fix},\, f_{fl},\, 1-\alpha}} \tag{4.30}$$

and

ii) $$limit_1 = \sqrt{F_{f_{Fix},\, f_{Fix},\, 1-\alpha}} \tag{4.31}$$

In practice the increasing degree of freedom will let the values for $limit_0$ and $limit_1$ tend to 1. (For degrees of freedom approaching '∞' the estimates for $\sigma_{fl}, \sigma_1, \sigma_2$ are virtually error-free and hence all differences are automatically significant). In practice a reasonable upper value for $limit_0$ and lower value for $limit_1$ are used.

Possible reasons for failure of the compatibility test (resulting $CF > limit_0$)

Since no boundaries for the search radius are used, if the correct solution is the best solution, it will automatically be found. A failure of the compatibility test is therefore only possible if undetected errors are still in the solution (e.g. ionosphere, undetected cycle slips) or if the chosen a priori value of the code weight does not correspond to the actual quality of the code measurements. An overweight of the code leads to a failure of the compatibility test and normally also to failure of the discrimination test.

Possible reasons for failure of the discrimination test (resulting $DF < limit_1$)

A failure simply means that there are more than one acceptable integer solutions. The best solution can not be considered as the correct one because the discrimination does not allow the exclusion of other combinations. This second criterion (a good value of the *DF*) is more stringent but also more critical.

4.3 Theoretical considerations

Let us study the discrimination potential of the ambiguity search strategy .

Starting with equation (4.7) and denoting the correct integer combination as $\vec{A}_0$, the $\Delta(\vec{v}^T P \vec{v})_i$ for any other integer combination $\vec{A}_i$ can be written as :

$$\begin{aligned}\Delta(\vec{v}^T P \vec{v})_i &= (\vec{A}_i - \vec{A}_{fl})^T N (\vec{A}_i - \vec{A}_{fl}) \\ &= ((\vec{A}_i - \vec{A}_0) + (\vec{A}_0 - \vec{A}_{fl}))^T N ((\vec{A}_i - \vec{A}_0) + (\vec{A}_0 - \vec{A}_{fl})) \\ &= (\vec{A}_0 - \vec{A}_{fl})^T N (\vec{A}_0 - \vec{A}_{fl}) + (\vec{A}_i - \vec{A}_0)^T N (\vec{A}_i - \vec{A}_0) + 2(\vec{A}_i - \vec{A}_0)^T N (\vec{A}_0 - \vec{A}_{fl})\end{aligned} \tag{4.32}$$

and the corresponding $(\vec{v}^T \boldsymbol{P} \vec{v})_i$:

$$\begin{aligned}(\vec{v}^T \boldsymbol{P} \vec{v})_i &= (\vec{v}^T \boldsymbol{P} \vec{v})_{fl} + \Delta(\vec{v}^T \boldsymbol{P} \vec{v})_i \\ &= (\vec{v}^T \boldsymbol{P} \vec{v})_{fl} + (\vec{A}_0 - \vec{A}_{fl})^T \boldsymbol{N} (\vec{A}_0 - \vec{A}_{fl}) \\ &\qquad + (\vec{A}_i - \vec{A}_0)^T \boldsymbol{N} (\vec{A}_i - \vec{A}_0) + 2(\vec{A}_i - \vec{A}_0)^T \boldsymbol{N} (\vec{A}_0 - \vec{A}_{fl}) \\ &= (\vec{v}^T \boldsymbol{P} \vec{v})_0 + (\vec{A}_i - \vec{A}_0)^T \boldsymbol{N} (\vec{A}_i - \vec{A}_0) + 2(\vec{A}_i - \vec{A}_0)^T \boldsymbol{N} (\vec{A}_0 - \vec{A}_{fl})\end{aligned} \tag{4.33}$$

The expectation value of $(\vec{v}^T \boldsymbol{P} \vec{v})_i$ becomes :

$$E\left\{(\vec{v}^T \boldsymbol{P} \vec{v})_i\right\} = E\left\{(\vec{v}^T \boldsymbol{P} \vec{v})_0\right\} + (\vec{A}_i - \vec{A}_0)^T \boldsymbol{N} (\vec{A}_i - \vec{A}_0) + 2(\vec{A}_i - \vec{A}_0)^T \boldsymbol{N} E\left\{(\vec{A}_0 - \vec{A}_{fl})\right\} \tag{4.34}$$

Taking into account that

$$E\left\{(\vec{A}_0 - \vec{A}_{fl})\right\} = 0 \tag{4.35}$$

and dividing equ (4.34) by the degree of freedom $f = n_{obs} - u_{Fix}$ we obtain :

$$E\left\{\frac{(\vec{v}^T \boldsymbol{P} \vec{v})_i}{f}\right\} = E\left\{\frac{(\vec{v}^T \boldsymbol{P} \vec{v})_0}{f}\right\} + \frac{1}{f}(\vec{A}_i - \vec{A}_0)^T \boldsymbol{N} (\vec{A}_i - \vec{A}_0) \tag{4.36}$$

and finally

$$\sigma_i^2 = \sigma_0^2 + \frac{1}{f}(\vec{A}_i - \vec{A}_0)^T \boldsymbol{N} (\vec{A}_i - \vec{A}_0) \tag{4.37}$$

where $\vec{A}_i - \vec{A}_0$ are integer values.

The following theoretical discrimination factor *DF* can now be defined :

$$DF = \frac{\sigma_1}{\sigma_0} = \sqrt{\frac{\sigma_0^2 + \frac{1}{f}(\vec{A}_1 - \vec{A}_0)^T \boldsymbol{N} (\vec{A}_1 - \vec{A}_0)}{\sigma_0^2}} = \sqrt{\frac{\sigma_0^2 + \Delta\sigma_1^2}{\sigma_0^2}} \tag{4.38}$$

DF represents the ratio of the *rms* of the best incorrect integer combination with respect to the correct combination and primarily decides on the success of the search.

Note that *DF* may be computed without actual measurements.

The normal equation matrix *N* only depends on :

- the satellite configuration.

- the *a priori rms* of the measurements (especially the resulting code weight).
- the integration time and the measuring frequency.
- the type of measurements (code , L1 phase, L2 phase).

For a given normal equation matrix N, the search algorithm as described in (chapter 4.2) is now used to find the theoretically best incorrect integer combination, which allows the computation of :

$$\Delta\sigma_1^2 = \frac{1}{f}(\vec{A}_1 - \vec{A}_0)^T N(\vec{A}_1 - \vec{A}_0) \tag{4.39}$$

The corresponding interesting discrimination factor DF is obtained from equation (4.38).

If we put the weight of a phase measurement (independent of L1 and L2) to 1, σ_0 corresponds to the *a priori rms* of a phase measurement in meters.

For the following investigation a value of $\sigma_0 = 5\ mm$ was used. Note that $\Delta\sigma_1^2$ is independent of the value of $\hat{\sigma}_0^2$ but that the discrimination factor DF depends on $\hat{\sigma}_0^2$ and deteriorates with increasing noise.

Below different characteristics of the ambiguity resolution are studied. Because the power of discrimination is significantly different for single or respectively dual frequency measurements, these two cases are dealt with separately.

All presented investigations are based on the satellite configuration given in figures (4.5) and (4.6).

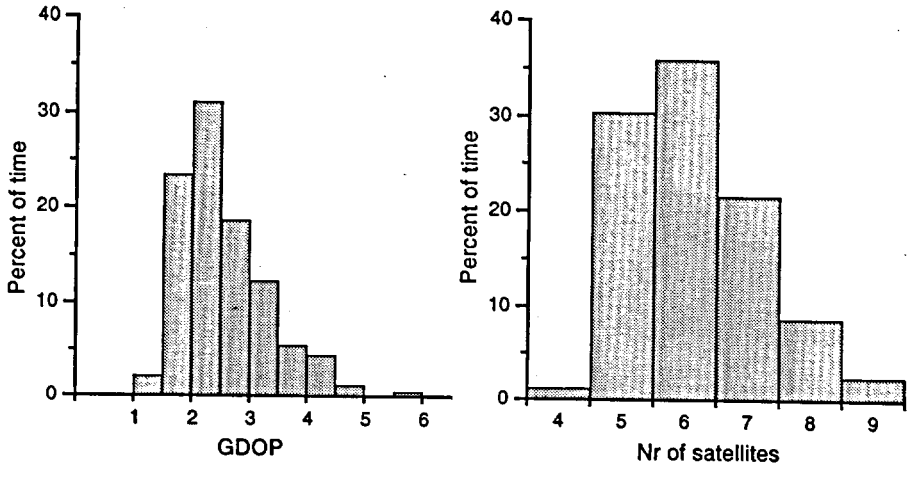

Figure. 4.5 : Histogram of the number of satellites and the GDOP in percent of time over the day (for station Zimmerwald).

Station : ***Zimmerwald*** minimal elevation 15°

latitude : 46° 52' N

longitude : 7° 28' E

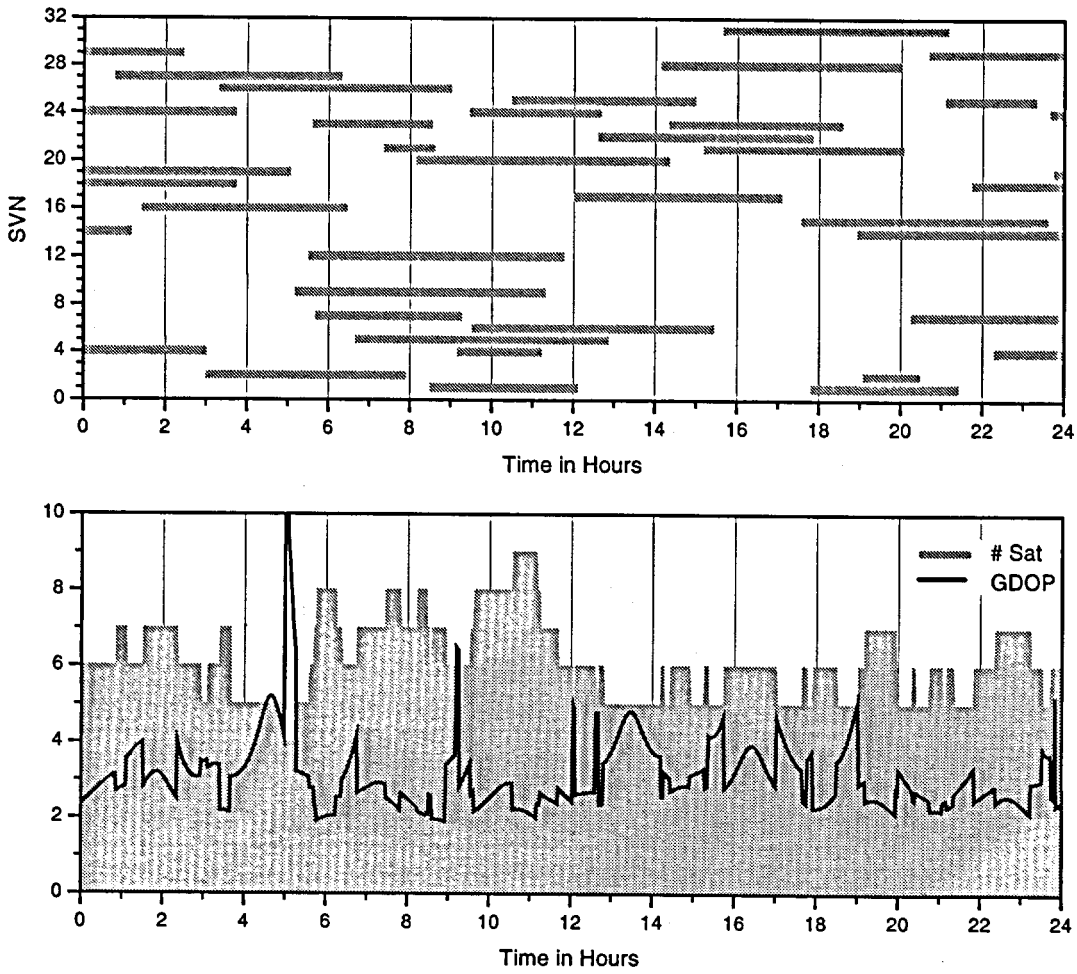

Figure 4.6 : Satellite configuration from 19. may 1994 for Zimmerwald.

4.3.1 Single frequency 'scenario'

We assume that continuos L1 measurements over 30 minutes are available. How does the discrimination factor *DF* behave as a function of time if we gradually add more and more measurement epochs to the NEQ system ?

For the computation of the a priori *DF* the following assumptions are made:

- 2-sec-data (measuring frequency = ½ Hz)
- phase quality $\sigma_{Phase} = 5\ mm$
- code quality

version 1	$\sigma_{Code} = 0.5\ m$	$weight_{Code}/weight_{Phase} = 10^{-4}$
version 2	$\sigma_{Code} = 5\ m$	$weight_{Code}/weight_{Phase} = 10^{-6}$

- *static mode* versus *kinematic mode*

Only 4 different sequences corresponding to different satellite constellations were analyzed and are presented in figure 4.7. The weakest constellation corresponds to Version (a) : 4-5 satellites, the best constellation to Version (d) : 9 satellites.

For every version (a) to (d) 4 different scenarios were computed :

- static mode $weight_{Code}/weight_{Phase} = 10^{-4}$
- static mode $weight_{Code}/weight_{Phase} = 10^{-6}$
- kinematic mode $weight_{Code}/weight_{Phase} = 10^{-4}$
- kinematic mode $weight_{Code}/weight_{Phase} = 10^{-6}$

These results are based on a special satellite constellation. It is therefore not possible to give a general rule here. Nevertheless the important characteristics of the behavior of the *DF* clearly show up.

In the static mode the change in geometry, due to the motion of the satellites, allows for reliable discrimination after some minutes, naturally depending on the quality of the constellation (compare [Frei, 1991, chapter V.3]). This result is not surprising and not new, since all conventional methods for solving the ambiguities in the static mode (see also chapter 4.1) are based on this feature.

In the kinematic mode, however, the discrimination power is much lower. As we have to solve for a new coordinate set every epoch, the ambiguities are much more sensitive to the number of satellites than in the static mode. With only 4-5 satellites the *DF* remains below 1.5 even after 30 minutes. Only with a constellation of 9 satellites, the *DF* for the static and kinematic mode are comparable.

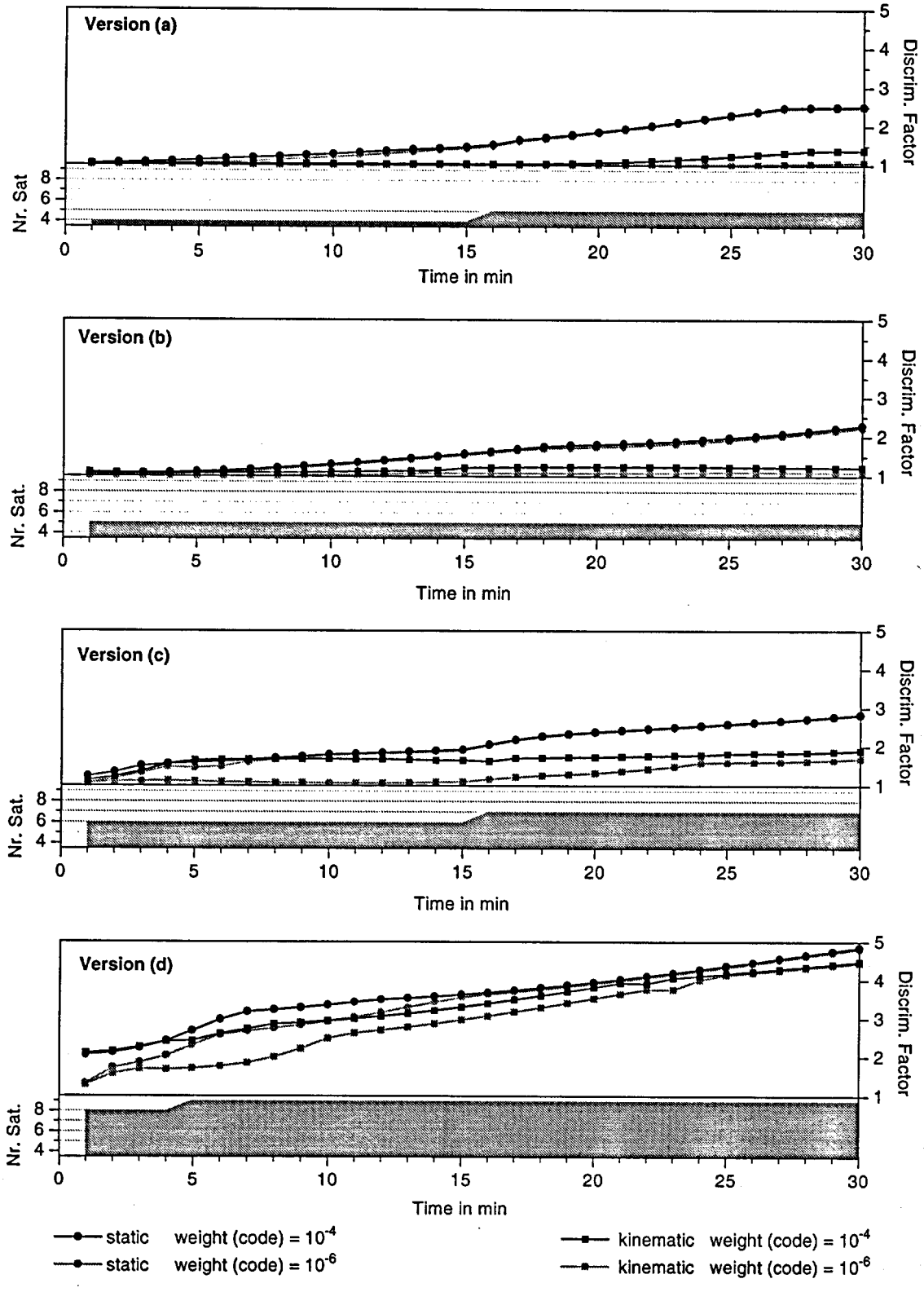

Figure. 4.7 : Theoretical discrimination factor (DF) over 30 minutes for different satellite constellations

The quality of the code measurements is essential in the kinematic mode; it is irrelevant in the static mode. In the static mode, the differences are often so small that in figure. 4.7 the corresponding curves cannot be distinguished.

We conclude that in order to resolve the ambiguities in the kinematic mode with single frequency measurements only, long observation periods (> 10 minutes) without major interruptions in the phase measurements and with good code measurements are required. A large number of satellites (>8) must be involved.

4.3.2 Dual frequency 'scenario'

The geometry is not substantially improved by the additional L2 phase measurements. Also the quality of the floating point solution is similar as in the single frequency mode. From the point of view of the discrimination of the ambiguity search algorithms the L2 measurements improve the performance in a significant way (see also [Frei, 1991]). The key to discriminating the correct solution from all other potential candidates lies in the fact, that the wavelength of the L1 and L2 phase are different but the integer values of the L2 phase ambiguities must correspond to the same coordinates as the integer L1 phase ambiguities.

For the following theoretical investigation each single epoch is treated separately. No change of the geometry in the satellite constellation helps the discrimination. This also means that there is no difference between the static and the kinematic mode.

The discrimination factor *DF* as given by equation (4.38) is computed for every single epoch. Parameters, influencing on the resulting value of the *DF* are :

- half- or full-cycle integer in the L2-phase ambiguities
- the *a priori rms* of the measurements (code and phase)

An important characteristic is given by the behavior of different receivers under anti-spoofing (AS). Some receivers reconstruct the L2 phase by squaring techniques. In this case the resulting unit of the L2 ambiguities are half cycles. Other receivers succeed in reconstructing the full cycle information.

Therefore two different scenarios are considered here :

- L1 full cycles / L2 full cycles
- L1 full cycles / L2 half cycles

For the quality of the measurements the following a priori values were adopted :

- phase quality $\sigma_{Phase} = 5\ mm$
- code quality

version 1 : $\sigma_{Code} = 0.5\ m$ $weight_{Code}/weight_{Phase} = 10^{-4}$
version 2 : $\sigma_{Code} = 1.5\ m$ $weight_{Code}/weight_{Phase} = 10^{-5}$
version 3 : $\sigma_{Code} = 5\ m$ $weight_{Code}/weight_{Phase} = 10^{-6}$

For all 6 resulting versions the computation of the instantaneous theoretical discrimination factor *DF* over a whole day, and based on the satellite configuration as shown in figure 4.5., was carried out with a time spacing of 1 minute. The results are given in figure 4.8.

For a better interpretation of the result, the mean values and the standard deviations of the *DF* as a function of the number of satellites are listed in table. 4.2 and drawn in figure 4.9.

Nr. of DF	#sat = 4	#sat = 5	#sat = 6	#sat = 7	#sat = 8	#sat = 9
(total = 1439)	17	441	511	309	126	35

Table 4.1 : Number of single DF used for the computation of the mean value.

L2-Half Cycle	#sat = 4	#sat = 5	#sat = 6	#sat = 7	#sat = 8	#sat = 9
$W_{co}/W_{ph} = 10^{-6}$	1.02 (0.00)	1.12 (0.03)	1.28 (0.06)	1.49 (0.08)	1.72 (0.10)	1.94 (0.11)
$W_{co}/W_{ph} = 10^{-5}$	1.09 (0.00)	1.26 (0.05)	1.50 (0.10)	1.77 (0.12)	2.07 (0.14)	2.30 (0.16)
$W_{co}/W_{ph} = 10^{-4}$	1.23 (0.00)	1.50 (0.14)	1.86 (0.17)	2.19 (0.20)	2.55 (0.13)	2.68 (0.19)
L2-Full Cycle	**#sat = 4**	**#sat = 5**	**#sat = 6**	**#sat = 7**	**#sat = 8**	**#sat = 9**
$W_{co}/W_{ph} = 10^{-6}$	1.02 (0.00)	1.19 (0.07)	1.51 (0.09)	1.84 (0.13)	2.24 (0.14)	2.62 (0.13)
$W_{co}/W_{ph} = 10^{-5}$	1.09 (0.00)	1.48 (0.13)	1.89 (0.16)	2.28 (0.19)	2.75 (0.19)	3.12 (0.23)
$W_{co}/W_{ph} = 10^{-4}$	1.64 (0.00)	2.01 (0.14)	2.50 (0.22)	2.96 (0.27)	3.42 (0.25)	3.81 (0.21)

Table 4.2 : Mean values of the instantaneous discrimination factor DF as a function of the number of satellites. (In brackets the standard deviations of a single DF).

Theoretically it is possible to fix the ambiguities with measurements from one single epoch. If we put, for example, the threshold value for the *DF* to 1.8, a constellation with 6 satellites would be sufficient with a phase quality of 5 mm, a code quality of 1.5 m and full cycles in L2. (Results of an instantaneous ambiguity fixing within one epoch of measurements with real data is given in chapter 5).

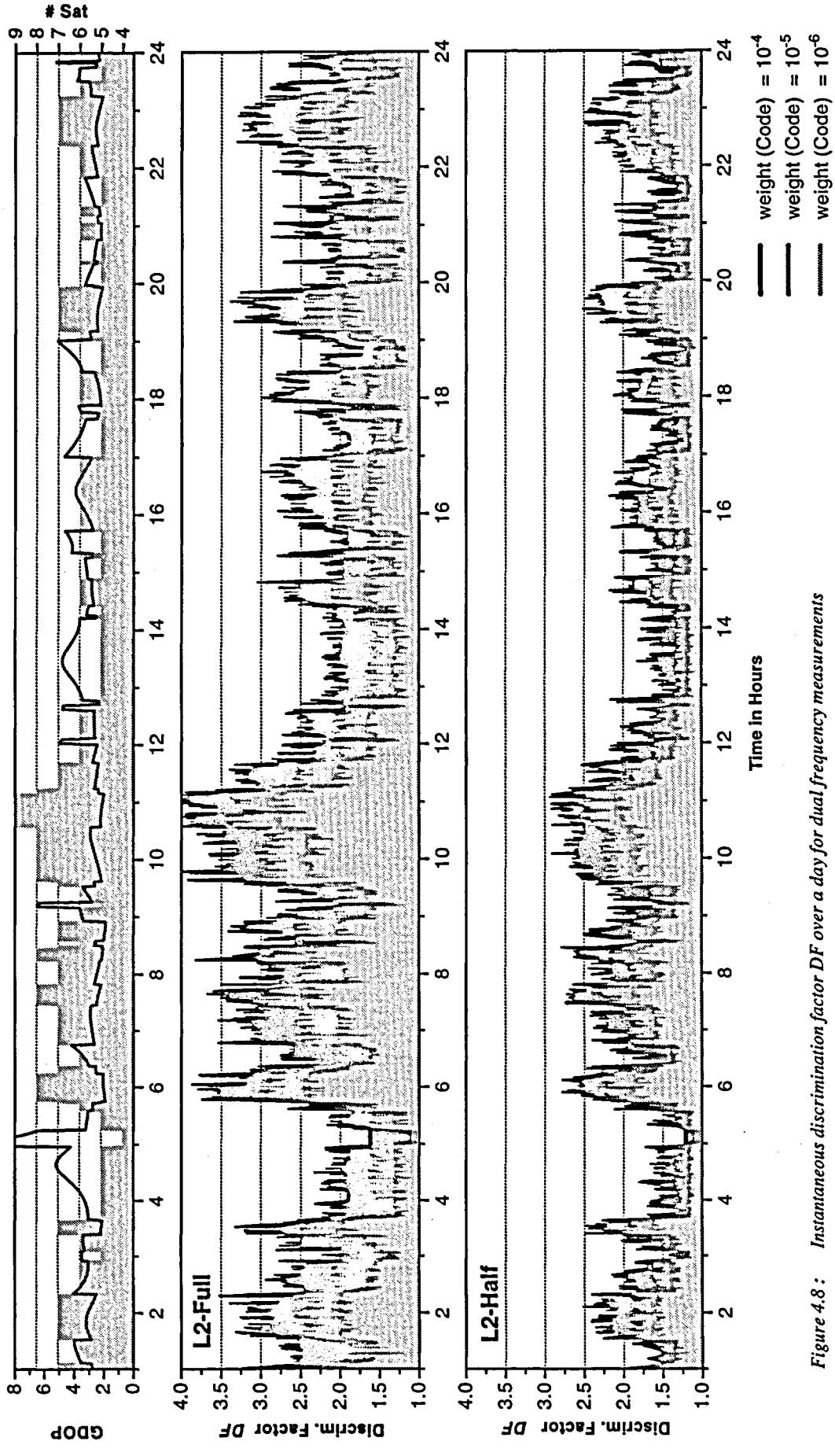

Figure 4.8 : Instantaneous discrimination factor DF over a day for dual frequency measurements

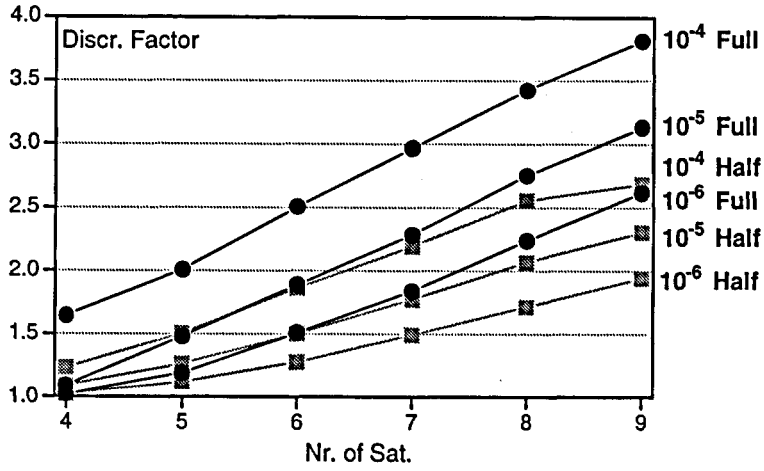

Figure 4.9 : The mean values of the instantaneous discrimination factor as a function of the number of satellites for different code weights ($w_{Code} / w_{Phase} = 10^{-6} / 10^{-5} / 10^{-4}$) and for half or full ambiguities in L2.

The following consideration leads to a more general interpretation of the instantaneous *DF* : If we integrate over more than one epoch but still over small time spans (<2-5 minutes) the gain for the resolution power due to the change in the satellite geometry in the kinematic mode is small. Because geometry is not substantially strengthened by the L2 measurements, it corresponds to the gain obtained with L1 measurements only (see chapter 4.3.1). The essential improvement consists in an effect of 'averaging' the code measurement, if more epochs are used. This means that in a first approximation

the *DF* over *n* epochs corresponds to the instantaneous *DF* with an improved code weight.

In the case of uncorrelated measurements the *DF* over *n* epochs with a *rms* of the code measurements σ_{code} would corresponds to the instantaneous *DF* with a *rms* for the code measurements $\overline{\sigma}_{code} = \sigma_{code} / \sqrt{n}$.

With this generalization of the *DF* in mind, two important conclusions may be drawn:

- In most static applications the code measurements are only used for the determination of the clock behavior of the receivers. They do not contribute to the ambiguity fixing either to the determination of the coordinates. In the kinematic mode, however, the quality of the code measurement becomes a decisive factor for a fast ambiguity resolution, the so-called 'on the fly' ambiguity resolution.

- The use of receivers reconstructing the full cycle in L2, even under AS conditions, has advantages. In our example the *DF* improves by a factor of 1.35 if full cycle L2 ambiguities instead of half cycle ambiguities are determined.

4.4 Stochastic modeling of the ionospheric path delay

Until now we have completely neglected the influence of ionospheric refraction on the measurements. Let us briefly discuss this topic:

When estimating in the case of dual frequency measurements coordinates with fixed L1 and L2 ambiguities, the ionosphere-free L3 combination may be used to eliminate systematic distortion due to the ionosphere. The problem, however, resides in the fixing of the ambiguities. The high discrimination potential of the ambiguity search in the dual-frequency mode lies precisely in the fact that unbiased L1 and L2 phase measurements are available. Fortunately for many applications over short distances the biases introduced by the ionosphere are small enough to be neglected entirely for the ambiguity search. In the following we outline a procedure taking ionospheric refraction into account.

4.4.1 The frequency dependency of the ionospheric path delay

The ionosphere is a part of the atmosphere situated above the troposphere and the stratosphere. It is characterized by the presence of ionized particles provoking a frequency dependent path delay of the GPS signal. A sufficient approximation for L-band frequencies is given by [Spilker 1980] :

$$\Delta\tau_{Ion} = 1.35 \cdot 10^{-7} \frac{TEC}{f^2} \tag{4.40}$$

with

$\Delta\tau_{Ion}$ ionospheric group path delay in [sec].

TEC *T*otal *E*lectron *C*ontent along the ray given in [electrons / m^2]

f the frequency of the signal in Hz
in the case of GPS : f_{L1} = 1.57542 GHz and f_{L2} = 1.22760 GHz.

For the code measurements the group path delay has to be used and for the phase measurement the phase path delay, which differs by the sign from the group path delay. By multiplying (eqn. 4.40) by the velocity of light c, we obtain the ionospheric path delay $\Delta\rho_{Ion}$ in meters.

$$\Delta\rho_{Ion} = 41 \frac{TEC}{f^2} \tag{4.41}$$

Due to this frequency dependency the ionospheric biases in the L1 and L2 measurements are different and it is possible to eliminate them by using the appropriate linear combination of L1 and L2. This ionosphere-free combination is also known as L3 combination.

The total ionospheric content, i.e. the values for activity of the ionosphere ,i.e. the TEC values, depend on the sunspot activity of the sun. For a given site on the surface of the earth a

strong daily variation is observed (maximum values in the afternoon, minimum values early in the morning).

4.4.2 The single layer model

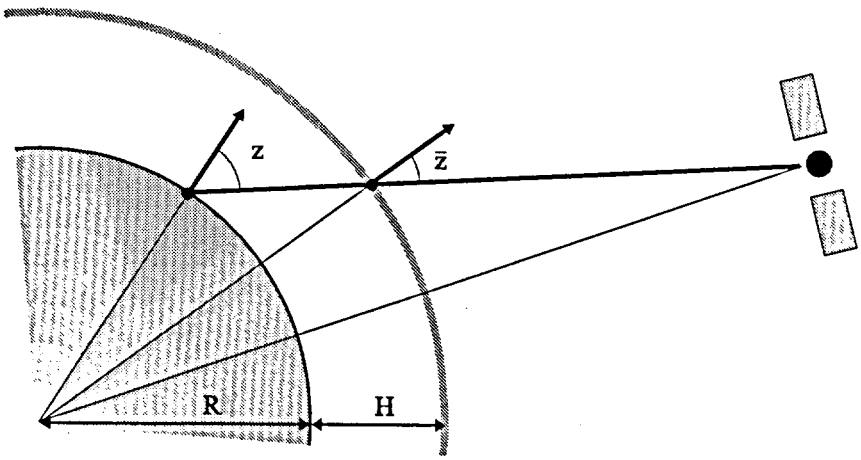

Figure 4.10 : Single layer model of the ionosphere.

The single layer model of the ionosphere concentrates the electrons of all ionospheric layers in a spherical layer of infinitesimal thickness at height H above the earth's surface. The total electron content TEC of the ionosphere can then be replaced in (equation. 4.40) and (equation. 4.41) by the electron density TEC_0 mapped with the $1/cos(\bar{z})$ of the zenith angle $\bar{z}$.

This single layer approach allows to express the ionospheric path delay as a function of the geometry given by the coordinates of the station and the satellite.

The zenith angle of the ray with respect to the ionospheric layer is given by :

$$\sin(\bar{z}) = \frac{R}{R+H}\sin(z) \tag{4.42}$$

with

R	Earth radius (6370 km)
H	Height of the ionosphere (~350 km).
z	Zenith angle from the station to the satellite.
$\bar{z}$	Zenith angle at the height of the ionosphere layer.

The ionospheric path delay may then be expressed by :

$$\Delta\rho_{Ion} = 41\frac{TEC_0}{f^2} \cdot 1/\cos(\bar{z}) \tag{4.43}$$

The electron density TEC_0 may now be modeled by an analytic function depending on the geomagnetic latitude and the hour angle of the sun where some coefficients of such a development may be estimated using dual frequency GPS measurements. [Wild, 1993] has shown that such GPS-derived ionosphere models approximate the real ionosphere quite well over time intervals of several hours. Short period fluctuations remain problematic, however. Note that for static surveys extended over several hours these short period variations in the ionosphere are not as critical as in the kinematic mode or for very short occupation times in the static mode (rapid static).

4.4.3 Stochastic approach

For 'stochastic' modeling of the ionosphere, we subdivide the ionospheric path delay in two parts. This model is very closely related to models presented by and [Bock et al., 1986] and [Beutler et al., 1989].

$$\rho_{Ion} = \rho_{Ion}^{model} + \delta\rho_{Ion} \tag{4.44}$$

A first part is given by a single layer model using the following approach for the TEC_0:

during 'night'

$$TEC_0 = E_0 \qquad t_{loc} \; from \; 20^h \; to \; 8^h \tag{4.45-a}$$

during 'day'

$$TEC_0 = E_0 + E_1 \cos((t_{loc} - 14^h)/24 \cdot 2\pi) \qquad t_{loc} \; from \; 8^h \; to \; 20^h \tag{4.45-b}$$

where

t_{loc} denotes the local time of the corresponding ionosphere point and is identical with the hour angle of the sun.

E_0 corresponds to TEC_0 during the night.

E_1 corresponds to the maximal raise of the TEC_0 at 14^h local time.

The model values used below are $E_0 = 10 \cdot 10^{16}$ and $E_1 = 30 \cdot 10^{16}$ and $H = 350\ km$ for the ionospheric layer.

For the second part $\delta\rho_{Ion}$ of the ionospheric path delay the two following approaches for an unknown ionospheric bias on the L1 or respectively L2 phase measurements may be used :

1.) Absolute ionospheric biases

$$\text{Phase meas. on L1 :} \quad \delta\rho^s_{Ion}(\varphi_{L1}) = \left({}^{1}\!/_{\cos(\bar{z}^s_m)} - {}^{1}\!/_{\cos(\bar{z}^s_f)} \right) \cdot IonBias^s_{Abs} \qquad (4.46\text{-a})$$

$$\text{Phase meas. on L2 :} \quad \delta\rho^s_{Ion}(\varphi_{L2}) = \gamma \cdot \left({}^{1}\!/_{\cos(\bar{z}^s_m)} - {}^{1}\!/_{\cos(\bar{z}^s_f)} \right) \cdot IonBias^s_{Abs} \qquad (4.46\text{-b})$$

2.) Differential ionospheric biases

$$\text{Phase meas. on L1 :} \quad \delta\rho^s_{ion}(\varphi_{L1}) = \left({}^{1}\!/_{\cos(\bar{z}^s)} \right) \cdot IonBias^s_{Dif} \qquad (4.47\text{-a})$$

$$\text{Phase meas. on L2 :} \quad \delta\rho^s_{Ion}(\varphi_{L2}) = \gamma \cdot \left({}^{1}\!/_{\cos(\bar{z}^s)} \right) \cdot IonBias^s_{Dif} \qquad (4.47\text{-b})$$

where

$\delta\rho^s_{ion}$ remaining ionospheric path delay for the phase measurements to the satellite *s* after subtraction of a correction deduced from a single layer model [in meters].

$\bar{z}^s_m$, $\bar{z}^s_f$ Zenith distances at the intersection with the ionospheric layers stemming

from the ray from the moving receiver $\bar{z}^s_m$, resp. from the reference station $\bar{z}^s_f$ to satellite *s* (see fig. 4.10).

$IonBias^s_{Abs}$ Normalized absolute ionospheric biases for the L1 phase measurement to

satellite *s* (along the normal to the ionospheric layer) [in meters].

$IonBias^s_{Dif}$ Normalized differential ionospheric biases for the L1 phase measurement to satellite *s* (along the normal to the ionospheric layer) [in meters].

$\gamma = \left({}^{f_1}\!/_{f_2}\right)^2 \approx 1.6$ scale factor to relate the L2 biases to the L1 biases.

In both cases we assume that *IonBias* is an unknown parameter. For both approaches, we may now extend our NEQ system by introducing an additional unknown ionosphere bias for every satellite.

If we would now simply pre-eliminate all *IonBias* parameters for every epoch together with the coordinates of the moving receiver and the clock biases (see chapter 2.2.3), the resulting NEQ system for the time-invariant parameters , i.e. the ambiguities, would become singular, even if we hold the ionospheric bias of a reference satellite fixed. Note that in this case we are trying to recover the individual L1 and L2 ambiguities from the L3 measurements only,

since using L1 and L2 measurements together with unknown ionospheric biases per epoch is strictly identical to the use of the ionosphere-free L3 combination.

The idea [Bock et al., 1986] is to postulate that the ionospheric biases constitute a white noise with zero-expectation values and known variances σ^2_{Ion} and to introduce this information as pseudo-measurements in the NEQ system.

$$\text{Distribution of } \textit{IonBias}: \quad N(0,\sigma^2_{Ion}) \tag{4.48}$$

The hypothesis that the ionospheric biases correspond to pure white noise is certainly not correct. They are strongly correlated in time and taking this correlation into account may improve the model. Our approach, however, has the advantage of being simple to implement.

By introducing these pseudo-measurements our NEQ system for the time invariant parameters becomes regular, but the solutions are weakened from a purely geometrical point of view.

The advantage of introducing absolute ionospheric biases consists of the fact that the coefficients indirectly depend (through the differences in the zenith angles $\bar{z}^s_m$ and $\bar{z}^s_f$) on the distance between the reference and the moving receiver. For a given noise level σ_{Ion}, there is a type of distance-dependent weighting of the measurements. During many kinematic surveys (e.g. flights) we often have a wide variation of the distance to the reference station. If differential ionospheric biases are used this distance dependent weighting effect vanishes and for all distances the same geometrical dilution depending on the choice of the noise level σ_{Ion}, is postulated.

The use of differential ionospheric biases leads to the simpler guesses for the noise level σ_{Ion}. We may put the noise for the differential zenith ionosphere bias of the L1 phase e. g. to 1 or 2 cm. In the case where absolute biases are used, the value for σ_{Ion} also corresponds to the noise of an absolute zenith delay of some meters.

The impact of additional stochastic ionosphere biases on the geometry and especially on the discrimination factor is unfortunately tremendous. On the one hand the ionospheric biases finally weaken the central relationship that the L1 and L2 measurements have to fit the same geometrical coordinates. On the other hand, however, they lead to a better, i.e. bias-free, estimation.

Results are presented in (section 5.2.4 , section 7.5 and chapter 8).

5. 'On the fly' ambiguity resolution from real data

5.1 Results from a short static baseline 'Thun 94'

In order to demonstrate that the theoretically derived discrimination level of dual frequency measurements (see section 4.3.2) may be achieved in practice, a first test with real data was performed using static measurements over a short baseline.

5.1.1 Overview

The data stem from a campaign carried out by the Swiss Federal Office of Topography for the study of antenna phase center variations. We gratefully acknowledge that this data set was made available to us.

This data set is of interest because of its duration of 24 hours and its ideal conditions: full-cycle ambiguities in L2 and good quality of code measurements. The baseline length of 10 meters guarantees, that the ionospheric refraction may be neglected in the differential measurements. The characteristics of the data set Thun are summarized in Table 5.1.

Data set : THUN	
Location : Thun (CH) Latitude : 46° 45' N Longitude : 7° 35' E	Start time : March 14, 1994 16 : 20 UT End time : March 15, 1994 16 : 15 UT Duration : ~ 24 h Measuring frequency : every 30 sec
Receiver TRIMBLE SSE (from the Swiss Federal Office of Topography)	Phase Meas. : L1-Phase L2-Phase (Full cycles) Code Meas. : C/A-code (*rms* < 0.5 m) (Anti-Spoofing ON)

Table 5.1 : Characteristics of the data set THUN used for instantaneous ambiguity resolution

5.1.2 Code solution

A differential kinematic code solution was computed and compared to the known reference coordinates. This gives a first impression of the quality of the code measurements (figure 5.1).

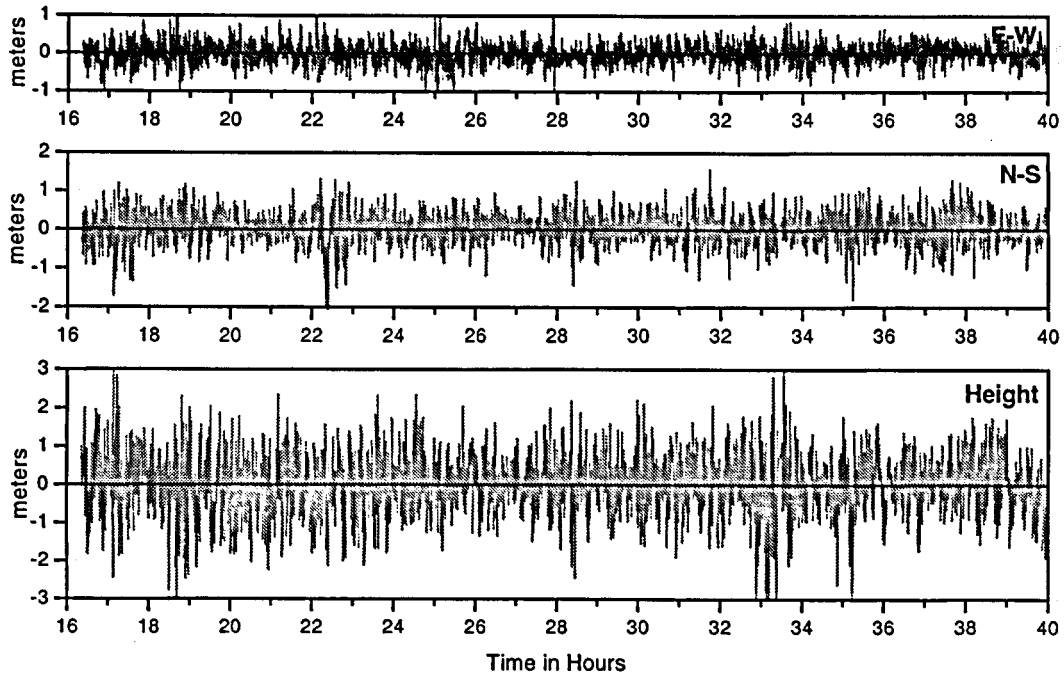

Figure 5.1 : Differences of a differential code solution to the reference coordinates (for the 10-m baseline Thun).

The average PDOP values for the entire day are 3.1, the average number of satellites 6.4. The standard deviation of the coordinates from the differential code solution for one epoch are :

$$\sigma_{E-W} = 0.28\ m \qquad \sigma_{N-S} = 0.40\ m \qquad \sigma_{Height} = 0.80\ m$$

This shows the good quality of the code measurements and allows the allocation of a high weight to the code ($weight_{Code}/weight_{Phase} = 10^{-4}$), from which the ambiguity search will benefit.

5.1.3 Ambiguity resolution on the single epoch level

First, a reference solution drawing on the phase measurements and interpreting these measurements as static was computed. The coordinates and the integer values for the ambiguities stemming from this solution were considered as valid for the subsequent test.

In the next step the measurements of every epoch are treated separately. The corresponding NEQ system is built up and the search performed. The best and second best integer combi-

nations are determined and from their σ values the empirical discrimination factor *DF* is computed. The best integer combination is then checked for correctness regardless of the value of the discrimination factor.

Let us summarize the procedure for computing the *DF* in table 5.2.

Input			
# of epochs	: 1		
Phase measurements	: L1	*weight (Phase L1)*	= 1
	L2 (Full cycle)	*weight (Phase L2)*	= 1
Code measurements	: C/A code	*weight (code)*	= 10^{-4}
Output			
σ_{fl}, f_{fl}	rms and degree of freedom of the floating point solution		
σ_1, f_{Fix}	rms and degree of freedom of the best integer combination		
σ_2, f_{Fix}	rms and degree of freedom of the second best integer combination		
$DF = \sigma_2/\sigma_1$	discrimination factor		
flag	best solution correct or false		

Table 5.2 : Summary of the procedure for the instantaneous ambiguity resolution.

The results of this single epoch ambiguity fixing are given in figure 5.2.

Those solutions, ending up with a wrong combination are marked with a bar in figure 5.2.II. From all 2796 epochs for only 2 epochs the best combination was not the correct one. The corresponding *DF* was in one case 1.0 and in the other case 2.8. This means that if we had chosen a threshold value of 2 for the *DF*, in one case we still would have accepted a wrong solution !

Figure 5.2.IV shows the obtained values of the three different rms. Their is a good agreement between σ_{fl} and σ_1 and the mean level for σ_1 is about 3.5, which corresponds to a *rms* a posteriori of 3.5 mm for the single difference measurements of the phase and to 35 cm for the code. Due to this low noise level the obtained values for the *DF* are even better than the prognosticated theoretical values, which were derived for $\sigma = 5$ mm (see figure. 4.5).

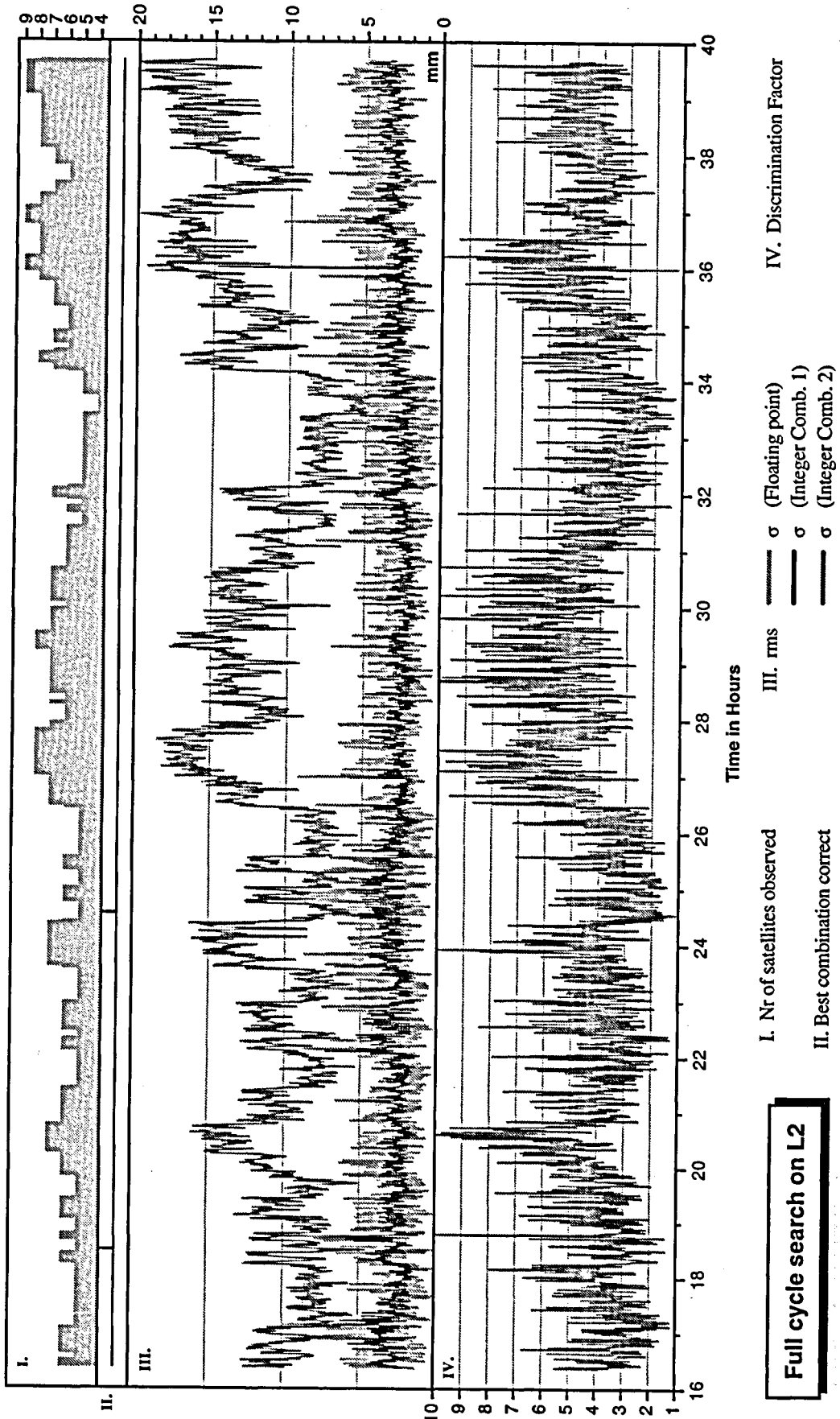

Figure 5.2 : Result of the single epoch ambiguity resolution on the 10-m baseline Thun with dual frequency measurements

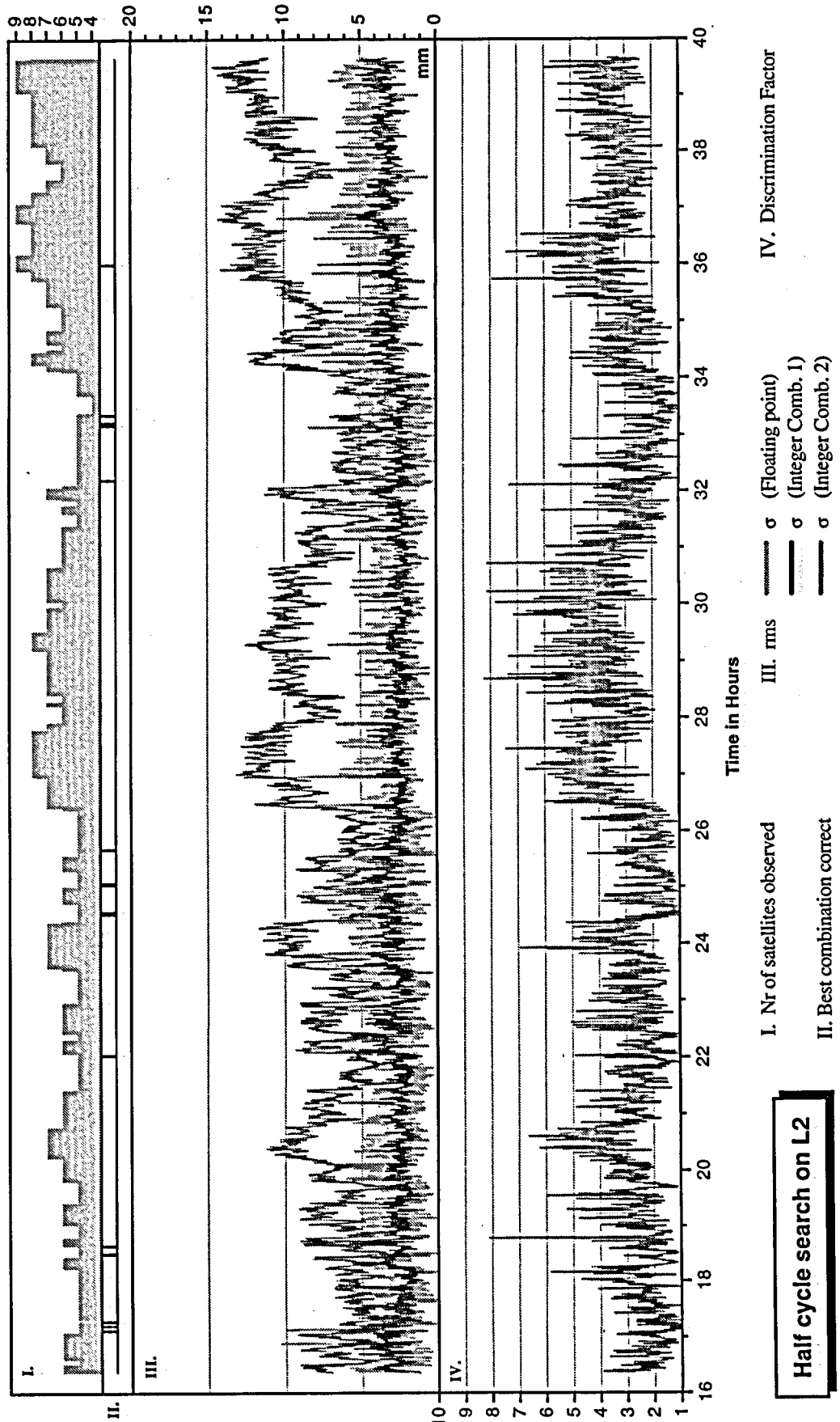

Figure 5.3 : Result of the single epoch ambiguity resolution on the 10-m baseline Thun with dual frequency measurements

The fact that the values of σ_{fl} are more noisy than the values of σ_1 is due to the small degree of freedom in the calculation of σ_{fl}, which is close to zero. From a statistical point of view, for a given error probability the threshold value for the *DF* increases with the decreasing degree of freedom, but fortunately for the calculation of σ_1 and σ_2, which correspond to solutions with fixed integer ambiguities, the degree of freedom is again increased to a reasonable level, since the ambiguities are no longer unknowns.

As already pointed out the search for half-cycles in L2 weakens the power of discrimination. Even though it was not necessary for this data set to look for half cycle ambiguities, the search was nevertheless also performed in this mode with the input parameters as in the full cycle mode. The results are presented in figure 5.3.

The number of epochs with a false ambiguity solution increases from 2 to 17 and all epochs correspond to a constellation with 5 satellites. The maximum value of the *DF* within this set of wrong solutions is $DF_{Half} = 1.5$ and the corresponding epoch is identical to the epoch with a wrong ambiguity solution in the full-cycle mode and a $DF_{Full} = 2.8$.

For a given *DF* the percentage of epochs *i* over the entire day with a value DF_i larger than *DF* can be computed for both modes and drawn as a function of *DF*. This corresponds to an empirically determined complementary distribution function and reflects the substantial decrease in the discrimination potential for the half-cycle mode compared to the full-cycle mode.

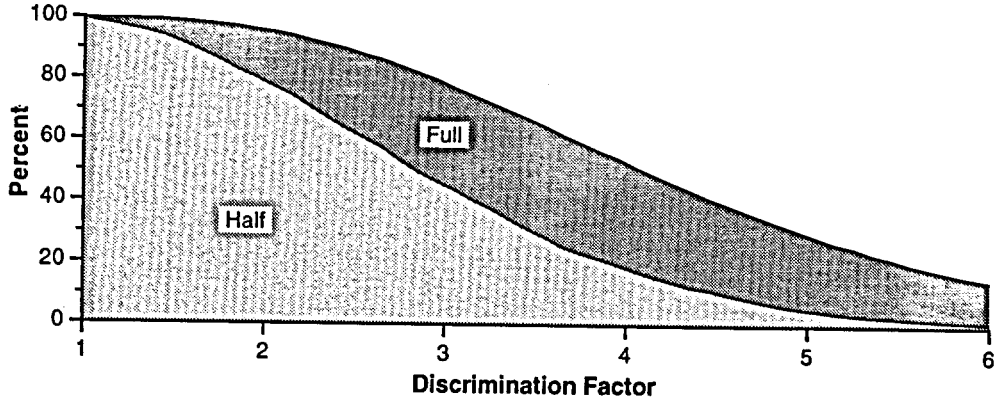

Figure 5.4 : Complementary distribution function of the discrimination factor DF in percent over the day.

For a constellation with a number of satellites ≥ 5, the degrees of freedom of the Fisher's probability density function for $DF^2 = \sigma_2^2/\sigma_1^2$ are > 8. With every additional satellite the degrees of freedom are increased by 2. If we use now a value of 8 for the degrees of freedom and an error probability of 1 %, we obtain a threshold value for *DF* :

$$DF_{limit}(\alpha = 1\%) = \sqrt{6.03} = 2.45$$

With a value of 2.5 in 90 % of the cases in the full-cycle mode and in 63% in the half-cycle mode a successful fixing of the ambiguities would have been possible for this data set. These are average values over the entire day. Note that in our example one epoch with a wrong result would still have passed this test.

5.1.4 Phase solution

If for a given epoch the ambiguities are solved correctly there is naturally no difference between the coordinates obtained directly from this single epoch or from the entire data set processed in the kinematic mode. To show the quality of the result obtained with phase measurements, the differences with respect to the reference coordinates are given in figure 5.5.

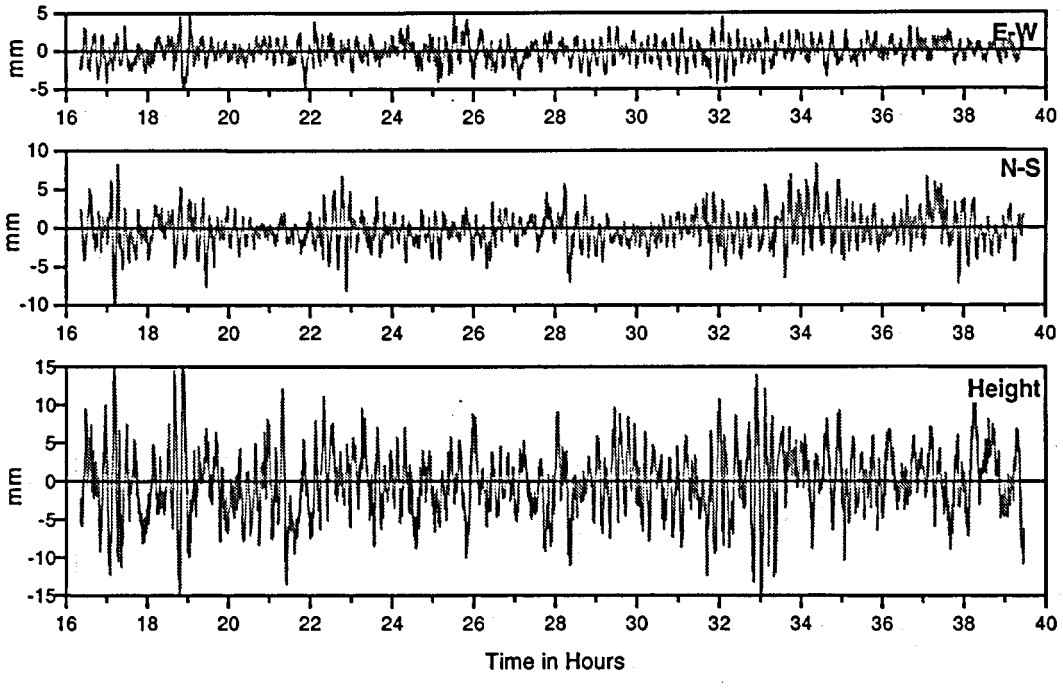

Figure 5.5 : Differences of a differential L1-phase solution to the reference coordinates (for the 10-m baseline Thun).

For this final computation the code measurements were deweighted. The result actually corresponds to a pure phase solution, where only L1 phase measurements with fixed ambiguities were used. The standard deviations of the coordinates for one epoch are :

$$\sigma_{E-W} = 1.3\ mm \qquad \sigma_{N-S} = 2.1\ mm \qquad \sigma_{Height} = 4.3\ mm$$

5.1.5 *Impact of incorrect integer ambiguities on the coordinates*

One interesting problem is the impact of a wrong integer solution on the coordinates. Let us just arbitrarily pick one epoch with 6 satellites and inspect the 10 best integer ambiguity sets. For every set the coordinates are evaluated and the difference to the reference values computed.

A first look at the values of the ambiguities shows that independent of the satellite the errors in the L1 and L2 ambiguities are almost linearly dependent (figure 5.6). This relationship is valid for all 9 incorrect versions and can easily be explained. If we assume that there is no frequency dependent error or influence on the L1 and L2 phase measurements, the double difference observation *DD* for the phase measurements on L1 and L2 may be written as :

$$DD(\varphi_1) = DD(d) + \lambda_1 A_1 \qquad \text{and} \qquad DD(\varphi_2) = DD(d) + \lambda_2 A_2 \tag{4.40}$$

By taking the difference, the geometrical term *DD(d)* is canceled out (a relation which was extensively used by [Frei and Beutler, 1989]).

$$DD(\varphi_2) - DD(\varphi_1) = \lambda_2 A_2 - \lambda_1 A_1 \tag{4.41}$$

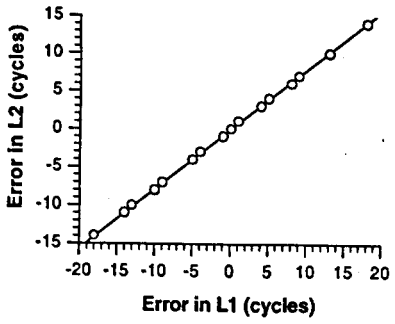

Figure 5.6: L2 error versus L1 error

This means on the other hand that the combination $\lambda_2 A_2 - \lambda_1 A_1$ is determined with the high accuracy given by the phase measurements. Formally we have :

$$\lambda_2 A_2 - \lambda_1 A_1 = const. \qquad \text{or}$$

$$\lambda_2 (A_2 + dA_2) - \lambda_1 (A_1 + dA_1) = const. \tag{4.42}$$

The relation between the errors dA_1 and dA_2 of the L1 and L2 ambiguities yields :

$$\lambda_2 dA_2 - \lambda_1 dA_1 \approx 0 \tag{4.43}$$

Even if this relationship is not explicitly used in the search algorithm, the NEQ system implicitly contains this information. This relation is the reason of the high discrimination power in the dual frequency mode, as it was already pointed out by [Frei, 1991].

The best solution ($\sigma_1 = 3\ mm$) is nicely discriminated as can be seen in figure 5.7. All other 9 combinations are at a level of about $\sigma_i = 11\ mm$. The resulting coordinates computed with these false integer combinations are widely spread with differences up to 6 meters as compared to the reference solution. The floating point solution of the coordinates is in this case directly identical to the code solution, because only one epoch has been used and the false integer solutions are worse in comparison with the floating point solution.

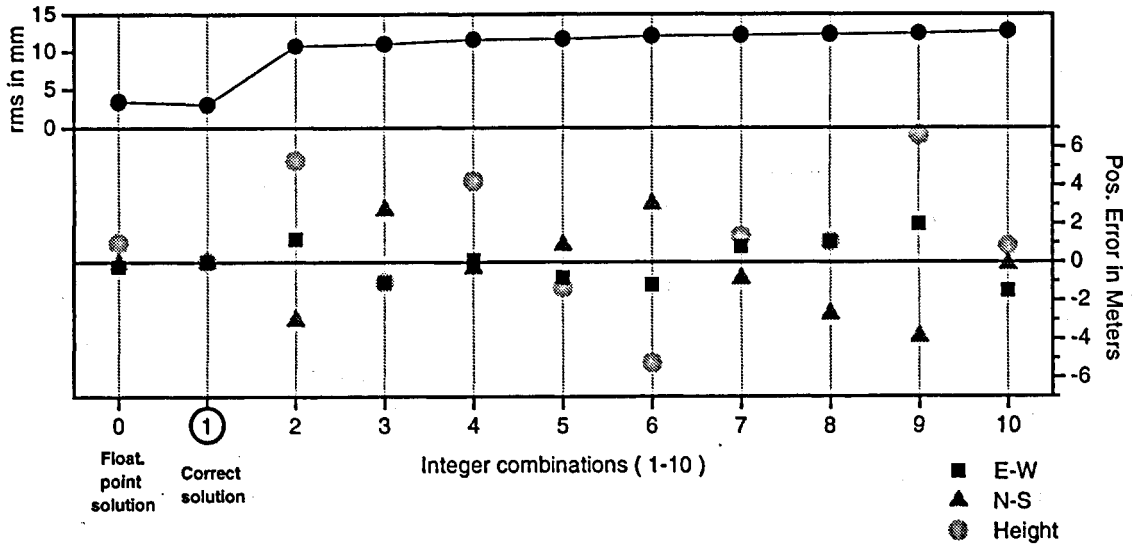

Figure 5.7 : Rms of the different integer combinations and their impact on the determination of the coordinates.

5.1.6 Conclusions

This example shows that for short baselines, where ionospheric refraction may be neglected, the discrimination power of dual frequency measurement allows the fixing of the ambiguities within one single epoch. The requirements are phase and especially code measurements of a high quality and a good satellite constellation. But even with 4 satellites it was possible, in our case to find the correct integer combinations. The integration of more than one epoch for the fixing of the ambiguities strengthens the discrimination. In particular, the statistics allow a better detection of outliers, which is not possible with data of one epoch only. An error of 0.3 cycle in a phase measurement e.g. can easily lead to a wrong integer combination with an acceptable *DF*.

An other important conclusion is that only the correct integer combination gives a valid result. All false combinations from the search, especially if dual frequency measurements are used, leads to results which can be offset several meters and can be worse than the code solution. This behavior is finally a consequence of the good discrimination potential in the dual frequency mode.

5.2 Results from real flight data : 'Laser Scanner flight 94'

In the previous section 5.1 we saw in an ideal example (10-m baseline) that it is in principle possible to retrieve the ambiguities with the measurements of one epoch only. How does the situation change with real kinematic data stemming from a flight with a receiver moving at a speed of about 200 km/h and a reference station on ground at a distance of 10 km or more ?

In this chapter we analyze a kinematic data set. Different strategies for retrieving the ambiguities were applied. Because two different reference stations on the ground at different locations could be used, the impact of the distance from the reference receiver to the moving receiver on the ambiguity fixing process, but also on the coordinate quality, could be studied.

5.2.1 Overview

This flight took place on May 17, 1994. Differential GPS measurements were collected in order to provide highly accurate positioning for an airborne Laser scanner. Different institutes and organizations were directly involved in or actively supported this project : The Swiss Cadastral Authority (Vermessungsdirektion), owner of the airplane, organized the flight. For the operation of their Laser scanner, an instrument which is still under development, DORNIER (Deutsche Aerospace) was responsible. A good part of the organization work was performed by the Remote Sensing Laboratory (RSL) of the University of Zurich. The task of our institute consisted of positioning with differential GPS. TRIMBLE SSE receivers (belonging to the Swiss Federal Office of Topography) could be used. The same institution also provided us with the 1-sec data from their permanent station of Zimmerwald (IGS-site). This means that the GPS data were made by the same receiver type as for the static baseline in Thun (see chapter 5.1).

Let us summarize the GPS-related characteristics of the campaign in table 5.3.

Data-Set : LASER-SCANNER FLIGHT	
Location : Grenchen (CH) Latitude : 47° 10' N Longitude : 7° 30' E	Take-off time : May 17, 1994 10 : 30 UT Landing- time : May 17, 1994 13 : 45 UT Flight duration : 3 h 15 min. Measuring rate : 2 Hz
Receiver TRIMBLE SSE dual frequency receivers (from the Swiss Federal Office of Topography)	Reference stations (see location in figure 5.8) FIX1: Distance to moving : 2 - 12 km Measuring rate : 2 Hz (Data set not complete) Zimmerwald Distance to moving : 28 - 35 km Measuring rate : 1 Hz

Table 5.3 : Characteristics of the data set 'Laser Scanner flight 94'

It was not possible to collect this large volume of data in the internal memory of the receivers. Therefore Laptop computers were connected to the receivers and the data downloaded onto harddisks. Unfortunately communication problems at the reference station FIX1 occurred and the L2 data were unusable after about 1 hour after take off (at $11^h\ 26^m$). No L2 data were stored at the FIX1 site. After an another 1½ hour (at $12^h\ 50^m$) the registration of the L1 measurements developed problems too and FIX1 could no longer be used. Fortunately the data of the permanent station Zimmerwald allowed completion the trajectory in the differential mode.

We focus our studies on two time windows :

Window 1 : from $10^h\ 34^m$ to $12^h\ 50^m$ Duration $2^h\ 15^m$ (L1 measurements only)

Window 2 : from $10^h\ 34^m$ to $11^h\ 26^m$ Duration 52^m (L1&L2 measurements)

In a first step the reference station FIX1 was connected to the permanent site Zimmerwald by means of a static baseline computed with the dual frequency measurements of window 2. This task was done using the Bernese Software (Version 3.4) The L1 and L2 ambiguities could be fixed and it was possible to compute an ambiguity-fixed, ionosphere-free solution for the coordinates of FIX1 with respect to Zimmerwald. These coordinates were then used as reference coordinates in the computation of the kinematic track of the airplane. This pro-

cedure allows us later on to compare the coordinates of the moving receiver obtained with respect to FIX1 with those obtained with respect to Zimmerwald.

Figure 5.8 gives an overview of the situation, showing the location of the two reference sites FIX1 and Zimmerwald and the area recorded by the Laser Scanner. The GPS trajectory covers the total flight duration of about 3 hours.

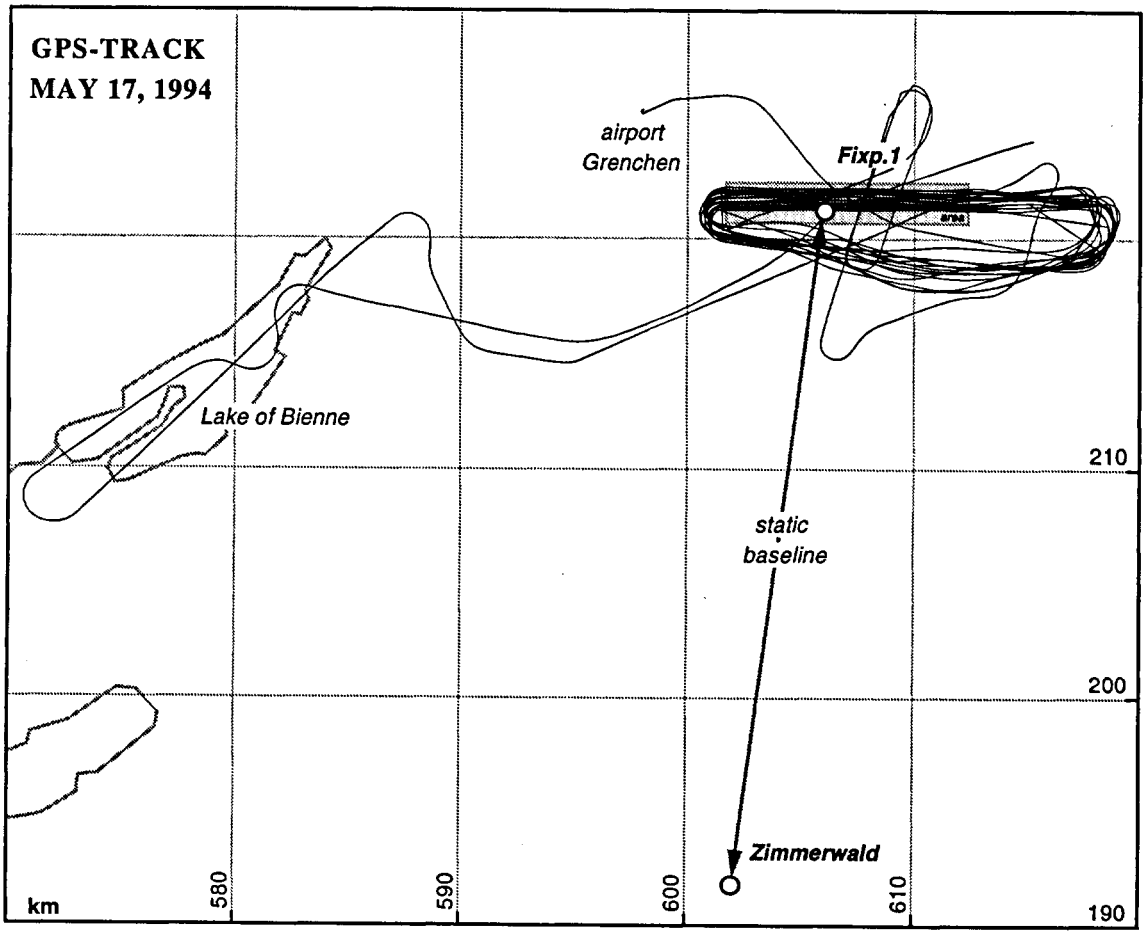

Figure 5.8 : Overview of the location of the reference sites and the GPS track for the 'Laser Scanner flight 94'

5.2.2 Ambiguity resolution in the single-frequency mode

Let us just start by using only the L1 data and let us introduce the measurements (code & phase) of window 1 over about 2 hours into our NEQ-system. For this integration we only use the data for every 5th second and we apply a ratio : $weight_{Code}/weight_{Phase} = 5 \cdot 10^{-4}$. For convenience the weight of the phase measurement is taken as unit, thus the *rms* of the unit weight a posteriori, which theoretically is dimensionless, corresponds to the a posteriori value of the *rms* of a single difference phase measurement in meters.

Over the entire time span there were no major interruptions in the phase measurements and the constellation varied from 5 to 8 satellites. In total 9 different satellites were involved and the single difference ambiguity of satellite 20 was kept fixed.

This leaves us with the NEQ system for the L1 ambiguities. By inverting the NEQ system the floating point solution is obtained. A careful conventional approach for fixing the ambiguities is used, where we fix in a single step only one ambiguity (the ambiguity with the best *rms*) and update the NEQ system after every step (see chapter 4.1).

The results may be found in table 5.4 (relative to the reference station FIX1) and in table 5.5 (relative to the reference station Zimmerwald). The ambiguities and their *rms* are given in units of L1 cycles. The formal error of the floating point values of the ambiguities are on the order of 0.02 cycles and reflect the quality of the constellation and the long integration time of 2 hours. Even if these values are far too optimistic, the stepwise fixing of the ambiguities showed in the trajectory relative to FIX1 that the fractional part of the real value of the ambiguity never exceeded 0.1 cycle. Using Zimmerwald as the reference, the fixing is more difficult or even impossible due to the larger distance. The *rms a posteriori* increases during the fixing from 5.9 mm to 7.8 mm compared to the increase of from 4.6 mm to 5.2 mm with FIX1. This indicates the presence of systematic errors. Nevertheless also with Zimmerwald as reference station the resolution of the L1 ambiguities in a single frequency scenario seemed to be successful.

In a second run we then held the L1 ambiguities fixed and introduced the L1- and L2-measurements in the NEQ system. If our L1 integer combinations were correct, the value of all L2 ambiguities from the floating point solution should be close to integer numbers. The result can be summarized by the mean and maximum value of the difference of the floating point value to the nearest integer value. With reference station FIX1 resp. Zimmerwald the mean values were 0.02 cycle resp. 0.05 cycle and the maximum values 0.07 resp. 0.13 cycle.

If a search in the dual frequency mode had been used to fix the ambiguities it would not be correct to conclude from a good correspondence of the L1 and L2 solutions that the corresponding ambiguities were resolved correctly, because for the search an implicit identity of the coordinates is postulated.

Floating point solution **Reference site** **FIX1**

L1 code & L1 phase

$weight_{Code}/weight_{Phase}$: $5 \cdot 10^{-4}$

Used data frequency : 5 sec σ_{fl} a posteriori of unit weight : 0.00456

SatNr	Freq.	StartTime	EndTime	#Epochs	Ambig.Value (in cycles)	Rms (cy.)
1	1	10:26:00	11:09:42	425	2250628.059	0.015
1	1	11:10:13	11:29:57	233	-1917201.935	0.016
1	1	11:32:37	11:40:15	88	-5921626.999	0.016
1	1	11:40:43	11:50:13	113	-7554982.112	0.016
1	1	11:51:43	12:00:22	45	-9999678.096	0.019
4	1	10:27:25	10:43:59	119	1769004.529	0.029
4	1	10:44:19	10:50:45	76	814967.474	0.030
5	1	10:26:00	12:24:51	1314	-1100752.235	0.017
6	1	10:26:00	12:51:55	1315	9064492.104	0.010
9	1	10:26:00	11:13:26	392	-5970502.131	0.013
12	1	11:20:00	11:33:36	152	-4521041.197	0.020
20 Ref.	1	10:26:00	12:51:55	1315	4625331.000	0.000
24	1	10:26:00	11:44:58	841	5940282.638	0.026
24	1	11:45:13	12:15:22	358	4524337.635	0.026
25	1	10:53:01	12:51:55	1088	-6930813.149	0.011

Stepwise fixing of the ambiguities

step	SatNr.	Frac (A_n)	Rms (A_n)	A (integer)	σ (unit weight)	#Epochs
1	6	0.104	0.0098	9064492	0.00459	1315
2	1	-0.089	0.0056	2250628	0.00464	425
3	1	0.015	0.0051	-1917202	0.00465	233
4	25	-0.054	0.0037	-6930813	0.00470	1088
5	5	-0.064	0.0037	-1100752	0.00477	1314
6	24	0.040	0.0018	5940283	0.00489	841
7	9	0.046	0.0021	-5970502	0.00500	392
8	24	0.058	0.0032	4524338	0.00508	358
9	12	0.056	0.0043	-4521041	0.00512	152
10	4	0.017	0.0052	1769005	0.00513	119
11	4	-0.023	0.0065	814968	0.00513	76
12	1	0.058	0.0077	-5921627	0.00515	88
13	1	0.013	0.0083	-7554982	0.00515	113
14	1	0.098	0.0148	-9999678	**0.00516**	45

Table 5.4 : Floating point solution and stepwise fixing of the L1 ambiguities for kinematic flight data over 2 hours of observation.(distance to the reference station 2-12 km).

Floating point solution **Reference site** **Zimmerwald**

L1 code & L1 phase

$weight_{Code}/weight_{Phase}$: $5 \cdot 10^{-4}$

Used data frequency : 5 sec σ_{fl} a posteriori of unit weight : 0.00593

SatNr	Freq.	StartTime	EndTime	#Epochs	Ambig.Value (in cycles)	Rms (cy.)
1	1	10:21:02	11:09:41	377	6838655.081	0.017
1	1	11:10:14	11:29:57	211	2670825.029	0.019
1	1	11:32:38	11:40:14	82	-1333600.030	0.020
1	1	11:40:44	11:50:13	105	-2966955.201	0.019
1	1	11:51:44	12:00:22	44	-5411651.470	0.024
4	1	10:27:26	10:43:59	105	2257462.425	0.034
4	1	10:44:21	10:50:44	62	1303425.509	0.036
5	1	10:21:02	12:24:51	1198	12220319.758	0.020
6	1	10:21:38	13:31:46	1199	8417601.095	0.011
9	1	10:21:02	11:13:26	348	-2625341.038	0.016
12	1	10:21:02	11:33:36	608	-1284804.226	0.023
20 **Ref.**	1	10:21:02	13:31:46	1199	15141977.000	0.000
24	1	10:21:38	11:44:58	752	6239028.686	0.030
24	1	11:45:14	12:15:21	341	4823083.799	0.030
24	1	12:15:51	12:24:59	98	-253037.031	0.052
25	1	10:53:02	13:31:46	998	1804433.970	0.014

Stepwise fixing of the ambiguities

step	SatNr.	Frac (A_n)	Rms (A_n)	A (integer)	σ (weight unit)	#Epochs
1	6	0.095	0.0110	8417601	0.00596	1199
2	5	-0.079	0.0068	12220320	0.00600	1198
3	12	0.065	0.0030	-1284804	0.00614	608
4	9	0.114	0.0026	-2625341	0.00673	348
5	24	-0.083	0.0040	6239029	0.00688	752
6	1	-0.086	0.0043	6838655	0.00703	377
7	25	0.021	0.0052	1804434	0.00703	998
8	1	-0.094	0.0039	2670825	0.00724	211
9	24	0.138	0.0048	4823084	0.00755	341
10	4	-0.166	0.0081	2257463	0.00772	105
11	4	-0.072	0.0108	1303426	0.00774	62
12	1	-0.062	0.0117	-1333600	0.00775	82
13	1	-0.132	0.0131	-2966955	0.00779	105
14	1	-0.282	0.0227	-5411651	0.00785	44
15	24	0.387	0.0291	-253037	**0.00793**	98

Table 5.5 : Floating point solution and stepwise fixing of the L1 ambiguities for kinematic flight data over 2 hours of observation.(distance to the reference station 28-35 km).

5.2.3 Ambiguity resolution in the dual-frequency mode

Instead of using only L1 measurements or L1 and L2 measurements in separate runs, a high potential of discrimination results if both measurement types are processed in the same run. For the ideal case of a 10 m baseline measured in static mode, the results were promising and it was even possible to retrieve the ambiguities in most cases within a single epoch (see chapter 4.4).

We will apply the same procedure to this kinematic data set and try to resolve the ambiguities within one single epoch. To check whether the result was correct (correct integer combination) we compare it with the ambiguities obtained by the stepwise conventional resolution using the total data set. (see section 5.2.2).

The results of the instantaneous ambiguity fixing are given in figure 5.9 for the reference station FIX1 and in figure 5.10 for the reference station Zimmerwald. Note that there is a slight difference in the constellation. Nevertheless in both cases the constellations were very good (6-8 satellites). The distance to the reference stations is given in figure 5.9.II resp. 5.10.II and varies from 2-12 km for FIX1 and 25-35 for Zimmerwald.

Comparing these results to the corresponding result obtained from the 10 m baseline (figure 5.2), it is interesting to note that the level of the *rms* of the floating point solutions σ_{fl} are more or less the same, but the values for the *rms* of the best solutions σ_1 are significantly higher. This is evident in particular for the results with Zimmerwald as reference station, but also noticeable in the result relative to FIX1. The values for *rms* of the second best solution σ_2, however, are again more or less at the same level. This behavior of σ_1 and σ_2 leads to a significant decrease in the discrimination power of the best solution. In the case of the result with Zimmerwald as reference station the values for σ_1 and σ_2 are practically identical over longer periods, and in 25% of the cases the search ended up with a wrong ambiguity combination (figure 5.10.III). The black vertical bars mark the epochs where the best integer combination for the ambiguities solution is <u>not</u> the correct one. With FIX1 as reference station, the results are far better even with one satellite missing in the constellation. The correct combination was found in more than 99% of the cases and the discrimination factor is accordingly better.

For completeness the baseline Zimmerwald-FIX1 was also treated as a kinematic data set and the same procedure to resolve the ambiguities within one epoch was applied. The results are given in figure 5.11. The distances from Zimmerwald to the moving receiver are similar to the distances to the reference station FIX1 and the results of the instantaneous ambiguity resolution are highly correlated. (compare figure 5.10 and 5.11). The shape of σ_2 are similar, leading to a similar DF. More or less over the same periods the correct solutions were found. In both cases the corruption by ionospheric refraction leads to a similar lack of discrimination.

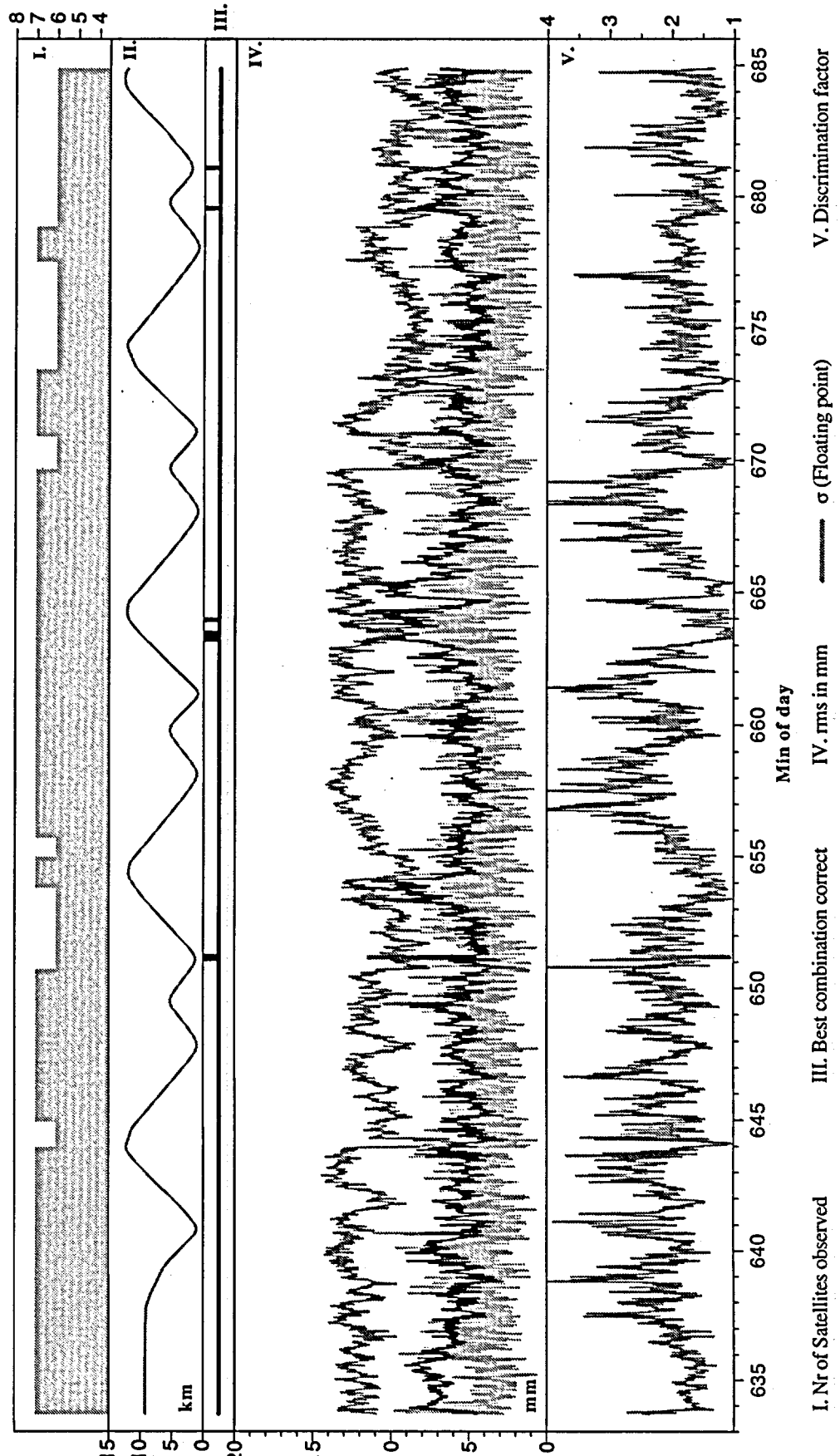

*Figure 5.9 : Result of the single epoch ambiguity resolution with **FIX1** as reference station. (Ful cycle search on L2)*

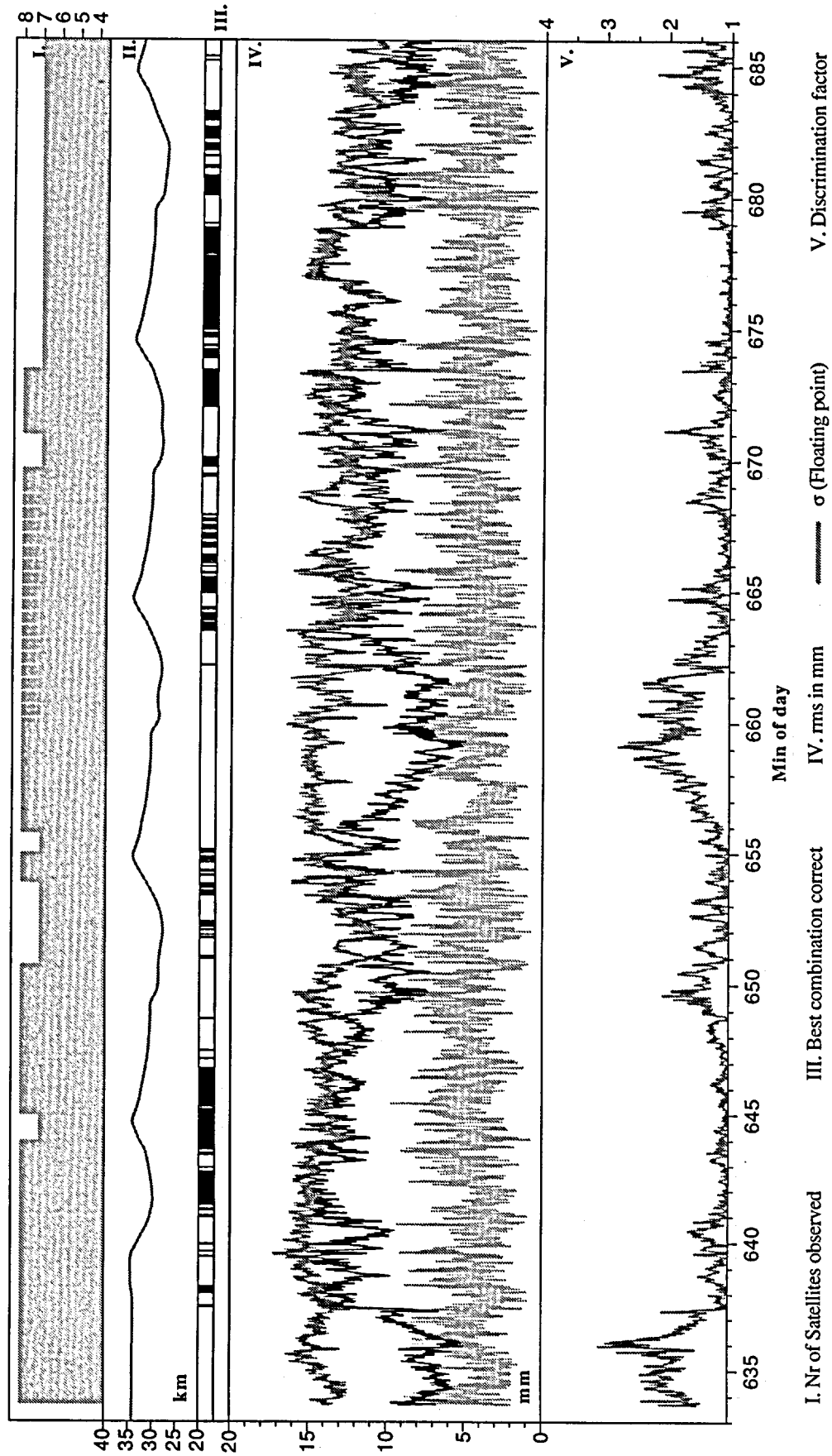

Figure 5.10 : Result of the single epoch ambiguity resolution with Zimmerwald as reference station. (Full cycle search on L2)

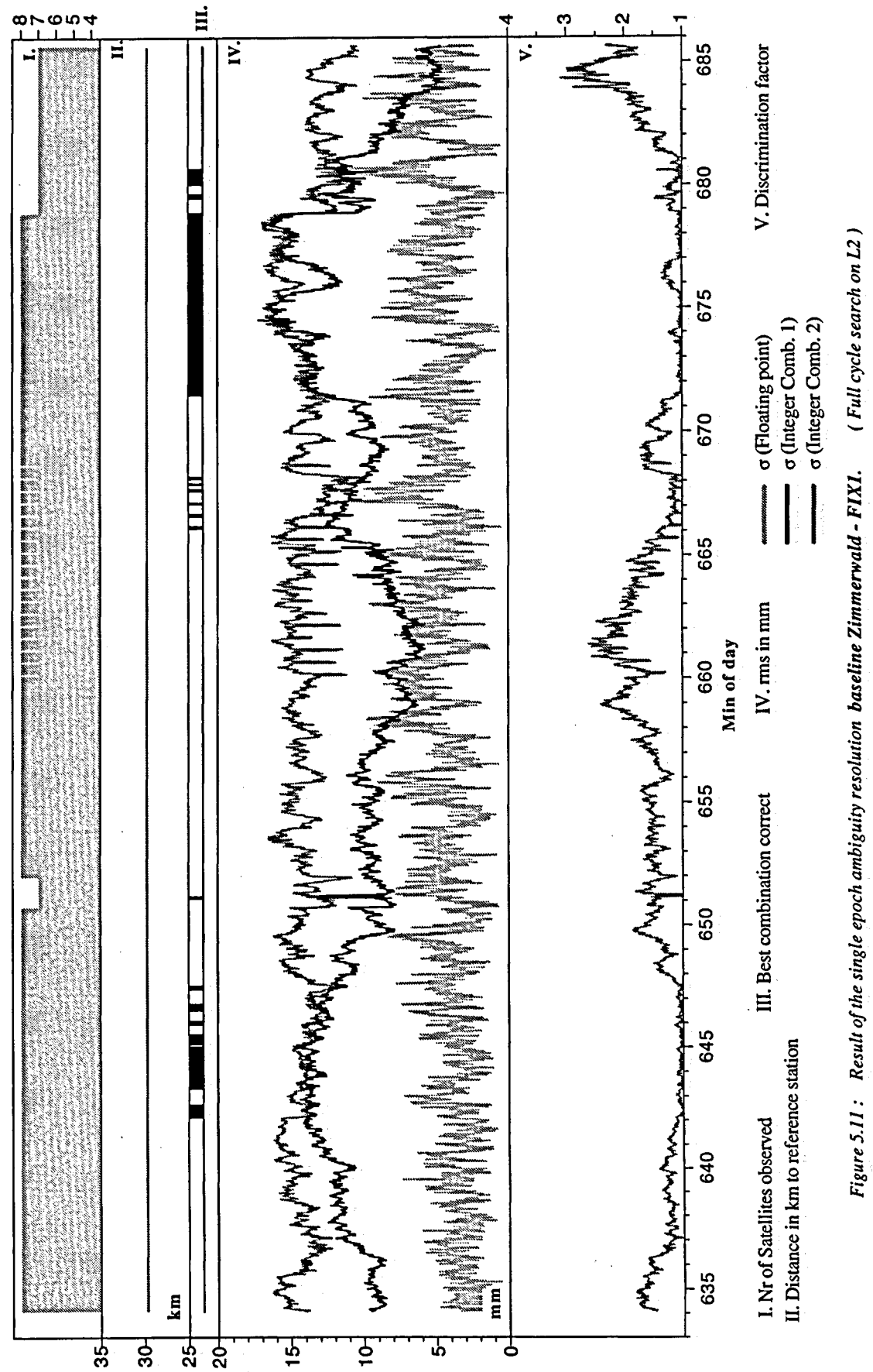

Figure 5.11 : Result of the single epoch ambiguity resolution ***baseline Zimmerwald - FIX1.*** *(Full cycle search on L2)*

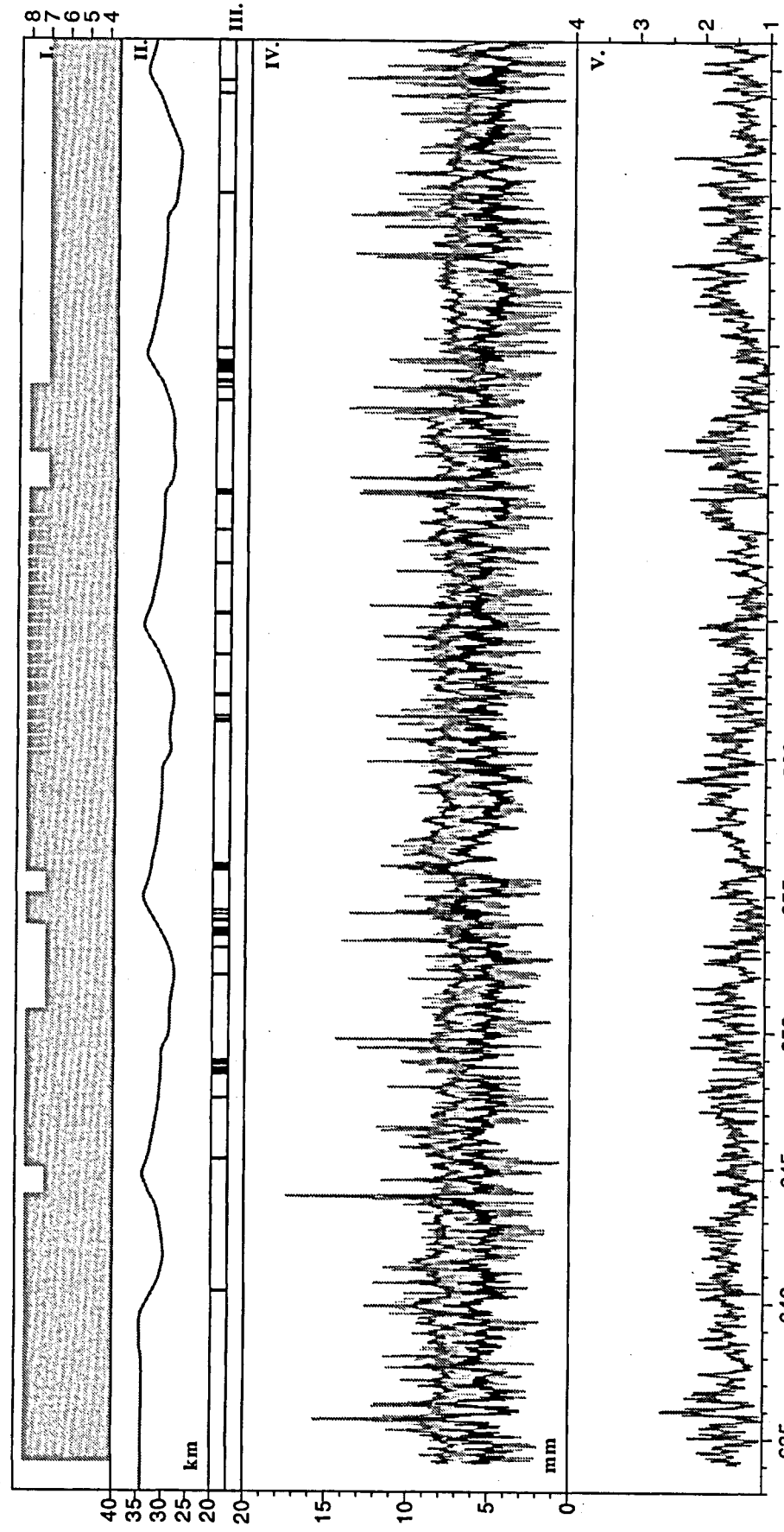

Figure 5.12 : Result of the single epoch ambiguity resolution with Zimmerwald as reference station (Full cycle search on L2)

(with additional stochastic ionospheric biases)

5.2.4 Impact of additional stochastic ionospheric biases on the ambiguity resolution

The main disturbing factor for the resolution of the ambiguities is ionospheric refraction. To account for the ionospheric path delay, the stochastic modeling as described in chapter 4.4 was introduced.

For the combination Zimmerwald - moving receiver the computation was repeated with additional differential ionospheric biases per epoch. A value of 1 cm for the white noise for a normalized differential ionospheric path delay on the L1 frequency in the zenith direction showed itself to be sufficient. No corrections for the single layer model were applied.

The results are given in figure 5.12 and show the impact of these additional biases on the ambiguity search. On the one hand the values for σ_{fl} become even more noisy, but on the other hand σ_1, the *rms* of the best solution, is significantly better and more homogenous than in the case without ionosphere biases. Due to the weakening of the geometry the level of σ_2, the *rms* of the second best integer combination, drops from about 15 mm to 8 mm. There are more possible integer combinations with a low resulting *rms*. Nevertheless, even if the geometry is weaker, the percentage of epochs with correctly resolved ambiguities is significantly higher, which shows the benefit of these additional stochastic biases to account for the ionospheric refraction.

5.2.5 Impact of short integration times on the ambiguity resolution

Even if it would be very nice to always solve the ambiguities instantaneously, a certain integration time may be necessary to stabilize and increase the reliability of the discrimination factor *DF*. The result of a computation using FIX1 as reference station and different integration times (1 sec / 15 sec / 60 sec/ 120 sec) is given in figure 5.13. The corresponding results related to Zimmerwald as reference station are drawn in figure 5.14 (without ionospheric biases) and figure 5.15. (with ionospheric biases).

It should be pointed out that for this computation the measured 2 Hz data (FIX1 and the moving receiver) was reduced to 1 Hz, thus for all 3 versions the number of epochs is identical with the integration time in seconds. For this representations the central epoch of the corresponding time intervals are used. The *DF* for the 1-sec version is identical to the instantaneous *DF* and corresponds to the results given in the figures 5.9.V, 5.10.V and 5.12.V.

For the version related to the near reference station FIX1 (figure 5.13), the best *DF* was obtained. In the case of the 15-sec integration time, one epoch was still solved incorrectly (at t = 663.25), where the *DF* value was particularly low. For all other longer integration intervals the search always led to the correct integer combination.

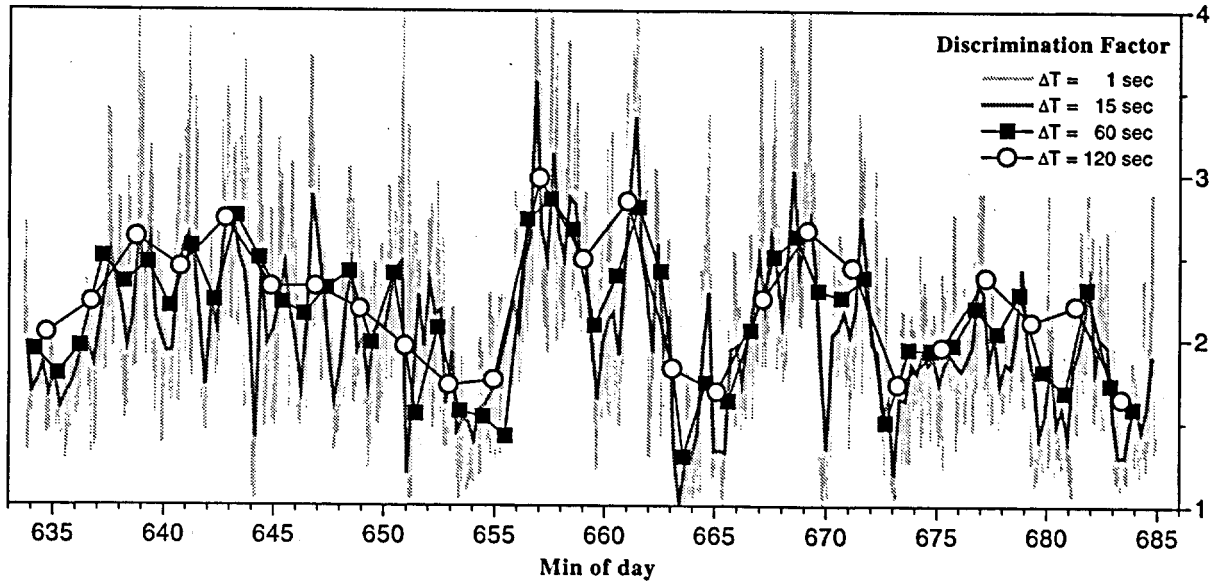

Figure 5.13 : The DF for different integration time ΔT. (reference site FIX1).

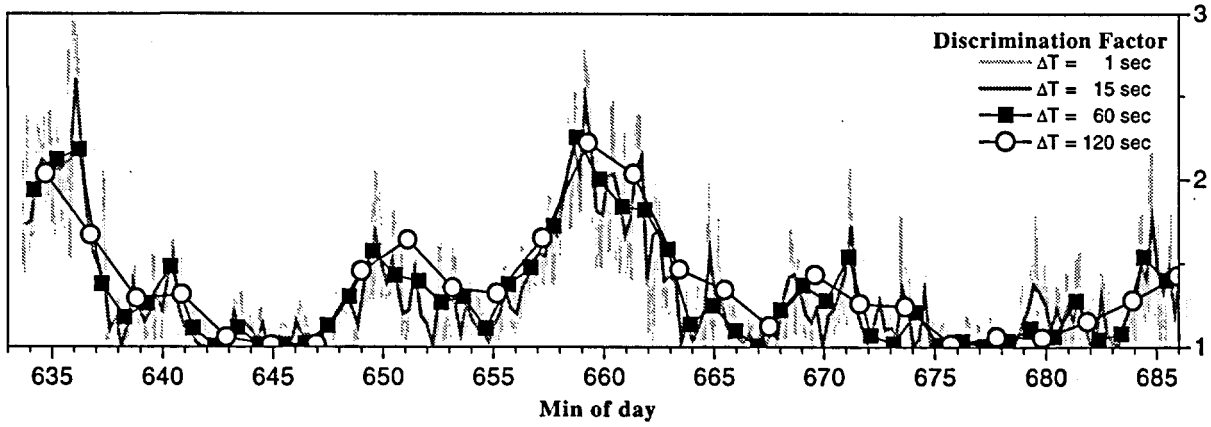

Figure 5.14 : The DF for different integration time ΔT. (reference site Zimmerwald / <u>without</u> ionospheric biases).

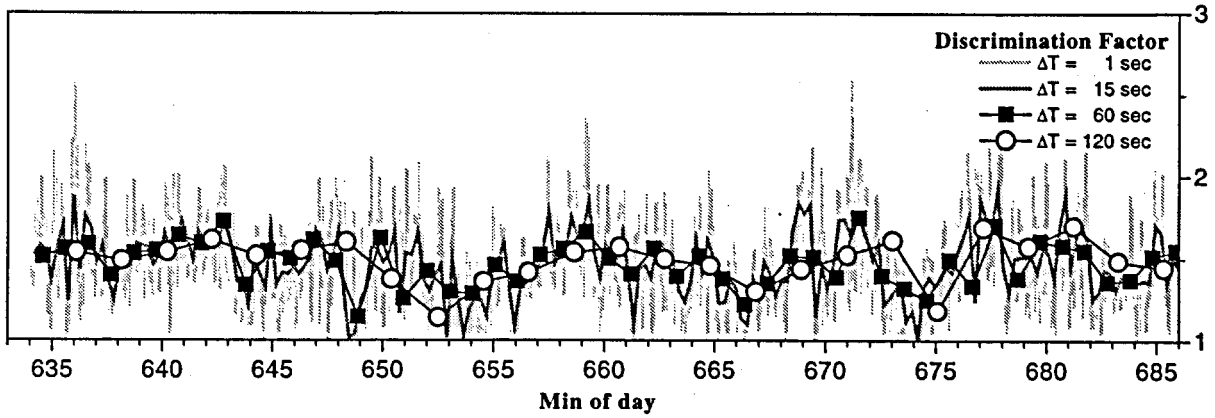

Figure 5.15 : The DF for different integration time ΔT. (reference site Zimmerwald / <u>with</u> ionospheric biases).

Using Zimmerwald as reference the *DF* is lower. In the solution where no stochastic ionospheric biases were estimated (figure 5.14), the impact of the ionospheric refraction on the *DF* is similar for all integration times from 1 sec to 120 sec. During the two time periods (from $t = 641$ to 647 and from $t = 675$ to 680) the ambiguities were solved incorrectly independent on the integration time. By introducing stochastic ionospheric biases (figure 5.15) a quite homogenous *DF* of about 1.4 led to the correct integer values for all epochs with an integration time of 60 seconds.

For all versions, as expected from theoretical considerations, a 'smoothing effect' and a slight increase in the *DF* is noticeable with increased integration time, but the basic capability of discriminating the correct solution is already present in a single epoch.

5.2.6 Comparison of the coordinates

Comparison of L1 and L2 solutions for the moving receiver :

We may derive separate ambiguity-fixed L1 and L2 solutions for the coordinates of the moving receiver using FIX1 resp. Zimmerwald as reference stations. The difference of the L2 minus the L1 solution (Fig. 5.16.) clearly shows a higher contamination by unmodeled effects in the solution related to Zimmerwald. The mean values and standard deviations of the differences are given in Table 5.6. The still good agreement of the coordinates reflects the low activity of the ionosphere in 1994.

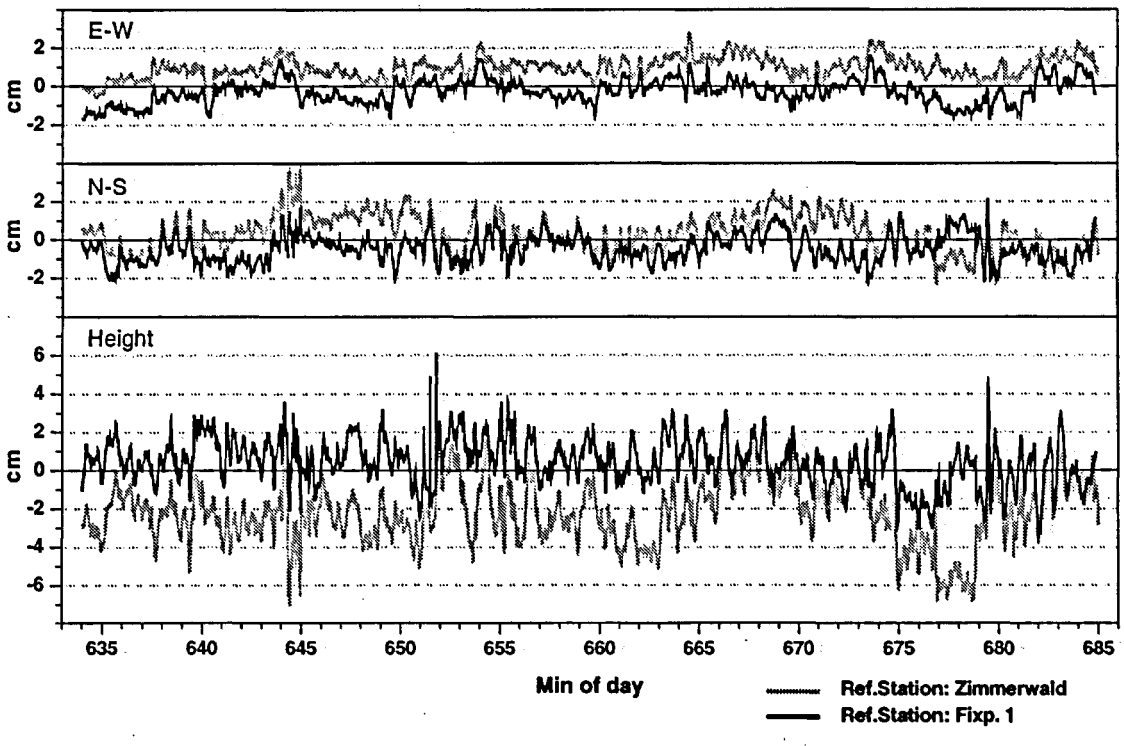

Figure 5.16 : Coordinate differences from L1- and L2- phase solutions for the two different reference stations (FIX1, Zimmerwald).

	Ref. Station : FIX1		**Ref. Station : Zimmerwald**	
	mean value	standard deviation	mean value	standard deviation
E-W	-2.8 mm	6.2 mm	9.7 mm	5.3 mm
N-S	-4.7 mm	7.2 mm	3.4 mm	9.4 mm
HEIGHT	4.5 mm	12.0 mm	-22.1 mm	16.1 mm

Table 5.7 : Mean values and standard deviations of the difference of the L1 and L2 phase solution.

Comparison of the L1 , L2 and L3 solutions for the baseline Zimmerwald - FIX1 :

The static baseline Zimmerwald-FIX1 has already been used for the investigation of the ambiguity search in the dual frequency mode. The coordinates of this baseline may also be processed in kinematic mode and compared to a reference solution. This reference solution was derived from a L3 ambiguity fixed solution using the Bernese Software (Version 3.4). The kinematic L3 solution shows good agreement in the horizontal components, but systematic errors up to 5 cm still disturb the height component (figure 5.17). The L1 and L2 solutions also show larger deviations in the horizontal components due to unmodeled systematic ionospheric path delays.

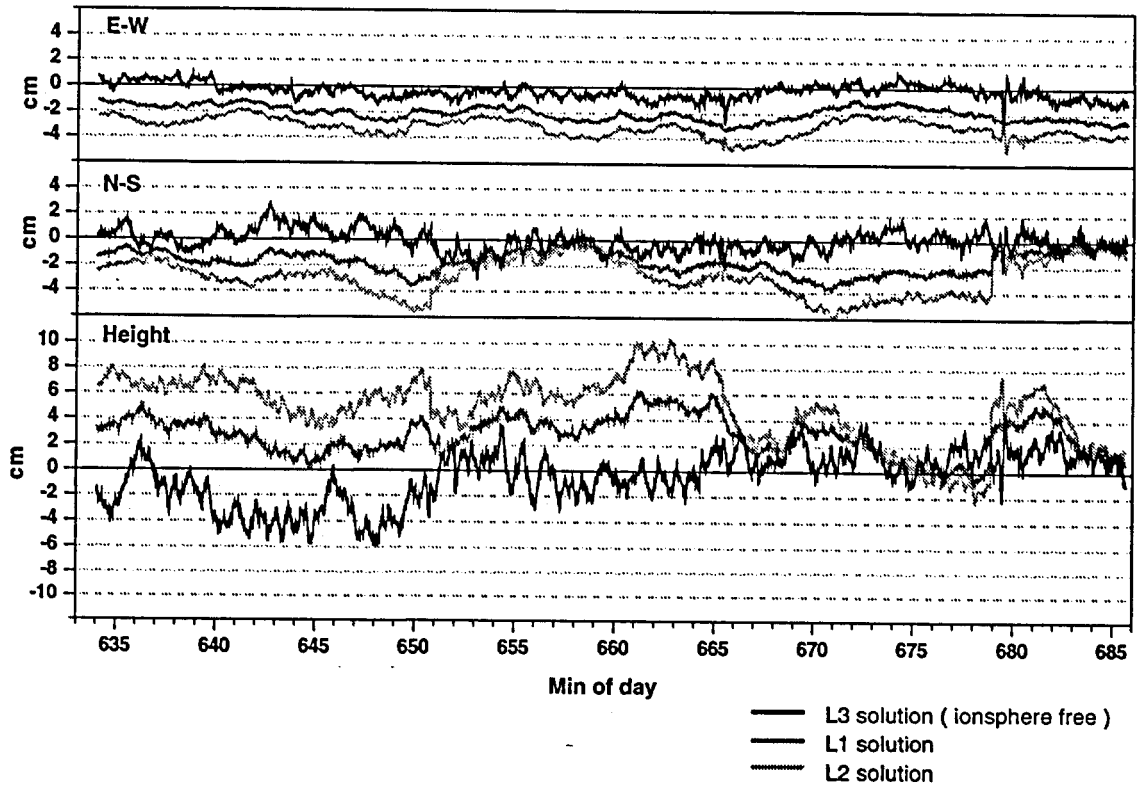

Figure 5.17 : Coordinate differences of the L1, L2 and L3 solutions for the baseline Zimmerwald - FIX1 (with respect to a static reference solution).

Comparison of the L1 solution for the moving receiver :

Using the resolved ambiguities L1 phase solutions for the moving coordinates relative to FIX1 or respectively Zimmerwald as reference station can be computed and compared. The agreement is satisfactory (see figure 5.18) although the difference indicates systematic behavior and has jumps of some centimeters coinciding with changes in the constellation. (As already mentioned L1 measurements from the reference station FIX1 were available over a longer time span than L2 measurements; thus the comparison extends over window 2).

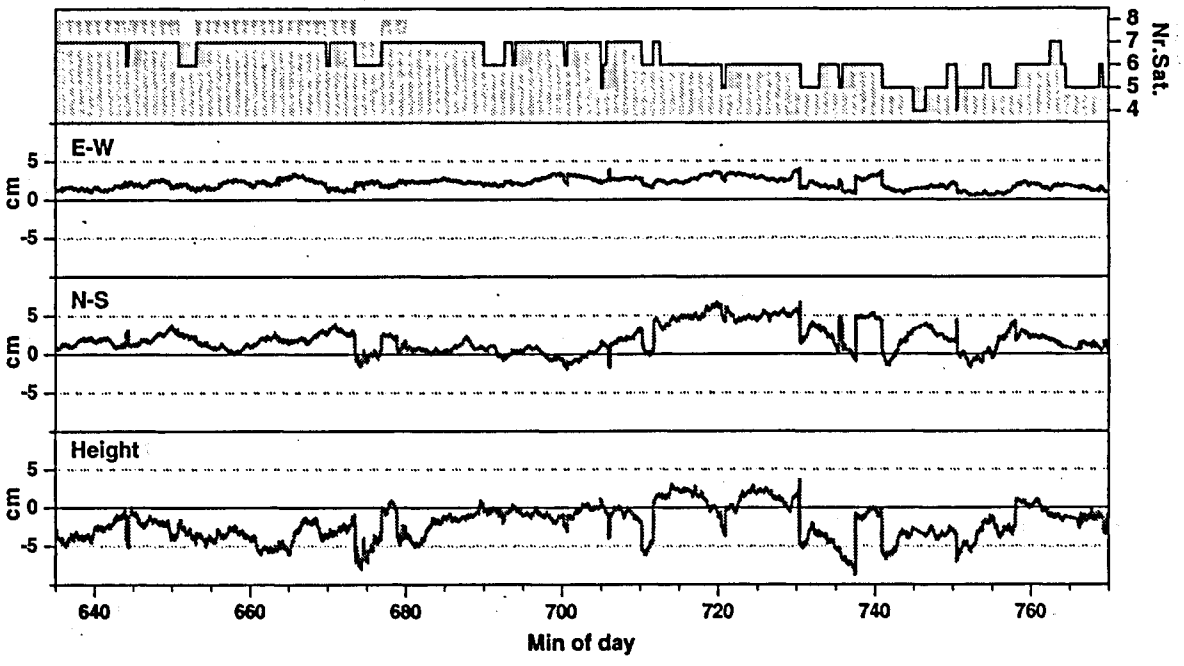

Figure 5.18 : Influence of the different reference stations on the coordinates of the moving receiver (Reference stations : FIX1 and Zimmerwald).

5.2.7 Conclusions

From these results we conclude that at least in our case ambiguity resolution in the kinematic mode is manageable over short distances provided a good constellation is available.

Even if in the kinematic mode where the geometrical constraints on the ambiguities are greatly reduced compared to the static mode it is still possible to retrieve the correct ambiguities in idealized cases even from single frequency data. The requirements in this case, however, is a strong constellation and continuous phase measurements over longer time periods. Narrow banking turns often leads to interruptions in the phase measurements. In practice there is often the unpleasant correlation that for the time period where the coordinates are of interest, losses of the phase lock to the satellites are more frequent, because flying over predefined lines requires a lot of banking turns.

In the case of dual frequency measurements, the time needed to fix the ambiguities is dramatically reduced. The ambiguities can in many cases be fixed quasi 'instantaneously'.

The example underlines the strength but also the limits of the single epoch approach for the ambiguity resolution in the dual frequency mode. In order to obtain valid results, the noise level of the correct combination must be low. Over longer distances, however, unmodeled effects, such as ionospheric, atmospheric biases, orbit errors or multipath effects are very harmful. With FIX1 as reference station (distance 2-12 km) the percentage of epochs with correctly resolved ambiguities and a good value for the corresponding *DF* is far higher as in the case where the data are related to Zimmerwald (distance 30-35 km). There is no apparent difference, at least for our data set here, between the results of using the data from a moving receiver (Zimmerwald - rover) or from a receiver at rest (Zimmerwald - FIX1). In both cases the corruption of the measurements by the ionospheric influence is similar and leads to the same lack of discrimination.

If we want to be able to resolve the ambiguities instantaneously, or within a very short time span (<2-5 min.), this will limit the maximum distance allowed from the reference station. If we take into account that the overall activity of the ionosphere in 1994 was low, this maximum distance allowed from the reference station could even be reduced (in periods or regions of high ionospheric activity). It is impossible to extract from one data set a value for such a maximum distance.

The introduction of stochastic biases to account for the ionospheric refraction may help to obtain a better, i.e. bias-free estimation, but weakens the discrimination of the integer combinations and thus requires longer integration times.

Longer integration times may help to stabilize and increase the capability to resolve ambiguities. If it is not possible to resolve the ambiguities, the floating point values may still be used in the computation of the coordinates. The quality of such a result then depends strongly on the quality of the code measurements and the integration time.

6 Comparison of GPS and Laser Tracker trajectories

6.1 Overview

The first experience with kinematic GPS at our institute was carried out in July 1989. We installed a mobile GPS receiver on a car (test in 'Rafz' July 18, 1989) and on a boat (test on the 'lake of Zurich' July 19, 1989). In both cases a reference receiver was operating in the vicinity. A first processing of the GPS data was restricted to an absolute and differential code solution [Cocard et al., 1989]. To get an impression of the quality of a code solution of the GPS trajectory a second independent tracking system was used. It consisted of a Laser Tracker allowing the measurement of a distance, a horizontal orientation and a vertical angle from the instrument to a mobile reflector ring, centered under the GPS receiver. The Laser Tracker, able to follow a moving target, collected measurements at a rate of about 1 Hz.

The results presented here are based on a later re-processing of the GPS data also integrating the phase measurements and allowing a comparison of two kinetically-determined trajectories.

Table 6.1 contains the technical specifications.

GPS	Laser-Tracker
2 TRIMBLE SST	Geodimeter 140T
single frequency measurements - C/A code - L1 phase	measurements - distance - horizontal orientation - vertical angle
Measurement rate : different - July 18, 1/15 Hz (Rafz) - July 19, 1/2 Hz (Lake of Zurich)	Measurement rate 0.8-1.2 Hz

Table 6.1 : Characteristics of the 'Laser Tracker 89' experiment

On the first day (July 18, 1989), the moving GPS receiver and the reflector ring of the Laser Tracker were installed on the roof of a car, in such a way that the GPS receiver with the integrated antenna was centered over the reflector ring. The test area was situated in a rural region with few trees and good conditions for both, GPS and Laser Tracker (Figure 6.1). The reference receiver was placed in the test field and the Laser Tracker on a hill overlooking the whole area. During the experience a certain number of stops (about 15) were made. The comparison of the coordinates was then limited to these check points.

On the second day (July 19, 1989), the configuration of the moving receiver and the reflector ring were identical, but this time they were installed on a small motorboat on the lake of Zurich (Figure 6.2). The measuring rate of the GPS was higher (1/2 Hz) than on the first day. Because no stops were possible the ambiguities had to be solved 'on the fly' using only L1 measurements.

Figure 6.1 : Overview of the test area from the site of the Laser Tracker. (Rafz / July 18, 1989)

6.2 *The Laser Tracker*

For the collection of the data and the computation of the coordinates a Laptop computer was used. To every received data set the computer time was added, and from the distance, horizontal and vertical angle the Cartesian coordinates in a not orientated local Cartesian frame were determined, thus allowing the comparison with the coordinates obtained by GPS.

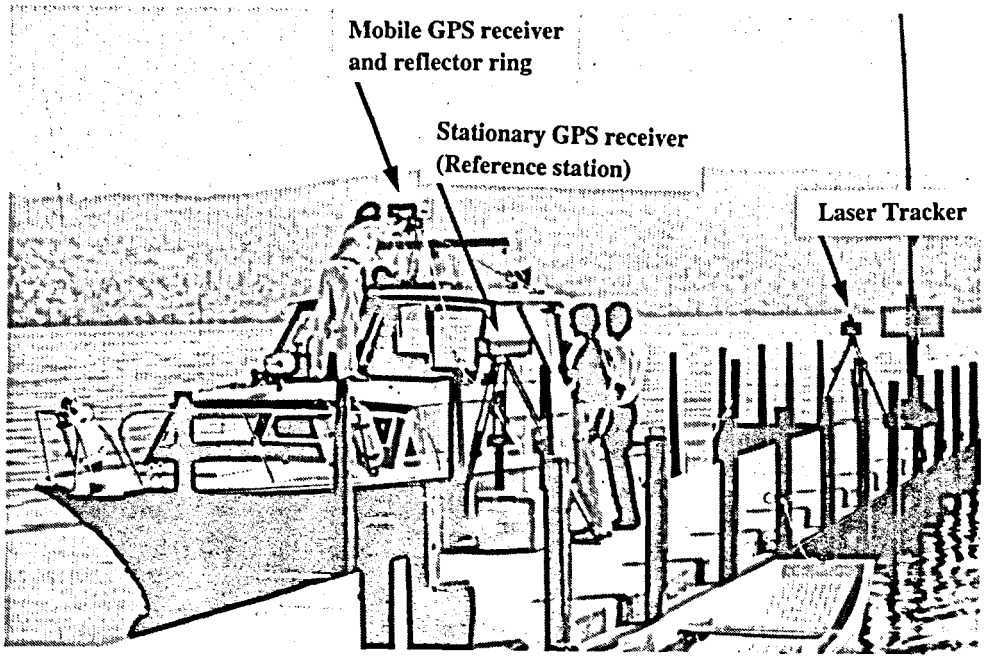

Figure 6.2 : Installation of the GPS receivers and the Laser Tracker on a boat. (Lake of Zurich / July 19, 1989).

6.3 Results of the test in 'Rafz'

6.3.1 GPS results

The collected GPS data consists of 80 minutes of data at a rate of 1/15 Hz with 5 satellites and a GDOP between 4.5 and 5. The constellation remained the same over this period. Satellites 3, 9, 11, 12, 13 were tracked.

A differential code solution and a differential code/phase solution were computed. For the code/phase solution $weight_{Code}/weight_{Phase} = 10^{-6}$ was assumed. It was possible to resolve the ambiguities by a conventional sigma dependent rounding technique. A detailed site allocation table defining 6 windows, where the moving receiver was at rest, allowed was used. In a second run the roving receiver was considered to be in motion over the entire period. In both cases it was possible to securely retrieve the integer valued ambiguities.

6.3.2 Comparison with the Laser Tracker results

For the coordinates obtained by the Laser Tracker mean values for the check points were calculated and both coordinate sets (GPS and Laser Tracker) were compared. Because the coordinate systems are different, a 3-D Helmert transformation had to be performed first. The resulting residuals after the transformation are given in Table 6.2. The coordinate system in which the residuals are given is the local coordinate system as defined by the unoriented Laser Tracker.

SiteNr	Residuals (Y-axis)	Residuals (X-axis)	Residuals (Height)
100	0.047	-0.023	-0.153
101	0.023	-0.128	-0.109
102	0.039	-0.173	0.011
S02	0.034	0.053	0.157
S04	-0.012	0.048	0.118
S05	-0.020	0.029	-0.004
S06	0.022	-0.066	-0.041
S07	-0.063	0.137	0.061
S08	-0.025	0.225	0.025
S09	-0.039	0.147	0.005
S10	-0.018	-0.177	-0.051
S12	-0.023	-0.004	-0.044
S13	0.061	0.174	0.080
S14	-0.065	-0.329	0.058
S15	0.038	0.087	-0.114

Table 6.2 : Residuals in meters between Laser Tracker and GPS coordinates at the check points.

The mean residual of one coordinate is 0.074 m. The difference between the y and x coordinate is due to the different accuracy of the Laser Tracker, since the x coordinate depends mainly on the distance and the y coordinate on the horizontal angle. The agreement corresponds to what can be expected.

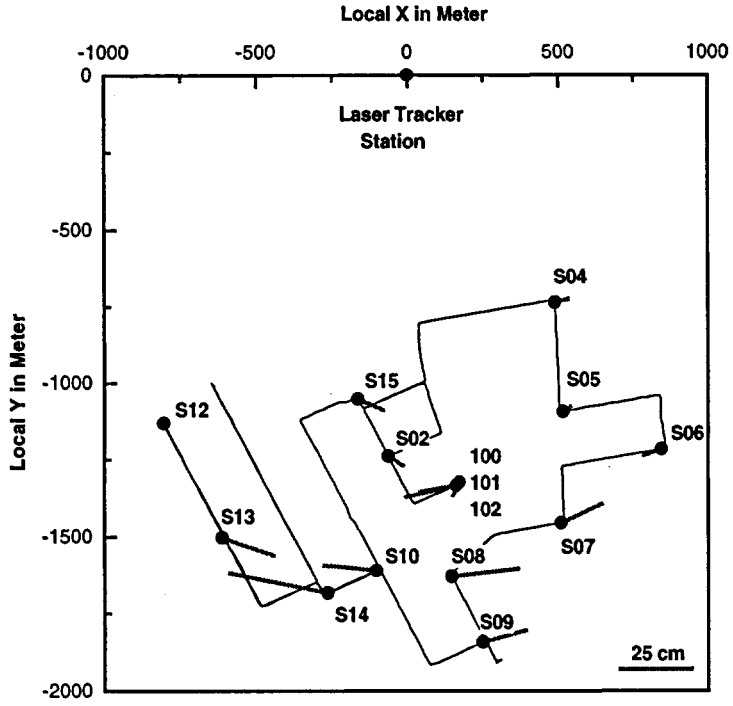

Figure 6.3 : Differences at the stationary sites between GPS and Laser Tracker solutions.

6.4 *Results of the test on the 'Lake of Zurich'*

6.4.1 *GPS results*

On the second day the measuring frequency of the GPS was 0.5 Hz. Because no stops could be made, the ambiguities had to be determined 'on the fly', using L1 measurements only. This was possible with the search algorithm described in chapter 4. The satellite constellation remained the same over the period of the survey. Satellites 3, 9, 11, 12, 13 were tracked. The duration of the entire experiment was about 60 minutes.

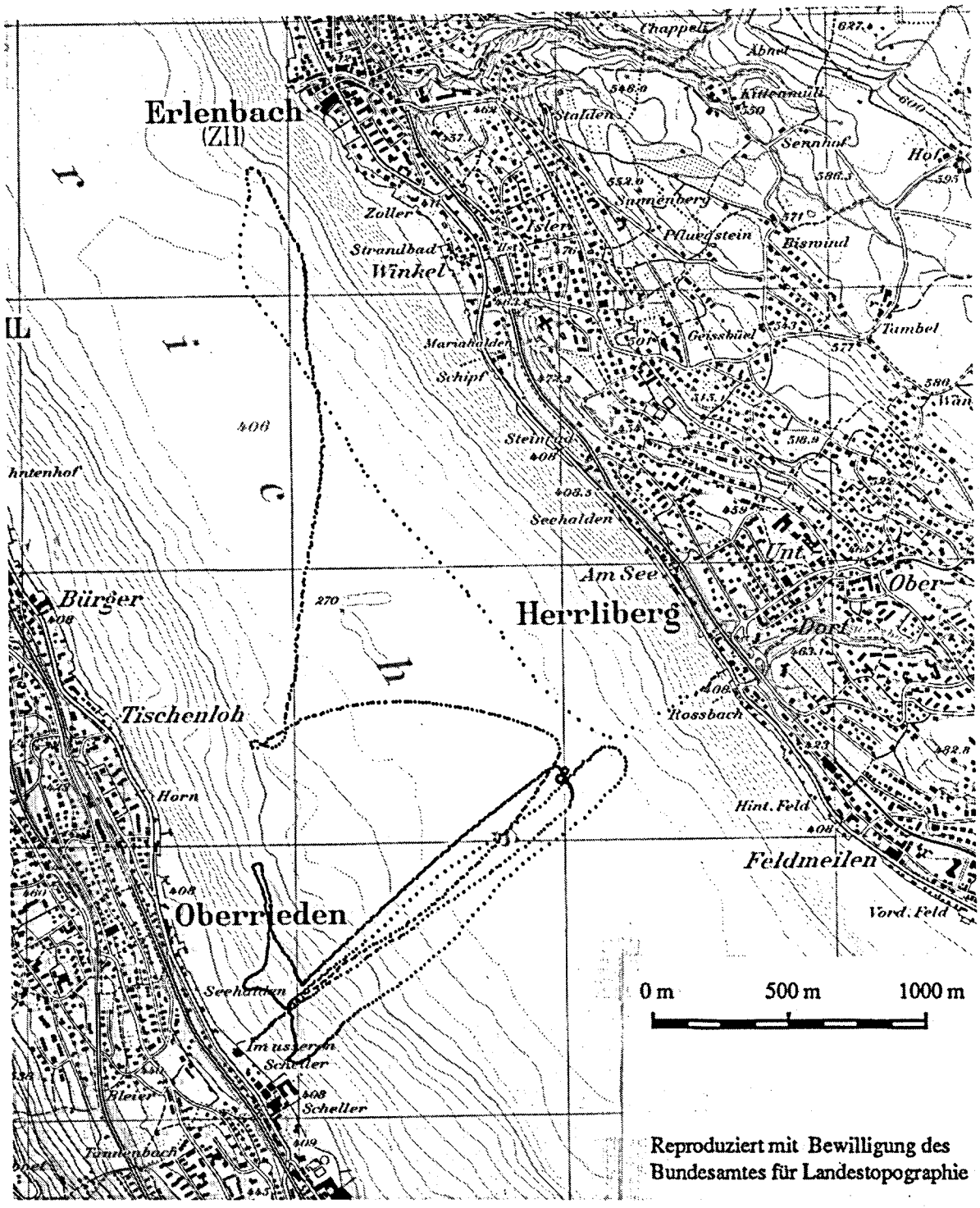

Figure 6.4 : GPS trajectory of the boat on the lake of Zurich (July 19, 1989)

The result of the search algorithm showed that due to the poor geometry of the constellation different possible combinations for the ambiguities were possible. Nevertheless the combination, considered by the algorithm as best, was the correct one. The stability of the height and the known height difference to the reference receiver proved this statement. Table 6.3 gives an overview of the result of the search.

Configuration parameters

measurements	C/A-Code L1-Phase
Nr of satellites	5
Nr of DD-Ambiguities	4
Reference Satellite	SVN12
rms(code)/rms(phase) a priori	1000
rms (float.)	**0.0076**

		Diff. to floating point solution [cycles]				Diff. to best solution			
	SVN	3	11	9	13	3	11	9	13
	rms (fixed)								
1	0.0077	1.5	-3.4	-2.9	-0.5	-	-	-	-
2	0.0082	2.5	-3.4	-2.9	-0.5	1	0	0	0
3	0.0086	0.5	-3.4	-2.9	-0.5	-1	0	0	0
4	0.0090	-3.5	0.6	1.1	0.5	-5	4	4	1
5	0.0092	2.5	-0.4	-0.9	-0.5	1	3	2	0
6	0.0106	-0.5	-3.4	-2.9	-0.5	-2	0	0	0
7	0.0111	-2.5	0.6	1.1	0.5	-4	4	4	1
8	0.0114	1.5	-0.4	-0.9	-0.5	0	3	2	0
9	0.0127	-2.5	2.6	2.1	0.5	-4	6	5	1
10	0.0128	-3.5	2.6	2.1	0.5	-5	6	5	1

Table 6.3 : Summary of the results of the ambiguity search, showing the 10 best integer combinations and their resulting rms.

The 10 best combinations and the differences in the corresponding integer valued ambiguities with respect to the floating point values as well as with respect to the best integer combination (version 1) are given in units of L1 cycles. It is interesting to see the results, obtained by any of these combinations and their influence on the coordinates. The difference in the coordinates of a solution obtained with a false ambiguity set is, in a first approximation, a linear function of time when compared to the 'true' solution. In our case the offsets are on the order of 1-2 meter and the linear drifts up to 50 cm/h. (Figure 6.5. shows the influence on the height component).

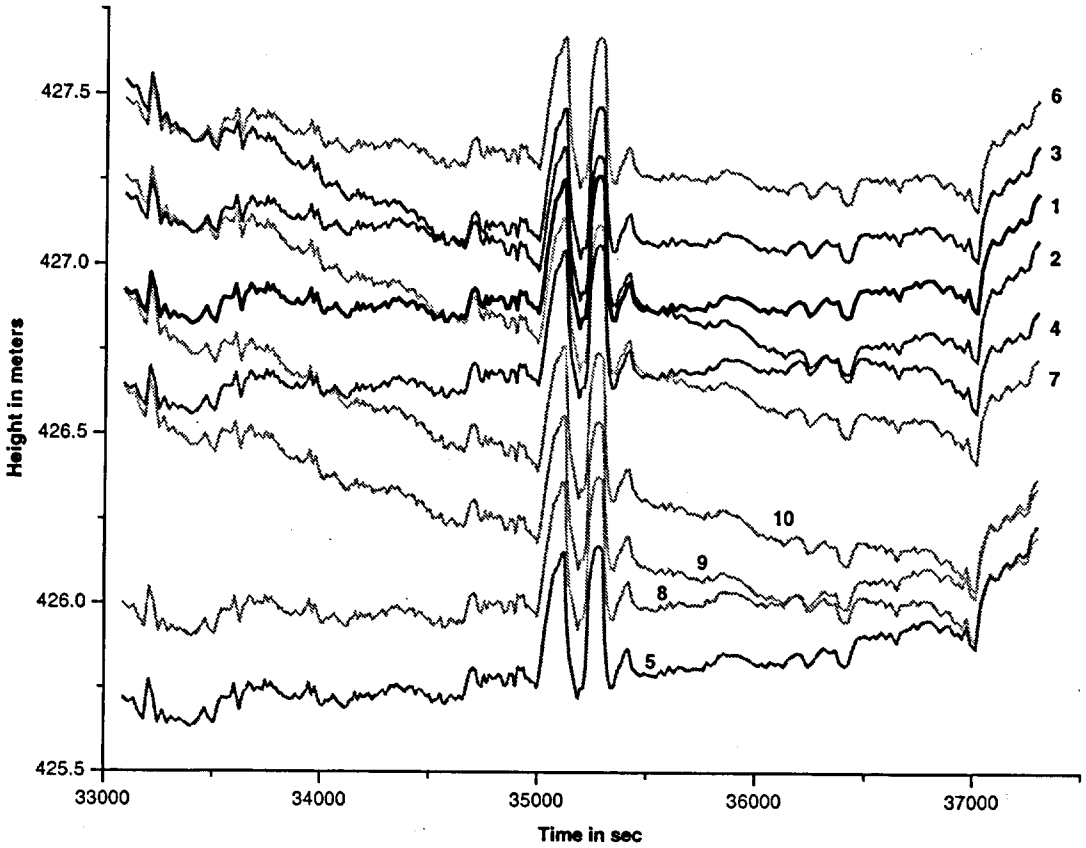

Figure 6.5 : Influence of wrong integer ambiguities on height determination.

If we assume that the first ambiguity set with $\sigma_0 = 7.7\ mm$ is the correct one, this solution can be used as a reference. The coordinate differences are fitted with a simple polynomial in time :

$$\Delta X_i(t) = \sum_{j=0}^{n} a_j (t - t_0)^j \qquad (6.1)$$

In particular the linear approximation (n=1) and the quadratic approximation (n=2) are of interest. The result of these fits are given in Table 6.4. The *rms* of the fits show that the quadratic terms are still significant.

	linear fit			quadratic fit			
	rms[m]	a0[m]	a1[m/h]	rms[m]	a0[m]	a1[m/h]	a2[m/h2]
	version 2			ambig. error. :	1	0	0 0
E-W	0.0037	-0.1167	-0.1873	0.0012	-0.1254	-0.1453	-0.0358
N-S	0.0061	-0.0433	-0.0664	0.0005	-0.0279	-0.1407	0.0633
H	0.0010	-0.2760	0.1185	0.0006	-0.2780	0.1276	-0.0078
	version 3			ambig. error. :	-1	0	0 0
E-W	0.0037	0.1167	0.1873	0.0012	0.1254	0.1450	0.0360
N-S	0.0061	0.0433	0.0663	0.0005	0.0279	0.1407	-0.0633
H	0.0010	0.2760	-0.1184	0.0006	0.2780	-0.1282	0.0083
	version 4			ambig. error. :	-5	4	4 1
E-W	0.0290	1.5947	0.3915	0.0008	1.5217	0.7437	-0.3002
N-S	0.0266	0.7035	-0.0036	0.0014	0.6366	0.3190	-0.2751
H	0.0160	0.5825	-0.8332	0.0018	0.6225	-1.0261	0.1644
	version 5			ambig. error. :	1	3	2 0
E-W	0.0095	0.2565	-0.5768	0.0011	0.2328	-0.4626	-0.0973
N-S	0.0090	0.4664	-0.4174	0.0009	0.4888	-0.5256	0.0922
H	0.0013	-1.2114	0.1990	0.0011	-1.2100	0.1919	0.0061
	version 6			ambig. error. :	-2	0	0 0
E-W	0.0073	0.2333	0.3749	0.0024	0.2507	0.2910	0.0715
N-S	0.0122	0.0868	0.1326	0.0007	0.0561	0.2810	-0.1265
H	0.0019	0.5520	-0.2368	0.0011	0.5560	-0.2559	0.0162
	version 7			ambig. error. :	-4	4	4 1
E-W	0.0325	1.4779	0.2043	0.0013	1.3962	0.5986	-0.3362
N-S	0.0205	0.6600	-0.0698	0.0011	0.6084	0.1791	-0.2123
H	0.0152	0.3065	-0.7147	0.0023	0.3443	-0.8974	0.1557
	version 8			ambig. error. :	0	3	2 0
E-W	0.0064	0.3732	-0.3894	0.0022	0.3582	-0.3171	-0.0616
N-S	0.0030	0.5098	-0.3511	0.0012	0.5169	-0.3852	0.0290
H	0.0021	-0.9353	0.0806	0.0017	-0.9320	0.0643	0.0138
	version 9			ambig. error. :	-4	6	5 1
E-W	0.0253	1.6412	-0.0614	0.0008	1.5776	0.2451	-0.2613
N-S	0.0205	1.0065	-0.2815	0.0020	0.9551	-0.0338	-0.2112
H	0.0176	-0.3335	-0.6133	0.0008	-0.2893	-0.8265	0.1818
	version 10			ambig. error. :	-5	6	5 1
E-W	0.0219	1.7578	0.1260	0.0019	1.7029	0.3910	-0.2259
N-S	0.0266	1.0498	-0.2151	0.0023	0.9830	0.1069	-0.2745
H	0.0184	-0.0575	-0.7318	0.0012	-0.0113	-0.9544	0.1898

Table 6.4 : Results of linear and quadratic interpolation

6.4.2 *Comparison with the Laser Tracker results*

Because the Laser Tracker and the GPS measurements could not be synchronized it is not possible to compare the two coordinate series directly. (In the 'Rafz'-experiment a direct comparison was possible for the fixed points of the trajectory).

Therefore in a first step a transformation had to be applied. If we think of the trajectory as a wire with a constant density, then the moment of inertia of this body does not dependent on the coordinate system. This property allows us to determine the parameters of a Helmert transformation without having to synchronize and to establish a correspondence between the points in the two data sets.

For every data-set the center of mass was calculated by :

$$\vec{c} = \frac{1}{n}\sum_{i=1}^{n}\vec{x}_i \tag{6.2}$$

In addition the tensor of the moment of inertia M was computed as :

$$M = \frac{1}{n}\sum_{i=1}^{n}(\vec{x}_i - \vec{c})(\vec{x}_i - \vec{c})^T \tag{6.3}$$

The matrix M may be diagonalized : $M = RDR^T$ (6.4)

Normalization leads to the scaling factor m : $\overline{D} = \frac{1}{trace(D)}D = m^2 D$ (6.5)

A part from measurement errors and discretization effects, the diagonal matrix $\overline{D}$ must be the same for the two data-sets. This fact allows us to establish the following identity for the two data sets $\vec{x}_1(t)$ and $\vec{x}_2(t)$:

$$m_1 R_1(\vec{x}_1(t) - \vec{c}_1) \equiv m_2 R_2(\vec{x}_2(t) - \vec{c}_2) \tag{6.6}$$

By rearranging this equation, one obtains the equation for the Helmert transformation :

$$\vec{x}_1(t) = mR\vec{x}_2(t) - \vec{x}_0 \tag{6.7}$$

with $m = m_2/m_1$ and $R = R_1^T R_2$ and $\vec{x}_0 = \vec{c}_1 - mR\vec{c}_2$

The next step consists of synchronizing the two data sets. Again a function which is independent of the coordinate system is used . For this purpose the distance function is best suited:

$$d(t) = \|\vec{x}(t) - \vec{c}\| \tag{6.8}$$

Because the two distance functions $d_1(t)$ and $d_2(t)$ describe in principle the same curve the unknown Δt can be determined by correlation techniques. The maximum of the cross-correlation function

$$\phi(\tau) = \int d_1(t) d_2(t-\tau) dt \tag{6.9}$$

may be calculated, using FFT calculus, where the convolution corresponds to a simple multiplication in the frequency domain and the synchronization error becomes:

$$\Delta t = \max(\phi(\tau)) \tag{6.10}$$

After these transformations it is now possible to compare the two data sets, using an 'extended' Helmert transformation. For this final adjustment, the more dense data set (Laser Tracker) is interpolated to the GPS epochs, thus creating the point correspondences in the two data sets. A part from the classical parameters (3 translations, 3 rotations, 1 scale) an additional small synchronization error is taken into account, using the velocity derived from the Laser Tracker coordinates.

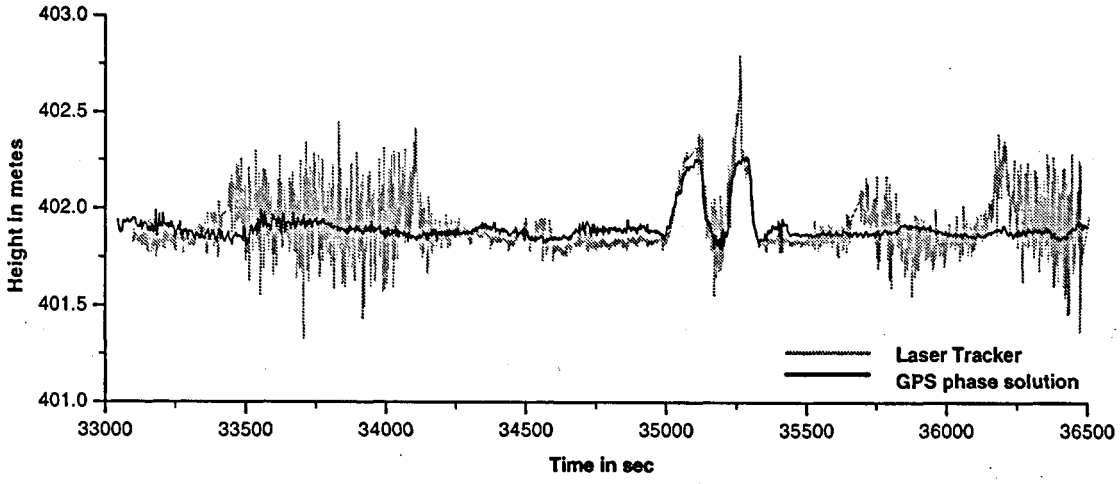

Figure 6.6 : The height component as function of time derived from GPS and Laser Tracker.

The residuals of the transformation, i.e. the coordinate differences after the transformation are given in Figure 6.7 as a function of time. The *rms* values over the total time span are

E-W = 0.361 m N-S = 0.405 m Height = 0.162 m

The two excursions around epoch 35200 correspond to loops which may be seen in Figure 6.4. Figure 6.8 focuses on these loops. Clearly there is a considerable increase in accuracy of the phase solution compared to the code-only solution.

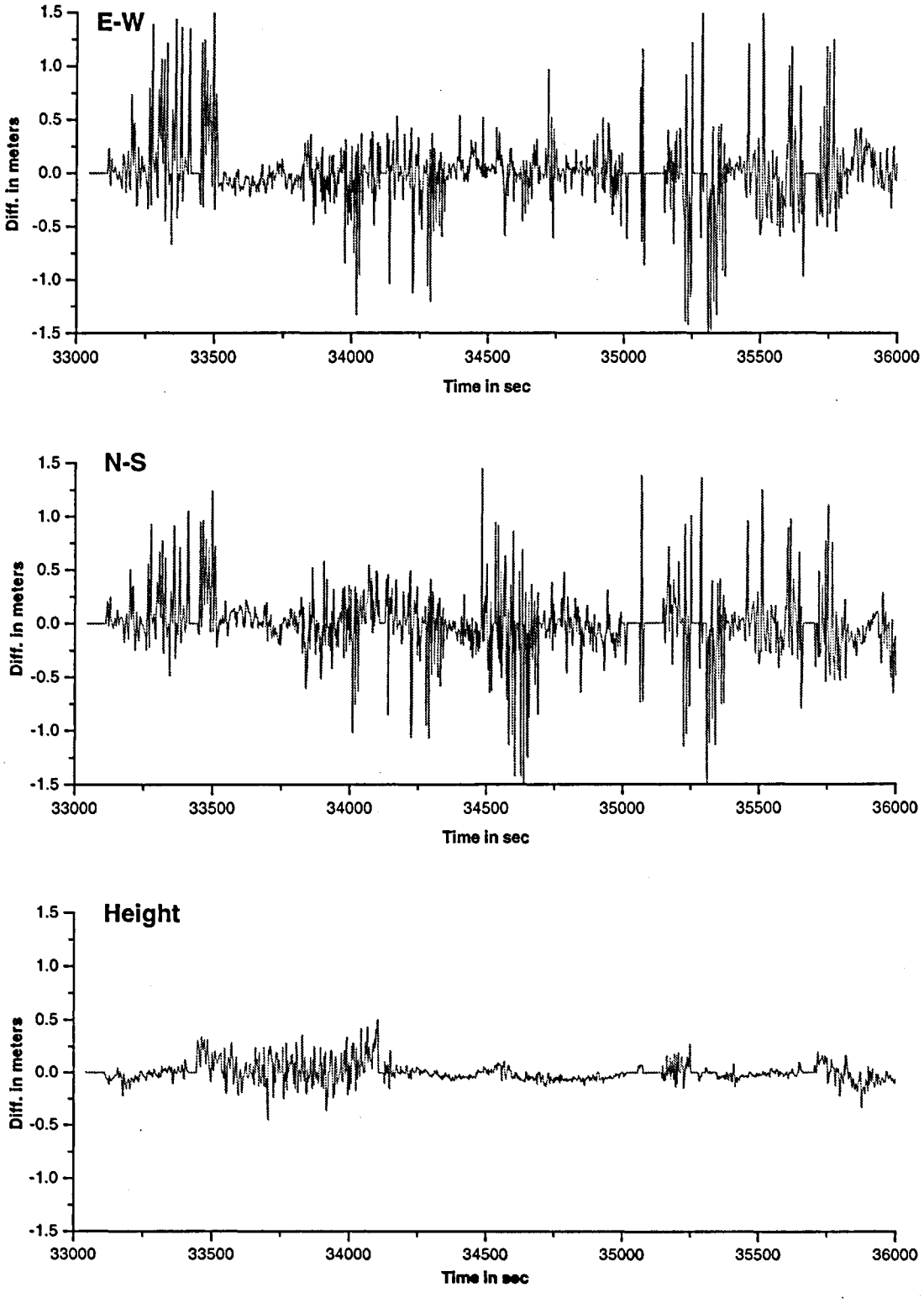

Figure 6.7 : Residuals between GPS and Laser Tracker result ('Lake of Zurich').

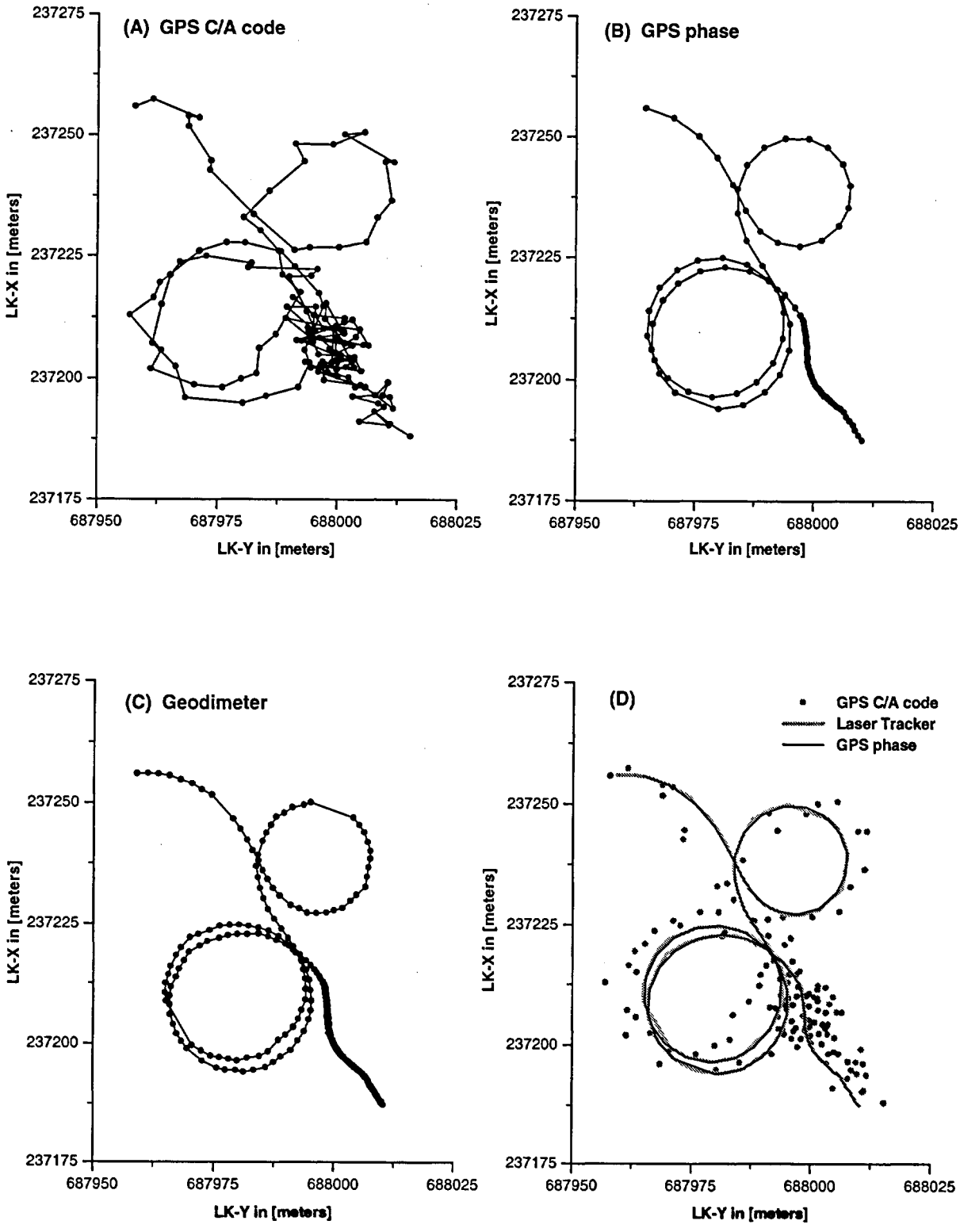

Figure 6.8 : Part of the trajectory (corresponding to the two excursions in Figure 6.7) gives an impression of the accuracy of the different methods involved. The coordinates are given in the Swiss projection system. (GPS code solution / GPS phase solution / Laser Tracker).

7 Kinematic GPS for Aerophotogrammetry

7.1 Introduction

Aerophotogrammetry is one of the various applications of kinematic GPS. In a bundle adjustment of an aerotriangulated photogrammetric block, the unknown parameters of the external orientation contains the coordinates of the projection centers of the camera and have to be determined. Even if these coordinates are normally of no interest in photogrammetry, they are inherent in the geometrical model. Conventionally, for the stabilization and orientation of a photogrammetric block, a certain amount of control points on the ground are required. Where the coordinates of the projection centers are determined by kinematic GPS, however, this information may be used in the bundle adjustment [Colomina, 1989]. In a study with synthetic data [Gruen et Runge, 1988] the accuracy potential of a combined GPS/bundle solution was demonstrated and the favorable structure of such a system with respect to the determinability of the additional parameter for self-calibration was shown. The consequence is a significant reduction of the number of control points on the ground needed for orientation. The basic idea is to replace the control points on the ground by control points on the flight trajectory (projection centers of the camera) which are determined by GPS.

7.2 Strategies for the recovery of the GPS trajectory

Different strategies for the disposition of the photogrammetric block, the processing of the projection centers from kinematic GPS, and the introduction into the photogrammetric bundle adjustment have been studied. The crucial question is whether it is possible to fix the ambiguities to integers. If this is possible the resulting coordinates of the ambiguity-fixed solution are of a much higher quality than in the case where real values for the ambiguities have to be used.

7.2.1 Continuous GPS trajectory after static initialization

A first approach for the recovering of kinematic GPS coordinates with integer ambiguities consists of using a static initialization phase before the flight. The reference receiver and the roving receiver in the airplane at rest collect GPS data for some 10 to 20 minutes. This data set may then be treated as a conventional static set and ambiguity fixing should not pose a problem. This initialization may also be repeated at the end of the flight, allowing the reconstruction of the trajectory from the end. During the kinematic phase the epochs are determined sequentially. If from one epoch to the next uninterrupted phase data to at least 4 satellites (with a reasonably good PDOP) is available, the coordinates of this new epoch may be computed. If new satellites enter the processing at a certain epoch during the flight, the integer values of their related ambiguities may easily be determined from these coordinates. This procedure provides good results, if it works. The main problem consists of major inter-

ruptions in the phase measurements. The integer values of the ambiguities are no longer valid and usually cannot be recovered. With real data, in particular of some years ago when the constellation was poor, this concept could not be used in an operational environment for aerotriangulation. A more robust method for dealing with this problem was required.

7.2.2 *Line-specific GPS trajectory from a floating point ambiguity solution*

Here we restrict the processing of the kinematic GPS data to the time windows of interest during the survey [Friess, 1990] and we treat the GPS data of every line separately. The typical duration of a line is on the order of a few minutes. If we take e.g. a length of 15 km and a velocity of 50 m/s we would end up with a flight time of 5 minutes for every line. In the single frequency mode it is usually not possible to fix the ambiguities within 5 minutes of data. It has to be pointed out that this concept was developed at a time when dual-band receivers were not commonly used in the kinematic mode.

If the ambiguities could not be resolved (normal case), the best possible real values for the ambiguities derived from the code plus phase measurements may be used instead. Consequently the GPS coordinates are affected by these wrong ambiguity values for every individual line. In a first approximation the coordinates of one line show linear behavior (offset and linear drift) compared to an ambiguity-fixed solution. If we want to introduce the projection centers related to this GPS information into a combined GPS/bundle block adjustment, we have to introduce in addition unknown drift-parameters for the GPS coordinates. They have to be determined by the constraint of the photogrammetric block itself. With a normal block geometry, consisting of a certain number of parallel strips, however, the constraint is weak and therefore adding two perpendicular strips at the end of the block was proposed in order to increase the determinability of the drift parameters [Ackermann, 1992]. Results published in [Høgholen, 1993] show that instead of perpendicular strips the block may also be stabilized with an appropriate distribution of control points along these two borders of the blocks.

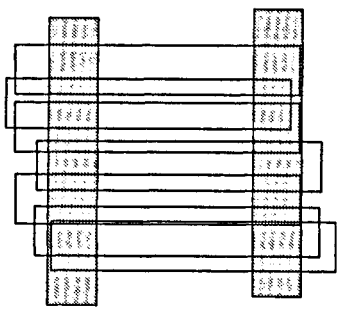

Figure 7.1 : Additional strips at the ends of the block

This approach is robust and therefore has big advantages. It only requires good GPS data in the single frequency mode during the flight over the surveying lines and is not affected by possible major interruptions in the phase measurements at the turns. Moreover the distance to the reference station is of secondary importance. The disadvantage, however, is the additional two strips. For a quadratic block of 10 strips e.g. this represents an increase of 20% for the photogrammetric images. In mountainous areas, where the strips are flown parallel to the terrain slope at different heights in order to have a more or less homogeneous scale over the entire block, the two perpendicular lines may be difficult or even impossible to achieve.

We will see in our example that the drift parameters are only necessary if it is not possible to resolve the integer ambiguities and the real values used are wrong by several cycles.

Not every banking turn produces major breaks. Even in the case where the integer values of the ambiguities cannot be retrieved a better estimate for the GPS coordinates is obtained by using the total amount of data in order to estimate the real values of the ambiguities. This procedure allows to selectively set up new sets of drift parameters only after interruptions in the GPS phase measurements.

7.2.3 GPS trajectory with ambiguities fixed 'on the fly'

The use of dual-band receivers in the kinematic mode changes the situation dramatically and makes possible the following approach. Dual-band instruments and a good local satellite constellation allow the fixing of the ambiguities even for short data spans. It also allows the use of drift-free GPS coordinates from an ambiguity fixed solution, making the introduction of additional drift parameters into the bundle adjustment obsolete. The advantage has to be seen in the fact that a conventional block geometry without additional strips is possible. There is, however, a disadvantage : it seems that the distance to the reference receiver must be kept short. This means in practice that a GPS reference station in the area of the block is required.

7.3 Results of the aerophotogrammetric test flight 'Uster 92'

The results presented here are part of the ETH project 'GPS-supported aerial triangulation' and have already partially been published in [Gruen et al. 1993a, 1993b], where the impact of GPS on photogrammetry is discussed in more detail. We will confine the discussion to the GPS problematic and use aerotriangulation only for external comparison purposes. Note that aerotriangulation is one of the very few possibilities allowing accurate external validation of kinematic GPS results.

This project was realizable thanks to the Swiss Cadastral Authority (Vermessungsdirektion), who provided the aircraft (a Twin-Otter) and the photogrammetric camera for the collection of a test data set. The camera operator R. Huebscher, who was always very responsive to our requests, was essential to the success of the experiment.

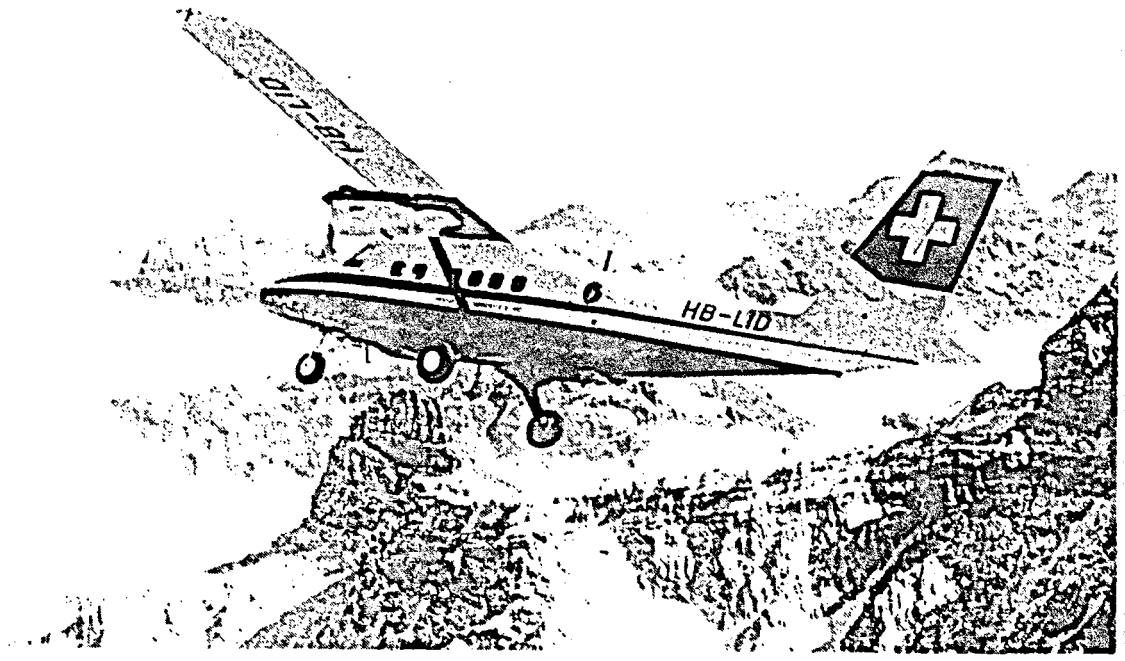

Figure 7.2 : Twin-Otter of the Swiss Cadastral Authority, used for the photogrammetric flight.

7.3.1 Test configuration and data acquisition

The selected test field of Uster near Zurich is well suited for the purpose. Its proximity to the airport and the availability of about 100 high quality reference points make it an ideal field for our investigation. The geodetic network points are known to have a coordinate accuracy of about 5 mm in planimetry and about 6 mm in height. The 94 points which were used in this test are distributed quite homogeneously over the entire area.

In March 1992, a GPS observation window of about 1 ½ hours with a good constellation (up to 6 satellites) was available. This window was used for two flights, taking place on two consecutive days. On the first day (March 4, 1992) five of eight strips were observed and on the second day (March 5, 1992) the remaining three strips. This short duration allowed collection of the GPS data in the internal memories of the receivers.

A reference receiver on the ground was installed at the airport (see figure 7.5) and two roving receivers were mounted on board the airplane. Trimble SST receivers belonging to our institute were used. The reference and one of the roving were dual frequency receivers. The second roving receiver, however, was a single frequency receiver. Its data was not used. The measurement rate was 1 Hz. Phase measurements on both frequencies, C/A-code measurements on the L1 band, and P code measurements on the L2 band were recorded. During the flight the data was only collected and then downloaded. The processing was done in the off-line mode.

The photogrammetric camera was a Wild RC20 with a camera constant of 15 cm. Eight strips with a lateral overlap of 60 percent were flown at a height of about 1500 m over the ground, leading to an image scale of 1:10'000. Within each strip, 19 pictures were taken with an overlap of 80 percent. For processing, only every second photograph was used, which led to an 60 percent forward overlap.

The project parameters are summarized in table 7.1.

Data set : AEROPHOTOGRAMMETRY BLOCK 'USTER'	
Test Area	Uster, near Zurich (CH)
Size	7.5 km by 9.5 km
Mean elevation	500 m
Number of check points	94
Airplane	Twin Otter
Dates of flights	March 4, 1992 (5 strips)
Flying height over ground	March 5, 1992 (3 strips)
Duration of the flights	about 1-1.5 hours
Photogrammetric block	
Photogrammetric camera	Wild RC20
Camera constant	153 mm
Image scale	1 : 10'000
Forward overlap	80 % (60 % used for processing)
Lateral overlap	60 %
Number of strips	8
Flight direction	Equal (South -North)
Number of exposures	152 (8 strips times 19 images per strip)
Number of photographs used	80
GPS receivers	Trimble SST
Code measurements	C/A code on L1
	P code on L2
Phase measurements	L1 &L2 (Full cycle on L2)
Measurement rate	1 Hz

Table 7.1 : Project parameters of the aerophotogrammetric test flight 'Uster 92'.

To connect the GPS results of the antenna coordinates to the coordinates of the projection centers, accurate knowledge of the time of exposure and the components of the eccentricity vector from the projection center of the camera relative to the phase center of the antenna is necessary. The synchronization problem was solved by recording the time of an incoming pulse sent by the camera during the exposure in the GPS receiver. This pulse was recorded in GPS time by the Trimble receiver (event marker) and stored in the raw data set. The time

of the computed GPS positions is also related to the same GPS time scale, This allows accurate interpolation. The pulse emitted by the camera deviates from the correct center time of exposure with an estimated standard deviation of 50 microseconds. Given a maximal airplane velocity of 300 km/h, this translates to only 4 mm uncertainty in the interpolation introduced by a synchronization error.

The eccentricity vector was determined on ground by terrestrial measurements with a theodolite, distance measurements and leveling. A set of attitude values of the camera was used to define a camera-related reference frame in which the components of the eccentricity vector are determined at the centimeter level. During the flight this set of attitude values of the camera was held fixed, thus the components of the eccentricity vector remained fixed in the coordinate system of the image.

These two pieces of information, the exposure time and the eccentricity vector, allow connection of GPS coordinates of the antenna with the coordinates of the photogrammetric projection centers.

7.3.2 Recovery of the GPS trajectory

The disposition and the smooth turns allowed collection of two data sets on two consecutive days without major interruptions: the number of tracked satellites was always ≥ 4.

Figures 7.3 and 7.4 show the GPS phase measurements as a function of time for the two days. It has to be pointed out that the minimal elevation angle during the data collection was put at zero. For the computation, however, only measurements with a minimum elevation of 15 degrees were used. The loss of lock to satellites with a low elevation angle are far more frequent, this is in particular true for the moving receiver. The elevation angle for SVNs 17 and 3 are below 15 degrees during the entire time span. SVN 2 was below 15 degrees elevation for about 40 % of the time span. These low elevation data were not used for computation, because the data noise and systematic errors were significantly higher.

Obviously the interruptions are more frequent in the data collected by the moving receiver and they are more frequent in L2 than in L1. This second phenomenon, however, strongly depends on the receiver type. These additional interruptions in the L2 measurements did not disturb ambiguity resolution too much.

Two static windows before and after the flight of about 10-20 minutes each with a constellation of 5 satellites allowed the fixing of the initial ambiguities on both days, the reference receiver at the airport being at a distance of about 200 m from the plane. As no major interruptions in the phase measurements occurred, the fixing of the additional ambiguities during the flight caused no major problems. No modeling of the ionosphere was necessary to resolve the ambiguities. Figure 7.5 gives an overview of the trajectory in Swiss projection coordinates. The height as a function of the N-S component (corresponding to the flight direction) is given in figure 7.6.

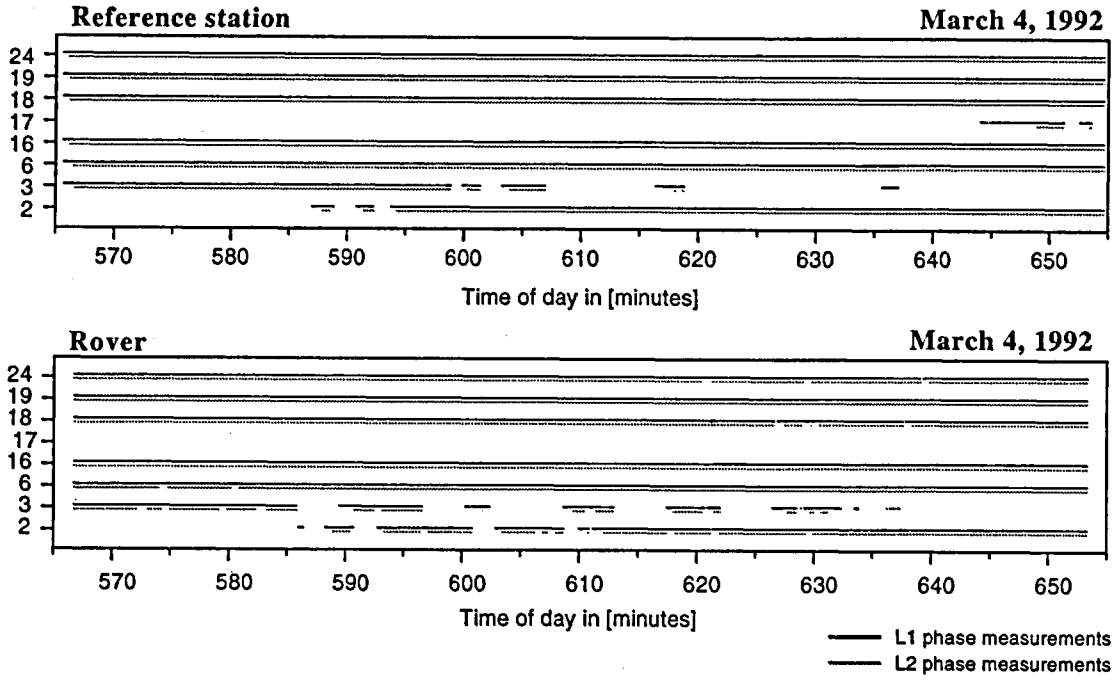

Figure 7.3 : Continuous phase measurements on L1 and L2 (March 4, 1992).

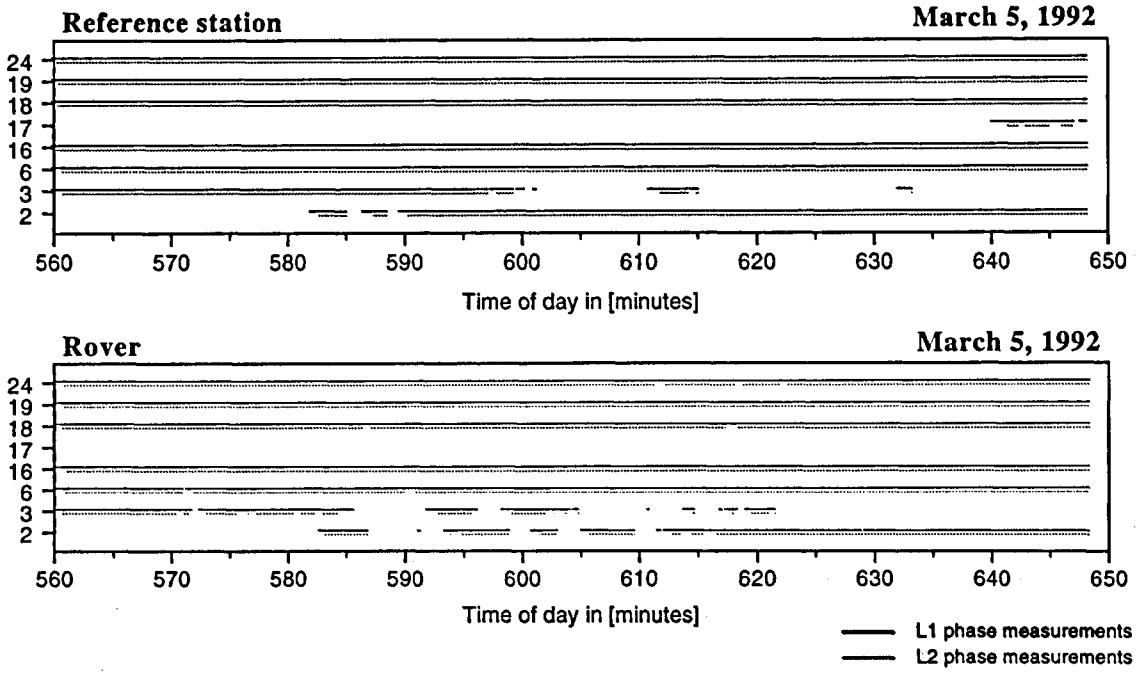

Figure 7.4 : Continuous phase measurements on L1 and L2 (March 5, 1992).

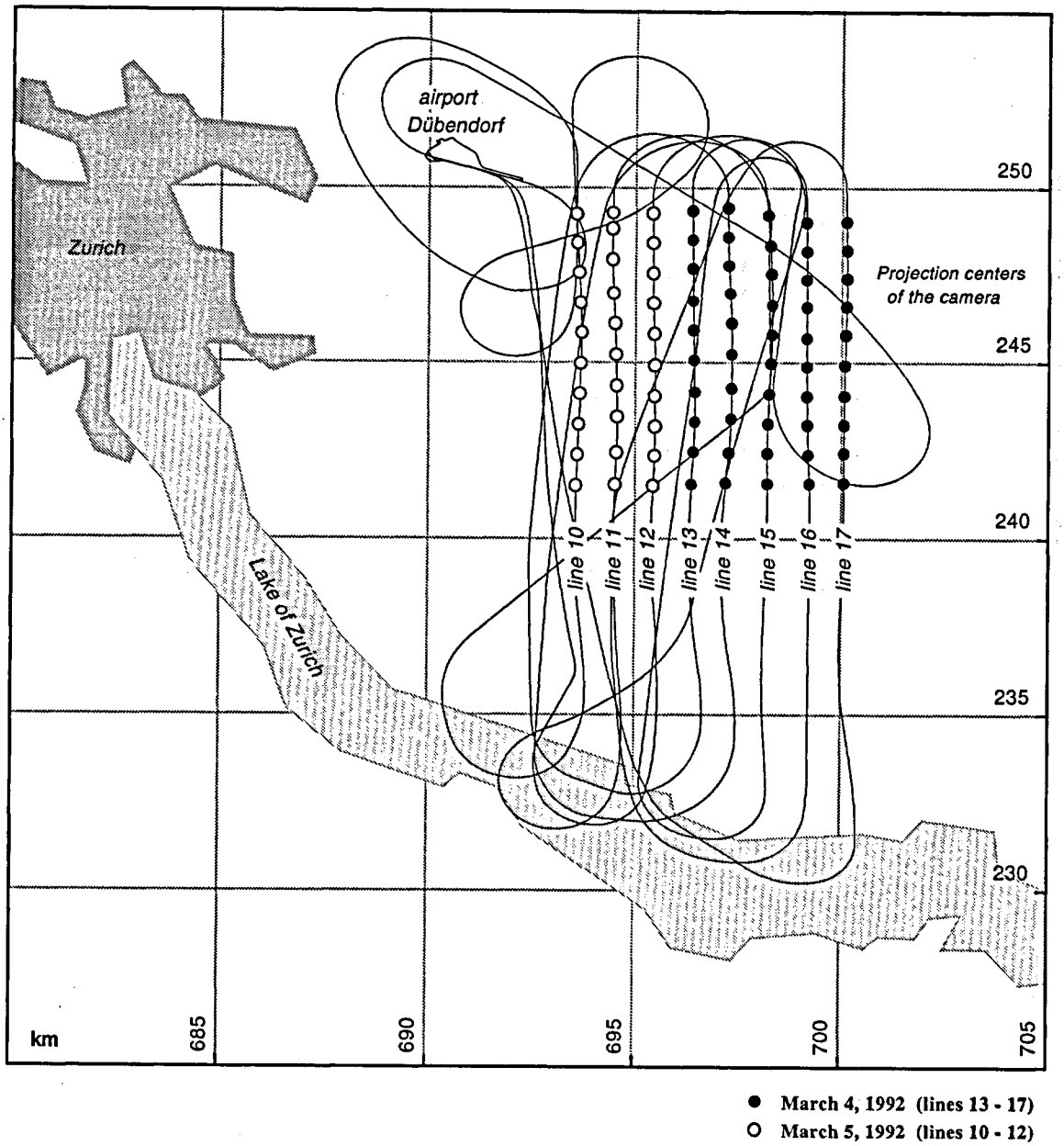

Figure 7.5 : GPS Trajectory of the aerophotogrammetric flight (March 4+5, 1992)

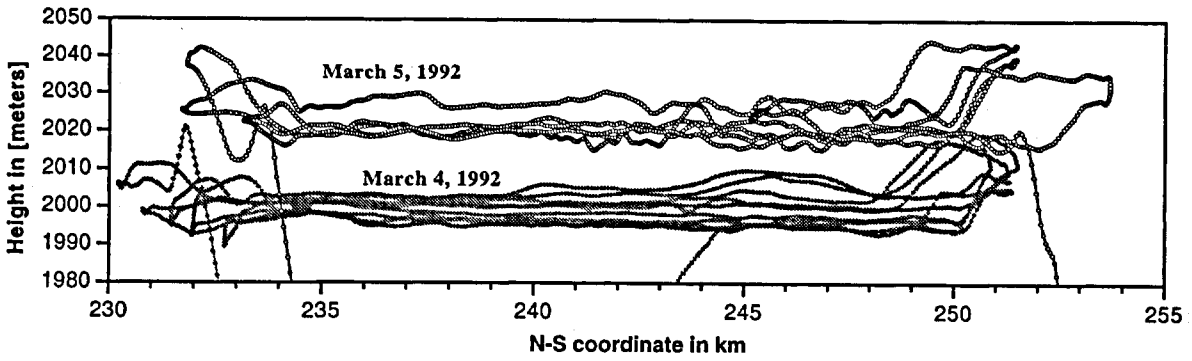

Figure 7.6 : GPS height of the aerophotogrammetric flight (March 4+5, 1992)

7.3.3 *Comparison of L1, L2, and L3 solutions with fixed ambiguities*

The procedure as described in chapter 2 was used to process the experiment. In a first iteration step the ambiguities were estimated and fixed to integers. In a second iteration step the fixed ambiguities were introduced as known into the processing and the coordinates of the moving antenna were computed.

For both days separate L1 and L2 solutions as well as an solution using the ionosphere-free combination of L1 and L2 with fixed integer ambiguities were computed. For convenience all geocentric coordinates were transformed to Swiss projection coordinates, using the same set of transformation parameters. This allows a separation into the E-W component (perpendicular to the flight direction), the N-S component (in the flight direction), and the height.

A first comparison of the L1 and the L3 solution shows discrepancies of up to 15 centimeters in the coordinates. (see figures. 7.7 and 7.9). Figures 7.7 - 7.10 also show the differences in the L2 solution with respect to the L3 solution. Note that they are linearly dependent on the differences of the L1 solution with respect to the L3 solution, and do not contain any new information. This linear dependency holds true in the case of identical constellations. As already pointed out and as one may see in the figures 7.7 and 7.9 there are small differences in the L1 and the L2 observation scenarios. Over small periods of time the L2 measurements are missing (black lines) whereas the L1 measurements are present (gray area). In some cases, where only four satellites were available, this produces bad PDOP values. Data with a PDOP >10 was left out. The L3 scenario is identical with the L2 scenario, which shows that it never occurred that only L2 data was recorded.

These discrepancies are mainly due to the ionosphere. As [Wild, 1993] showed the ionospheric influence introduces in a first approximation scale factors into the L1 and L2 solutions. For geodetic GPS networks, based on longer observation time spans, this scaling effect is then the principal systematic effect of the ionosphere. In the kinematic case, however, where for every epoch a new set of coordinates is produced, the short period fluctuations of the ionosphere may lead to more general distortions in the L1 and L2 solution.

To extract a possible scaling factor from the differences of this kinematic solution the error in the horizontal distance as a function of the horizontal distance itself is given in figure 7.8 (March 4, 1992) and figure 7.10 (March 5, 1992). For the first day a clear scale factor of $-3.7\ ppm$ for the L1 solution with respect to the L3 solution may be extracted (figure 7.8). For the second day, however, a constant scale factor is not so obvious. But still the distance deduced from a L1 solution is shorter than from the L3 solution (figure 7.9).

The comparison of the L1 and L3 solution reveals that the measurements are significantly corrupted by the ionosphere. This effect will disturb the ambiguity-fixing process if only short time intervals are used (see chapter 7.4). If, however, the integer ambiguities are known the bias introduced by the ionosphere may be eliminated by using the L3 combination.

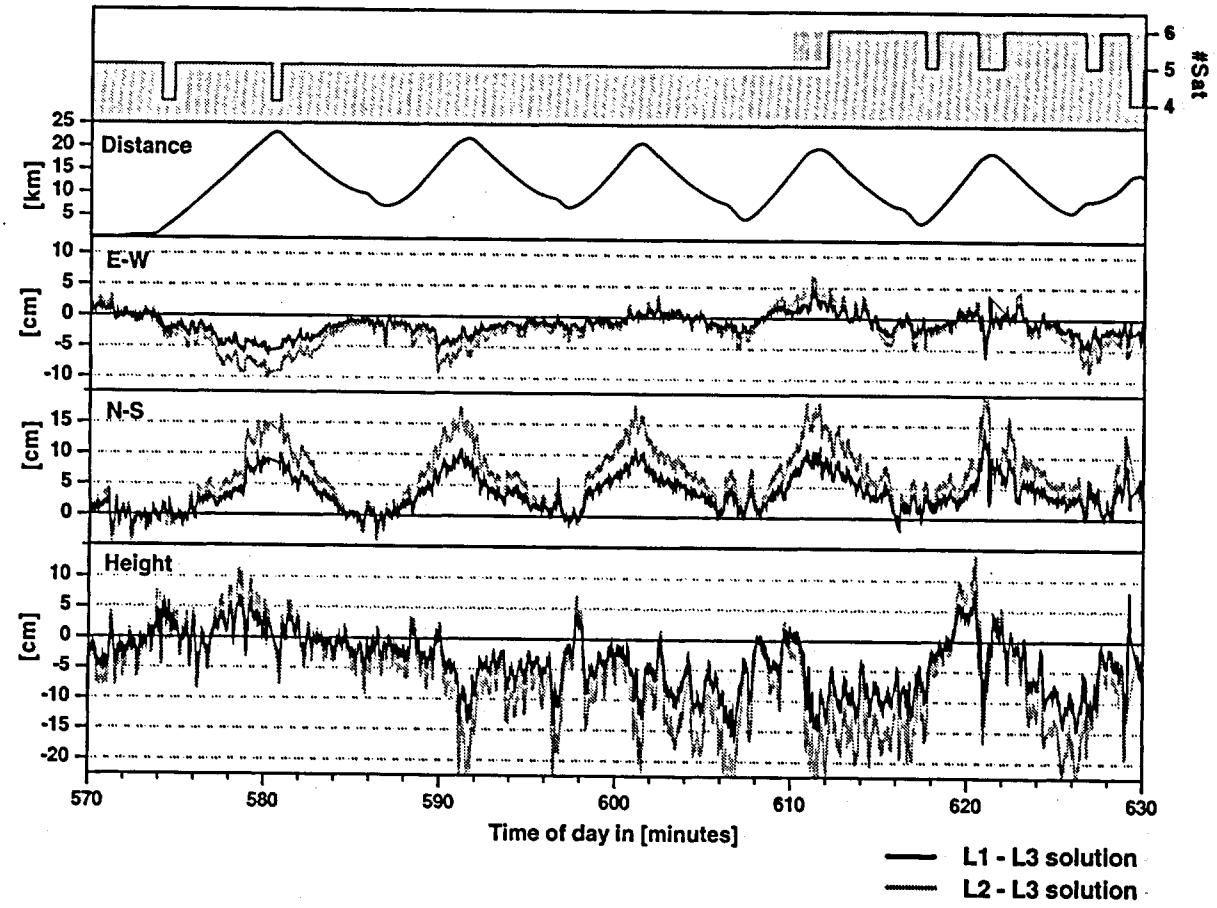

Figure 7.7 : Coordinate differences of the L1 and L2 solutions with respect to the L3 solution as a function of time (March 4, 1992).

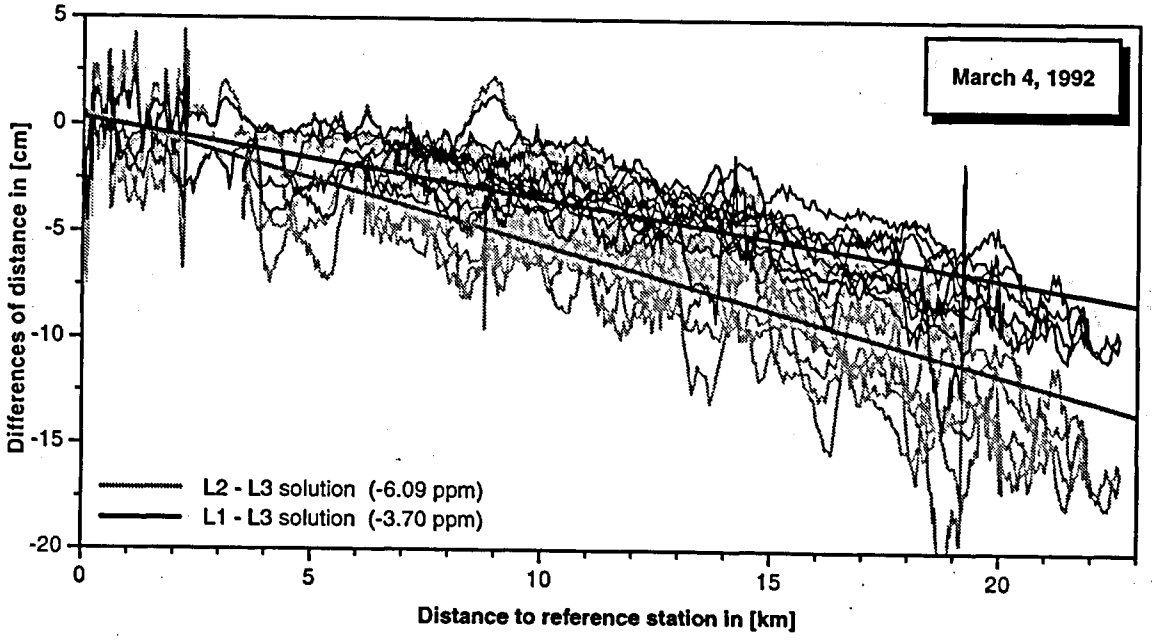

Figure 7.8 : Differences of the horizontal distance of the L1 and L2 solution with respect to the L3 solution as a function of the distance (March 4, 1992).

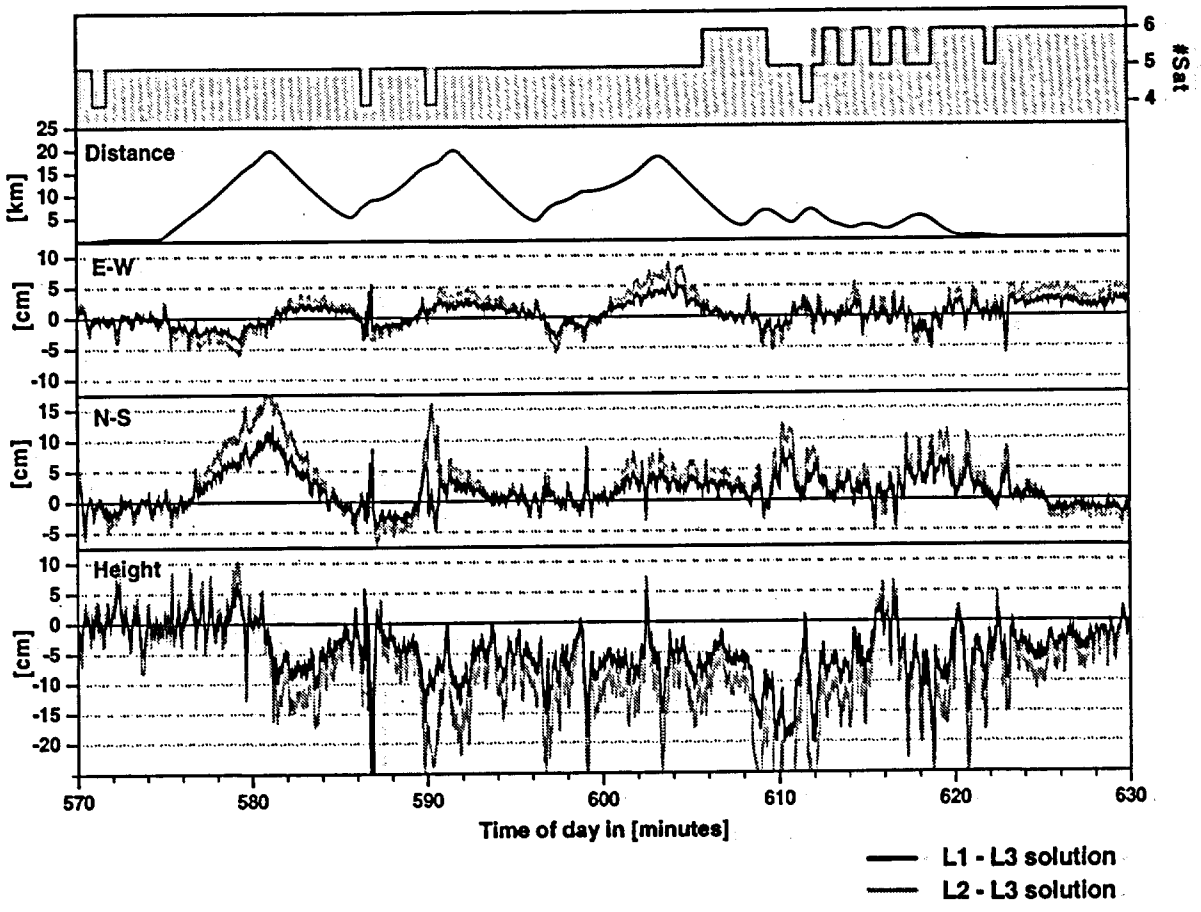

Figure 7.9 : Coordinate differences of the L1 and L2 solution with respect to the L3 solution as a function of time (March 5, 1992).

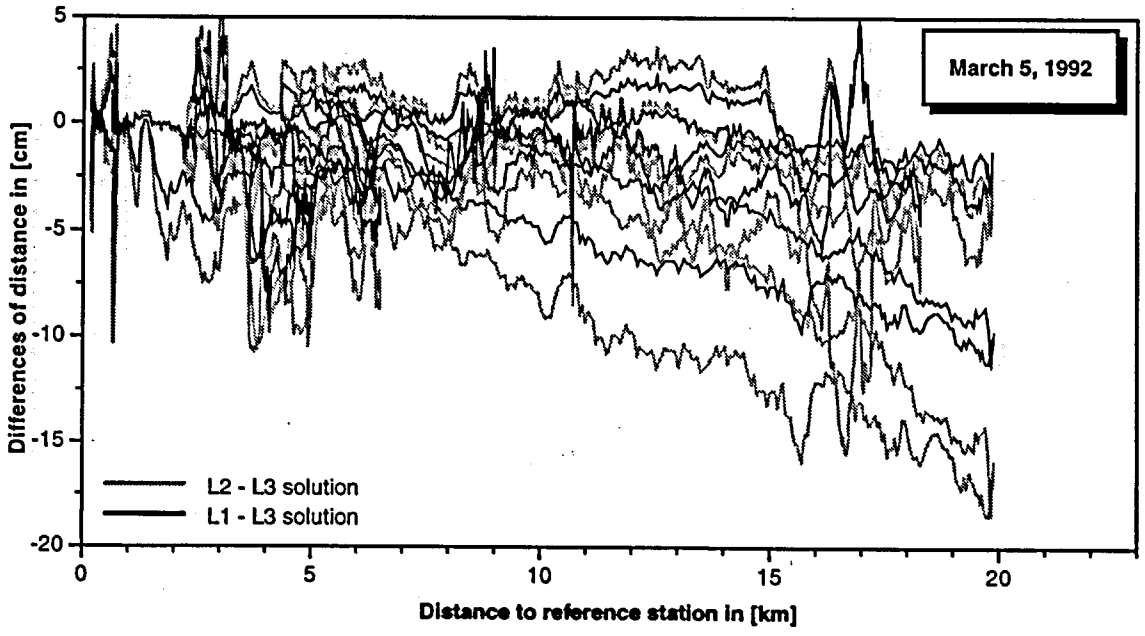

Figure 7.10 : Differences of the horizontal distance of the L1 and L2 solutions with respect to the L3 solution as a function of the distance (March 5, 1992).

7.3.4 *Interpolation to the exposure time*

The positions of the antenna from the L1 or respectively L3 solution refer to the 1-sec GPS epochs. Because the precise times of the camera exposures were also recorded by the receiver, it is possible to interpolate the antenna coordinates to the epochs of interest to the photogrammetry.

The following procedure should give an idea of the interpolation error : For every line the original 1-sec data-set was reduced to a 2-, a 4- and an 8-sec data set. By interpolating the coordinates in the reduced data sets to the middle of the corresponding time intervals, a direct comparison of the interpolated with the measured values allows derivation of a *rms* error of the interpolation as a function of the measurement interval.

Because only the interpolation of coordinates during the survey is of interest only data from the first to the last exposure time of every surveying line was used. Results using the total data set including all maneuvers would be much worse. The results of the individual lines have been regrouped to daily values (mean over 5 lines for March 4, over 3 lines for March 5, 1992).

A linear and a quadratic interpolation were considered. For the quadratic interpolation 2 epochs before and 2 epochs after the central epoch of the reduced data set were used and a least square fit was applied. The results may be inspected in figure 7.11.

For the extrapolation of the *rms* error for the interesting 1-sec data set, the following empirical formula was used :

$$rms(\Delta t) = a_1 (\Delta t)^{a_2} \tag{7.1}$$

with the measurement interval Δt and the two unknown parameters a_1 and a_2. The values for the 1-sec data-set ($\Delta t = 1$) are then $rms = a_1$. The values for a_1 and a_2 for the two days and for the linear or quadratic interpolation are summarized in table 7.2. and show the overall good interpolability.

Error [meters]	March 4, 1992 linear interpolation	March 4, 1992 quadratic interpolation	March 5, 1992 linear interpolation	March 5, 1992 quadratic interpolation
E-W	$0.013 \cdot (\Delta t)^{1.92}$	$0.0005 \cdot (\Delta t)^{2.81}$	$0.024 \cdot (\Delta t)^{1.79}$	$0.0089 \cdot (\Delta t)^{1.89}$
N-S	$0.002 \cdot (\Delta t)^{1.91}$	$0.0002 \cdot (\Delta t)^{2.62}$	$0.006 \cdot (\Delta t)^{1.82}$	$0.0012 \cdot (\Delta t)^{2.21}$
Height	$0.005 \cdot (\Delta t)^{1.74}$	$0.0017 \cdot (\Delta t)^{2.11}$	$0.048 \cdot (\Delta t)^{1.23}$	$0.0295 \cdot (\Delta t)^{1.45}$

Table 7.2 : Results of the fitted interpolation error function for the linear and quadratic interpolation on March 4+5, 1992.

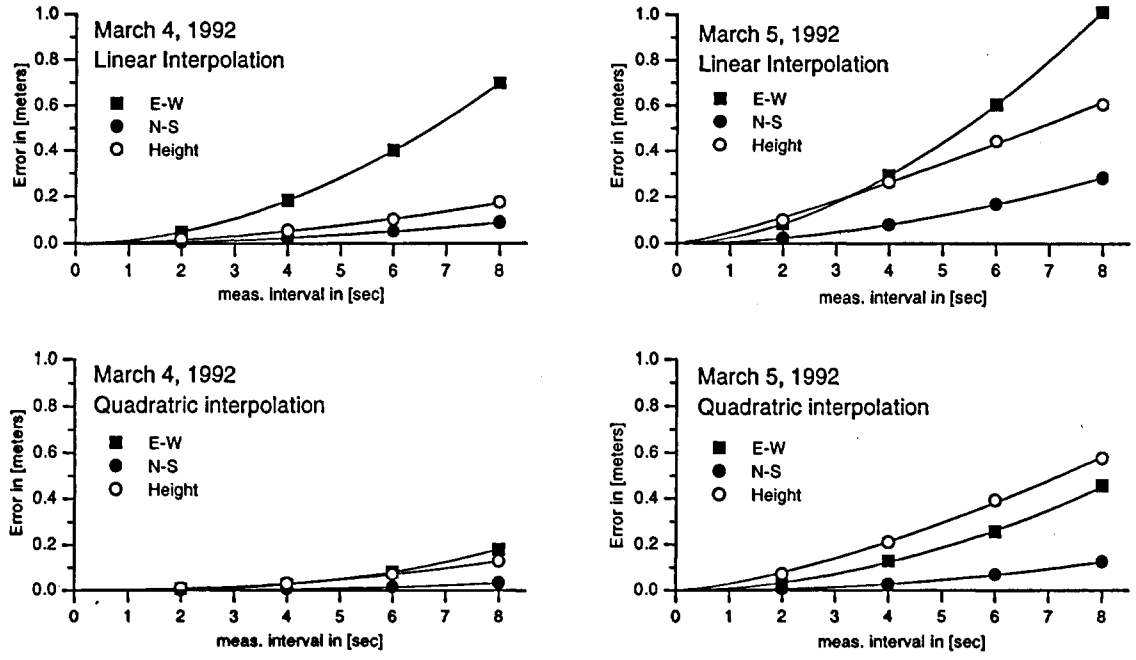

Figure 7.11 : Errors (in meters) introduced by a linear or quadratic interpolation as a function of the measurement interval (in seconds) for the two days separately (March 4+5, 1992)

Let us point out that the N-S component, corresponding to the flight direction, provides in all cases the best result. The critical component is the one perpendicular to the flight direction (E-W).

The values given above reflect only the error introduced by the interpolation and depend on the dynamic behavior of the airplane and the air turbulence. All systematic errors, which have a linear or quadratic behavior over some seconds, cancel out. Thus the same quality for the interpolability may be obtained e.g. from a solution with floating point estimated ambiguities.

The deteriorated quality of the interpolability on the second day (March 5, 1992) compared to the first day (March 4, 1992) may be attributed to more enhanced air turbulence along the trajectory. This different behavior shows up in the height profiles of the lines (figures 7.12).

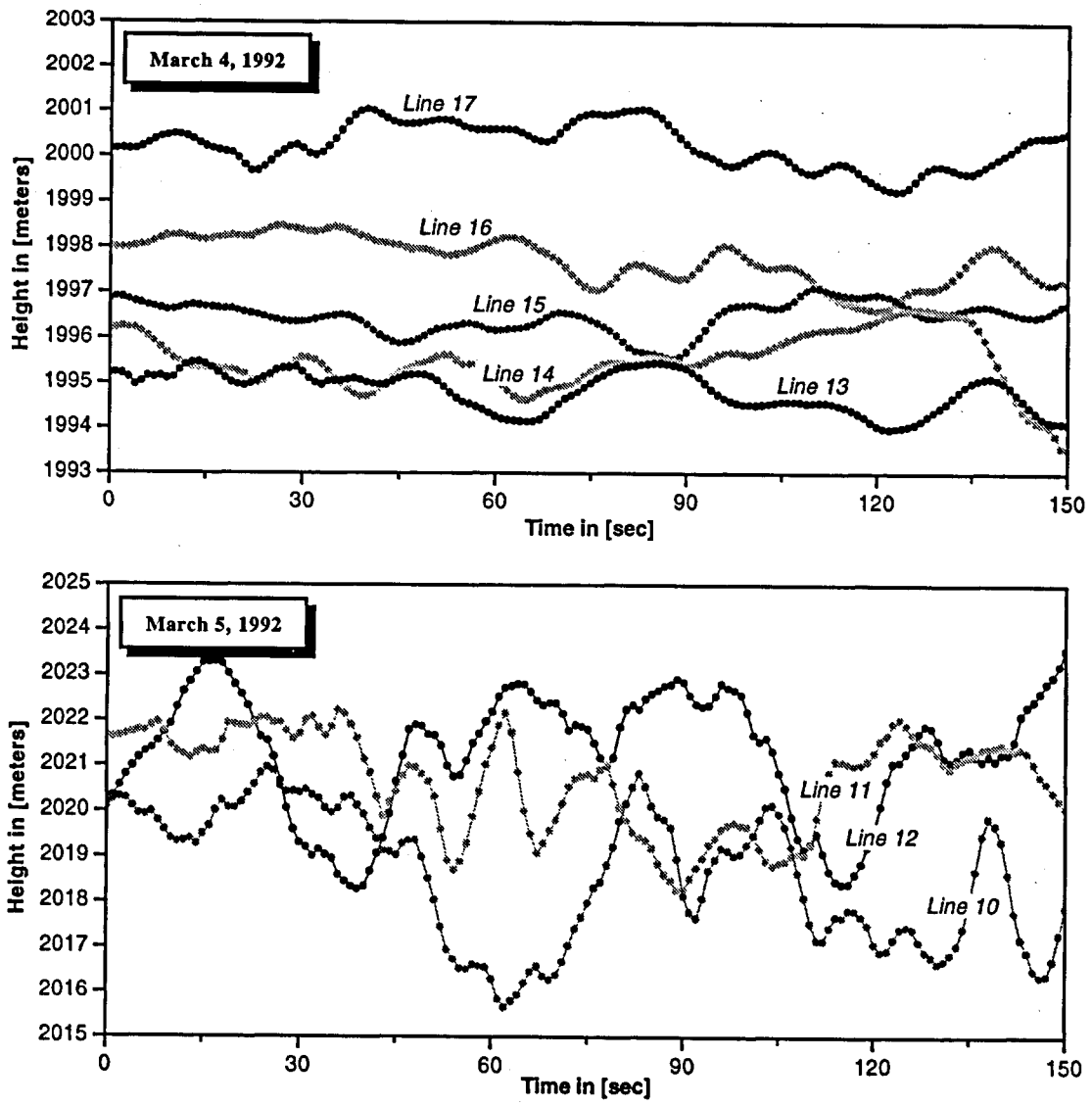

Figure 7.12 : Height profiles for the individual lines as a function of the time for both days separately. The velocity is about 70 m/s and the 150 sec corresponds to 10 km.

Note that for both days the atmospheric conditions were excellent and in the end the interpolation did not cause much trouble also on the second day, where the maximum *rms* error yields 4.8 cm for the height component with a linear interpolation method and 2.9 cm with a quadratic interpolation.

7.3.5 External comparison with antenna coordinates from aerotriangulation

The 80 photographs of the block were measured on the Wild AC3 Analytical Plotter. In addition to the 94 signalized points, 313 natural tie points had to be included. This resulted in a average density of about 25 points per photograph. Using the total amount of 94 control points, the coordinates of the projection centers of the camera may be accurately determined in a bundle block adjustment. The standard deviations from the bundle adjustment were 7.4 cm for the horizontal coordinates and 3.6 cm for the height component.

The eccentricity vector from the projection center of the camera to the phase center of the GPS antenna is known and was held fixed in the image-coordinate system. From the photogrammetric block adjustment the absolute orientation of the image coordinate system is also known. This allows correction for the eccentricity vector and computation of the coordinates of the GPS antenna from the photogrammetric projection centers.

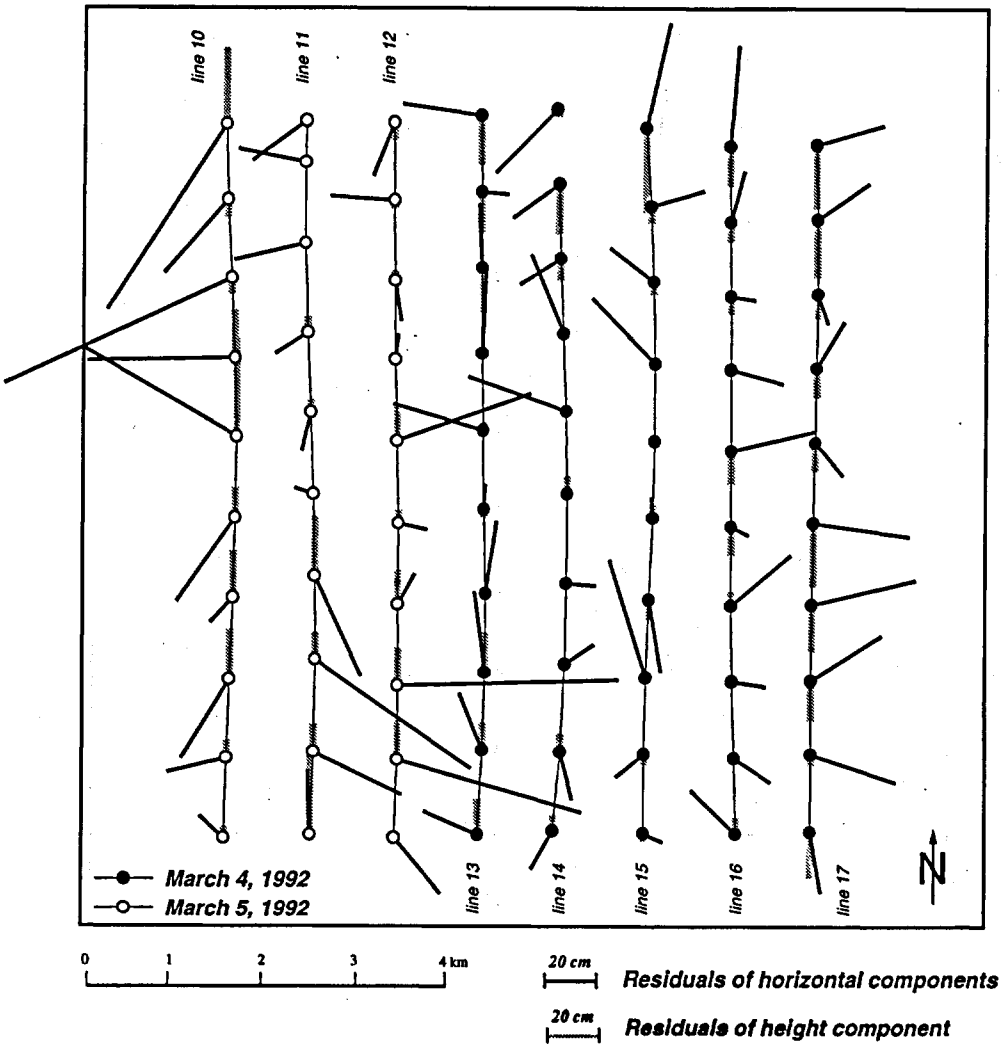

Figure 7.13 : Differences of the antenna coordinates between GPS coordinates (L1 solution with integer ambiguities) and coordinates from aerotriangulation (with all 94 control points).

This result was then compared to the GPS coordinates. One problem was the use of different coordinate systems. In principle the GPS coordinates were connected to the geocentric coordinates of the permanent IGS site Zimmerwald by means of a static GPS baseline from Zimmerwald to the reference site at the airport. The coordinate system used in the bundle block adjustment, however, is derived from the Swiss projection coordinates of the 94 control points in Uster. Because of the distortion in the Swiss projection coordinates (the distance Zimmerwald - Uster being approximately 100 km) an unknown translation vector, constant for the entire block, had to be considered in the comparison.

The GPS coordinates may either be derived from the L1 solution or from the L3 solution with fixed ambiguities. Using a pure L2 solution does not make much sense, since the ionospheric refraction is larger. The translation vectors and the *rms* of the residuals using either the L1 or the L3 solutions are given in table 7.3.

	translation vector [meters]			rms of the residuals [meters]		
	E-W	N-S	Height	E-W	N-S	Height
L1-solution	-0.822	0.244	-0.391	0.152	0.106	0.075
L3-solution	-0.825	0.265	-0.450	0.155	0.107	0.080

Table 7.3 : Translation vector and rms of the residuals from the external comparison between antenna coordinates determined with GPS and aerotriangulation.

The L1 residuals (figure 7.13) show that there are no systematic errors over the entire block and the integration of the GPS measurements in the bundle adjustment could be done without introducing additional drift parameters, with the exception of one translation vector to account for the inaccuracies of the coordinate transformation.

The L3 solution gives the same pattern of residuals as in figure 7.13 and is therefore not explicitly presented. The comparison with the formal accuracy of the aerotriangulation (7.4 cm in planimetry and 3.6 cm for the height) shows that the values obtained externally are about a factor of 2 worse. The errors of the GPS coordinates do not explain this discrepancy. Nevertheless it was shown [Gruen et al. 1993a, 1993b] that by integrating the GPS coordinates in the bundle block adjustment a similar level of accuracy of the ground check points could be obtained with only four control points at the corners of the block as compared to a conventional version with a large number of ground control points (bridging distance $i = 2b$) without integration of the GPS information.

7.4 Impact of unresolved ambiguities on the coordinates

One possible way to recover the coordinates of the projection centers of the camera is to process the kinematic GPS data separately for every line. We define as a line not only the time from the first to the last exposure time of the camera, but extend it to the turns. In our case the duration of such a line is about 5 minutes.

Let us additionally assume that only phase on the L1 band and code measurements are available. From these 5 minutes of GPS data a real valued solution for the ambiguities using the procedure as described in chapter 2 may be produced and the coordinates can be derived from this floating point solution.

Since two different code measurements with a different accuracy are available (C/A code and P Code) the following two versions with different code weighting will be considered :

Version 1 : C/A code $weight_{Code}/weight_{Phase} = 10^{-6}$

Version 2 : P code $weight_{Code}/weight_{Phase} = 0.5 \cdot 10^{-4}$

For latter versions and for every line the coordinates are computed from the corresponding floating ambiguities and compared to the reference solution (the L1 solution with the correct integer ambiguities). The coordinate differences contain only the errors introduced in the solution by the wrong ambiguity values. For every line these differences are approximated by a linear fit, characterized by an offset, a linear drift and the *rms* error of the residuals after the linear approximation. The results are given in table 7.4. The *rms* of the linear fit are on the order of a few millimeters. This clearly shows the linear behavior of our 'floating' solutions over 5 minutes worth of data.

Obviously the drift parameters depend on the quality of the code measurements. With the C/A code we obtain offset values of a few meters, and with the P code all values are below 1 meter. The linear drifts are also smaller in the case where the P code is used (typical values 10-20 cm/min. for the C/A code versions and 5-10 cm/min. for the P code versions).

The consequence for the integration of GPS coordinates into the bundle block adjustment, using such 'floating' solutions, is obviously that drift parameters have to be taken into account and that they must be determined through photogrammetric constraints. The impact on the block design (as mentioned in chapter 7.1.2) are two additional perpendicular strips at the block boundaries.

DRIFT PARAMETERS	C/A code ($w_C / w_P = 10^{-6}$)			P code ($w_C / w_P = 0.5\ 10^{-4}$)		
LINE 10	**OFFSET**	**LIN.DRIFT**	**RMS FIT**	**OFFSET**	**LIN.DRIFT**	**RMS FIT**
E-W	1.342	-0.0133	0.0009	0.013	0.0068	0.0010
N-S	1.698	0.0180	0.0017	0.863	0.0079	0.0018
HEIGHT	-0.565	-0.0519	0.0029	-0.806	-0.0183	0.0020
LINE 11	**OFFSET**	**LIN.DRIFT**	**RMS FIT**	**OFFSET**	**LIN.DRIFT**	**RMS FIT**
E-W	0.108	-0.0041	0.0003	0.321	-0.0055	0.0003
N-S	0.284	0.0007	0.0005	0.431	0.0015	0.0005
HEIGHT	-0.855	-0.0016	0.0026	0.961	0.0053	0.0028
LINE 12	**OFFSET**	**LIN.DRIFT**	**RMS FIT**	**OFFSET**	**LIN.DRIFT**	**RMS FIT**
E-W	-0.631	-0.0200	0.0012	0.265	0.0025	0.0004
N-S	4.422	0.0566	0.0028	0.009	0.0001	0.0006
HEIGHT	-0.918	-0.1431	0.0076	0.966	0.0019	0.0031
LINE 13	**OFFSET**	**LIN.DRIFT**	**RMS FIT**	**OFFSET**	**LIN.DRIFT**	**RMS FIT**
E-W	2.817	-0.0364	0.0003	0.166	-0.0056	0.0034
N-S	3.157	0.0799	0.0014	0.727	0.0100	0.0066
HEIGHT	2.756	-0.1553	0.0040	-0.003	-0.0190	0.0015
LINE 14	**OFFSET**	**LIN.DRIFT**	**RMS FIT**	**OFFSET**	**LIN.DRIFT**	**RMS FIT**
E-W	0.025	-0.0021	0.0004	0.110	-0.0038	0.0004
N-S	0.386	-0.0003	0.0007	0.602	0.0021	0.0008
HEIGHT	-0.563	-0.0010	0.0016	-0.648	-0.0063	0.0021
LINE 15	**OFFSET**	**LIN.DRIFT**	**RMS FIT**	**OFFSET**	**LIN.DRIFT**	**RMS FIT**
E-W	-0.536	-0.0148	0.0009	0.401	-0.0030	0.0003
N-S	2.026	0.0351	0.0004	0.231	-0.0024	0.0005
HEIGHT	-0.332	-0.0748	0.0021	-0.646	0.0068	0.0014
LINE 16	**OFFSET**	**LIN.DRIFT**	**RMS FIT**	**OFFSET**	**LIN.DRIFT**	**RMS FIT**
E-W	-0.103	0.0062	0.0005	0.474	-0.0023	0.0003
N-S	-0.940	-0.0126	0.0004	0.311	0.0015	0.0003
HEIGHT	0.419	0.0345	0.0004	-0.073	-0.0076	0.0003
LINE 17	**OFFSET**	**LIN.DRIFT**	**RMS FIT**	**OFFSET**	**LIN.DRIFT**	**RMS FIT**
E-W	-0.497	0.0036	0.0004	0.357	0.0021	0.0004
N-S	-0.039	0.0023	0.0005	-0.123	-0.0030	0.0004
HEIGHT	0.954	0.0068	0.0028	0.834	0.0106	0.0021

Table 7.4 : Offset and linear drift from 'line-wise' GPS-solutions with floating ambiguities. The offset is given in [m], the linear drift in [m/min.] and the rms of the linear fit in [m].

7.5 *'On the fly' ambiguity resolution per line*

As we saw in chapter 7.4 the fixing of ambiguities is important in obtaining drift-free GPS coordinates. Using the total amount of 1½ hours of dual frequency data or even only single frequency data the quality of the floating point solution is sufficient to allow secure fixing of the ambiguities. The demand for uninterrupted phase measurements over a longer time period is hard to fulfill in practice. Therefore we want to see, whether it is possible to securely retrieve the integer values of the ambiguities over shorter time periods for this specific 'Uster 92' data et.

As in chapter 7.4 we deal with every line separately, using the same windows of 5 minutes. To be successful we must rely on the dual frequency data and trust in its discrimination power. We also take advantage of the high quality of the P code measurements, introducing them in the NEQ system with a weighting ratio of $weight_{Code}/weight_{Phase} = 0.5 \cdot 10^{-4}$. Because Anti Spoofing (AS) was turned off, the search could be performed in the full cycle mode for the L2 ambiguities. The satellite constellation is similar for all lines. The number of observed satellites and the corresponding mean value of the PDOP may be found in table 7.5.

	line 10	line 11	line 12	line 13	line 14	line 15	line 16	line 17
# Sat	5-6	5	5	6	6	5	5	5
PDOP	4.1-3.8	4.4	4.4	3.4	3.7	4.2	4.5	4.2

Table 7.5 : Satellite constellation for the individual lines.

The corruption of the measurements by the ionosphere poses some problems. In section 7.3.3 the differences in the L1 and L2 solutions with respect to the L3 solution and systematic errors up to 10 cm for the L1 and 15 cm for the L2 solutions showed up.

Therefore it was necessary to introduce ionospheric biases parameters (see chapter 4.4 Stochastic modeling of the ionosphere). The approach using differential ionospheric biases was adopted and different levels for the a priori noise σ_{Ion} of a L1 ionospheric bias normalized to the zenith direction were tested.

By putting the a priori value for the *rms* error of a single difference phase measurement to 5 mm the following levels for the a priori σ_{Ion} were analyzed :

σ_{Ion} = 0 mm 2.5 mm 5 mm 10 mm 25 mm 50 mm

March 5	without input model					with single-layer model				
LINE 10	σ_{f1}	σ_1	σ_2	DF	CORRECT	σ_{f1}	σ_1	σ_2	DF	CORRECT
σ_{Ion} = 0	8.2	13.4	14.8	1.11	(15.6)	6.9	12.1	13.4	1.10	(16.6)
σ_{Ion} = 2.5	5.7	10.1	10.6	1.06	OK	5.0	10.3	10.6	1.03	(10.6)
σ_{Ion} = 5	4.5	7.2	9.0	1.26	OK	4.0	7.5	9.0	1.21	OK
σ_{Ion} = 10	3.4	5.1	6.9	1.36	OK	3.2	5.2	6.7	1.28	OK
σ_{Ion} = 25	2.6	3.7	4.6	1.25	OK	2.6	3.8	4.6	1.22	OK
σ_{Ion} = 50	2.4	3.4	3.6	1.06	OK	2.4	3.4	3.6	1.06	OK
LINE 11	σ_{f1}	σ_1	σ_2	DF	CORRECT	σ_{f1}	σ_1	σ_2	DF	CORRECT
σ_{Ion} = 0	4.1	10.2	11.7	1.15	(18.0)	3.9	10.3	10.7	1.04	(20.4)
σ_{Ion} = 2.5	3.7	9.4	10.3	1.09	(10.8)	3.5	9.4	9.5	1.01	(12.1)
σ_{Ion} = 5	3.3	7.1	8.0	1.12	OK	3.1	7.9	8.1	1.03	OK
σ_{Ion} = 10	2.9	4.8	6.1	1.28	OK	2.8	5.2	6.0	1.16	OK
σ_{Ion} = 25	2.5	3.2	3.7	1.15	OK	2.5	3.4	3.7	1.10	OK
σ_{Ion} = 50	2.4	2.9	3.1	1.06	OK	2.4	2.9	3.1	1.05	OK
LINE 12	σ_{f1}	σ_1	σ_2	DF	CORRECT	σ_{f1}	σ_1	σ_2	DF	CORRECT
σ_{Ion} = 0	9.9	12.3	12.4	1.01	(18.1)	9.2	11.6	12.0	1.04	(16.7)
σ_{Ion} = 2.5	8.0	10.8	11.0	1.02	(11.7)	7.1	9.6	10.4	1.09	(10.7)
σ_{Ion} = 5	6.5	8.5	9.5	1.12	OK	5.8	7.7	8.6	1.11	OK
σ_{Ion} = 10	4.7	6.0	6.6	1.11	OK	4.2	5.5	6.1	1.11	OK
σ_{Ion} = 25	3.1	4.0	4.3	1.08	OK	3.0	3.8	4.1	1.08	OK
σ_{Ion} = 50	2.7	3.5	3.7	1.07	OK	2.6	3.4	3.7	1.07	OK

Table 7.6a: Result of a line-wise ambiguity search in the dual frequency mode with additional stochastic ionosphere biases (lines 10 - 12 / March 5, 1992)

σ_{Ion} A priori *rms* in [mm] of a stochastic ionospheric bias normalized to the zenith's direction and the L1 phase. (*rms* of the unit weight a priori = 0.005)

σ_1 *Rms* in [mm] a posteriori of the best integer solution from the search.

σ_2 *Rms* in [mm] a posteriori of the second best integer solution from the search.

DF Discrimination factor : $DF = \sigma_2 / \sigma_1$

CORRECT Independent of the value of the obtained *DF* the best integer solution is compared to the correct one, and marked with OK if they agree. In the case where the search ended up with a wrong integer set, the *rms* in [mm] of the correct integer solution is given in brackets. Note that in the case where the best integer solution is the correct one its *rms* is identical to σ_1 .

March 4	without input model					with single-layer model				
LINE 13	σ_{f1}	σ_1	σ_2	DF	CORRECT	σ_{f1}	σ_1	σ_2	DF	CORRECT
σ_{Ion} = 0	11.2	16.4	16.9	1.03	(22.9)	9.2	15.0	15.4	1.03	(21.5)
σ_{Ion} = 2.5	7.8	13.0	13.2	1.02	(13.4)	6.5	11.4	12.7	1.11	(12.7)
σ_{Ion} = 5	5.9	8.9	10.8	1.21	OK	5.0	8.5	10.0	1.18	OK
σ_{Ion} = 10	4.4	6.1	8.1	1.33	OK	3.9	5.8	7.5	1.29	OK
σ_{Ion} = 25	3.3	4.4	5.1	1.16	OK	3.2	4.3	5.1	1.20	OK
σ_{Ion} = 50	3.1	4.0	4.2	1.05	OK	3.0	3.9	4.1	1.03	OK
LINE 14	σ_{f1}	σ_1	σ_2	DF	CORRECT	σ_{f1}	σ_1	σ_2	DF	CORRECT
σ_{Ion} = 0	7.2	12.3	13.8	1.12	OK	6.4	13.8	13.9	1.01	(13.9)
σ_{Ion} = 2.5	6.0	9.0	11.6	1.29	OK	5.3	9.9	11.0	1.11	OK
σ_{Ion} = 5	5.3	7.3	9.0	1.23	OK	4.8	7.7	8.9	1.16	OK
σ_{Ion} = 10	4.5	5.7	7.2	1.26	OK	4.1	5.8	7.1	1.21	OK
σ_{Ion} = 25	3.8	4.5	5.2	1.17	OK	3.7	4.5	5.1	1.15	OK
σ_{Ion} = 50	3.6	4.2	4.4	1.05	OK	3.6	4.2	4.4	1.05	OK
LINE 15	σ_{f1}	σ_1	σ_2	DF	CORRECT	σ_{f1}	σ_1	σ_2	DF	CORRECT
σ_{Ion} = 0	4.8	8.6	10.6	1.23	OK	3.9	8.0	10.3	1.29	OK
σ_{Ion} = 2.5	4.5	7.1	8.7	1.23	OK	3.7	6.9	8.5	1.23	OK
σ_{Ion} = 5	4.0	5.9	7.4	1.25	OK	3.3	5.9	6.8	1.15	OK
σ_{Ion} = 10	3.2	4.5	6.0	1.34	OK	2.7	4.5	5.5	1.23	OK
σ_{Ion} = 25	2.3	3.1	4.3	1.39	OK	2.1	3.1	4.0	1.27	OK
σ_{Ion} = 50	2.0	2.7	3.2	1.18	OK	2.0	2.8	3.2	1.15	OK
LINE 16	σ_{f1}	σ_1	σ_2	DF	CORRECT	σ_{f1}	σ_1	σ_2	DF	CORRECT
σ_{Ion} = 0	3.4	8.6	10.4	1.20	(11.2)	2.8	7.0	8.5	1.22	(8.5)
σ_{Ion} = 2.5	3.1	7.3	8.3	1.14	OK	2.5	5.6	6.6	1.18	OK
σ_{Ion} = 5	2.8	5.4	6.9	1.29	OK	2.3	4.2	6.3	1.49	OK
σ_{Ion} = 10	2.4	4.0	5.5	1.37	OK	2.1	3.4	5.1	1.52	OK
σ_{Ion} = 25	2.0	3.0	4.3	1.43	OK	1.9	2.8	3.7	1.32	OK
σ_{Ion} = 50	1.9	2.7	3.1	1.13	OK	1.9	2.7	2.9	1.08	OK
LINE 17	σ_{f1}	σ_1	σ_2	DF	CORRECT	σ_{f1}	σ_1	σ_2	DF	CORRECT
σ_{Ion} = 0	5.9	10.6	11.0	1.03	(13.1)	4.9	9.7	10.0	1.03	(11.1)
σ_{Ion} = 2.5	5.2	08.9	9.1	1.02	(9.1)	4.3	7.2	8.9	1.23	OK
σ_{Ion} = 5	4.5	7.0	7.8	1.12	OK	3.8	5.4	7.7	1.44	OK
σ_{Ion} = 10	3.5	5.2	6.9	1.32	OK	3.0	4.1	6.6	1.61	OK
σ_{Ion} = 25	2.5	3.6	4.5	1.25	OK	2.4	3.3	4.6	1.39	OK
σ_{Ion} = 50	2.3	3.2	3.2	1.00	OK	2.3	3.1	3.3	1.06	OK

Table 7.6b : Results of a 'line-wise' ambiguity search in the dual-frequency mode with additional stochastic ionosphere biases (lines 13 - 17 / March 4, 1992). (see explanations to table 7.6a)

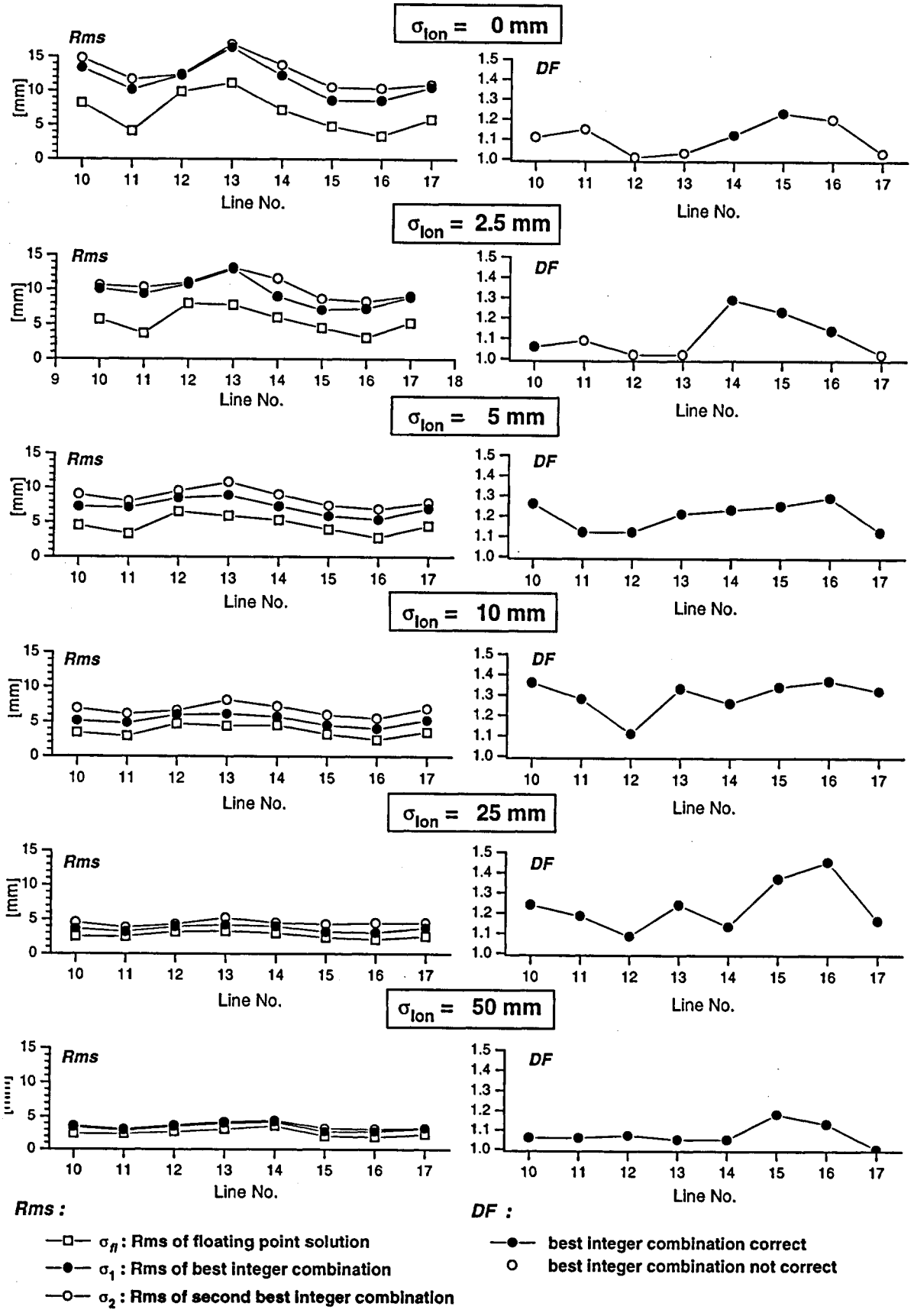

Figure 7.14 : 'Line-wise' ambiguity search in the dual frequency mode with additional stochastic ionosphere biases.(Note that the lines are not in chronological order).

Two sets of versions were computed : a first set without any a priori-model for the ionosphere correction and a second set which already corrected for a single layer model. The details and used parameters of this model are described in chapter 4.4.3. We hoped that the a priori model would already remove the greater part of the ionospheric path delay and that a lower noise level σ_{Ion} for the remaining stochastic bias could be used as in the case without input model. Note that the lower we are able to choose σ_{Ion} the better the discrimination will be. The results are summarized in table 7.6a and 7.6b. Figure 7.14 gives an impression of the impact of the stochastic ionosphere parameters on the ambiguity search process.

The introduction of our parameters removes ionospheric biases on the one hand. On the other hand the values for σ_1 and σ_2 become closer and the discrimination factor is thus weakened. But obviously data corruption by the ionosphere is significant, and the benefit of introducing ionospheric biases is important.

Without stochastic ionosphere parameters, the search ended up with a wrong integer combination for 6 out of 8 lines. The *rms* of the correct integer combination was on the order of 10 - 20 mm and at least one, normally even several, wrong integer combinations with a lower resulting *rms* could be found. The distortions due to a not properly modeled ionosphere lead to a 'biased' and thus unreliable discrimination factor.

By gradually increasing the value of σ_{Ion} the situation improves. For the versions with $\sigma_{Ion} \geq 5$ mm the search always ended up with the correct solution, and the discrimination factor reaches an optimum somewhere for a value between 10 mm and 25 mm. This optimum is obtained by attempting to use a value for σ_{Ion} as small as possible (to not weaken the search) and as high as necessary to remove the systematic errors introduced by the ionosphere. The optimum therefore is in principle different for every data set. A to large value of σ_{Ion} damages the discrimination factor. This means that for big ionospheric activity (where we have to choose a large value for σ_{Ion}) it becomes more and more difficult or even impossible to securely retrieve the ambiguities.

For the best version with $\sigma_{Ion} = 10$ mm the discrimination factor for all lines with the exception of line 12 is of the order of 1.3. A closer look at the result of line 12 showed that in fact a similar value for the discrimination factor from the best to the third best integer solution was obtained. leaving us with two candidates. (An idea which has not been tested would be to use the photogrammetry to discriminate between these two solutions.)

The differences between the versions (without any a priori model for the ionosphere or using a single layer model) are very small. There is no noticeable benefit in our single layer model for our purpose. It seems that there is only a small decrease of σ_{fl}. Better modeling might change the situation but the results show that already with the simple hypothesis of a white noise for the ionospheric error and a careful definition of the noise level σ_{Ion}, the results of the ambiguity search could be significantly improved.

8 Kinematic GPS for Aerogravimetry

8.1 Introduction

The key problem in monitoring the earth's gravity field with a gravity meter, installed on board a moving vehicle, is the separation of the signal (acceleration due to the earth's gravity field) from the noise (acceleration due to the motion of the vehicle).

In the case of a ship, adequate filter techniques allow this separation without additional external information of the acceleration of the vehicle. Since 1950 gravity meters, installed on ships revealed themselves to be a practicable way to monitor the earth's gravity field [LaCoste and Romberg, 1967]. Due to the high velocity of an airplane accurate external information of position, velocity and acceleration are required for reducing the measured accelerations in order to retrieve gravity. [Brozena et al, 1989] for example have shown that kinematic GPS is a powerful tool for this task.

The ultimate goal of every airborne gravimetric survey is the mapping of the anomalies of the earth's gravity field. To achieve this task there are various requirements for aerogravimetry on the GPS trajectory. The horizontal coordinates are only needed for the spatial location of the measurement and do not cause any problems with the achievable accuracy of kinematic GPS. Assuming a desired accuracy of 1 mgal (1 mgal = 10^{-5} m/s^2) and a gradient of -0.3 mgal/m for the gravity a height accuracy of 3 meters is required. For the correction of the Coriolis acceleration the horizontal velocity (East-West component) is needed with an accuracy of 7 cm. The required accuracy of the vertical component of the acceleration, however, directly correspond to the desired accuracy of the gravity determination. Similar values are given e.g. in [Hehl, 1992].

horizontal position	10 - 100 m
height component of the position	1-3 m
horizontal velocity	7 cm
vertical acceleration	1 mgal

Table 8.1 Required accuracy of the GPS trajectory for aerogravimetry.

The key problem is vertical acceleration. It is obvious that with a simple numerical differentiation of the GPS positions a noise level of 1 mgal is not achievable. Therefore elaborated filtering techniques (normally low pass filters) are applied [Hehl, 1992], [Klingelé et al, 1993], [Bagnaschi, 1993]. By low pass filtering with a cutoff frequency of 0.01 Hz an accuracy of 1 mgal for the vertical acceleration from kinematic GPS put on a vertical motion machine were reported by [Wei et al., 1991].

In the following results from a gravimetric airborne survey with GPS are presented. We will focus in particular on the GPS part ot the survey namely : the determination of the trajectory and the derivation of velocity and acceleration.

8.2 GPS-results from an aerogravimetric survey 'Aerograv 92'

8.2.1 Overview

In November and December 1992 an airborne gravimetric survey was carried out over Switzerland by our institute in collaboration with LaCoste and Romberg, who provided for the gravity meter. A LaCoste Romberg Model S Marine relative gravity meter, mounted on a gyro stabilized platform, was installed on board an airplane and collected raw data at a rate of 1 Hz. (For details concerning the gravity meter see e.g. [Valiant, 1982]). The airplane was a Twin Otter belonging to the Swiss Cadastral Authority (Eidgenössische Vermessungsdirektion).

During the flights 6 Trimble SST receivers were operating (2 receivers on board the airplane, 4 receivers at ground stations). Because of the importance of the project and the long distances (the survey covered the entire territory of Switzerland) we installed 4 suitably distributed reference stations : Zimmerwald, Zurich, Engadin and Lausanne (see figure 8.1).

In addition to the 3 receivers, owned by our institute, the University of Braunschweig provided us with 2 further receivers. The Swiss Federal Office of Topography permanently operates a receiver at the IGS site at Zimmerwald. At our special request the data rate was put to 2 Hz during the surveying flights. The Institute of Geodesy of EPF Lausanne was in charge of the receiver at the Lausanne reference site. We gratefully acknowledge the help and cooperation of all the institutions involved, which actively contributed to the success of the mission. Tables 8.2 and 8.3 give an overview of the GPS part of the 'Aerograv 92' survey.

Data set : AEROGRAV 92		
GPS receivers :	6 Trimble SST	
Collected measurements :		
1 single-frequency receiver	C/A code (on L1)	L1 phase
5 dual-frequency receivers	C/A code (on L1) P code (on L2)	L1 phase L2 phase
Measurement rate	2 Hz	
(Data directly downloaded to the harddisk of laptop computers)		

Table 8.2 : Parameters related to GPS of the 'Aerograv 92' data set

Distribution of GPS receivers (see also figure 8.1)		
Airplane 1	dual	Swiss Federal Institute of Technology (ETHZ)
Airplane 2	single	Swiss Federal Institute of Technology (ETHZ)
Zimmerwald	dual	Swiss Federal Office of Topography (L+T)
Zurich	dual	Swiss Federal Institute of Technology (ETHZ)
Lausanne	dual	University of Braunschweig (Germany)
Engadin	dual	University of Braunschweig (Germany)

Table 8.3 : Distribution of the GPS-receivers

Eight flights were performed between November 24 and December 11, mainly during the night. The duration of the individual flights was about 4 to 5 hours, which corresponds the maximal possible flight duration of the airplane. Figure 8.1 shows the design of the surveying lines, comprising 20 lines in the East-West direction and 4 crossing lines.

In the following we focus only on the flight of December 10. The total duration of this particular flight was about 4 ½ hours and the following 3 lines were flown :

	duration	flight direction	remarks
Line 12	60 min.	East-West	(only partially)
Line 10	1 h 40 min.	West-East	(total line)
Line 8	50 min.	East-West	(total line)

Table 8.4 : Overview of the lines surveyed on December 10.

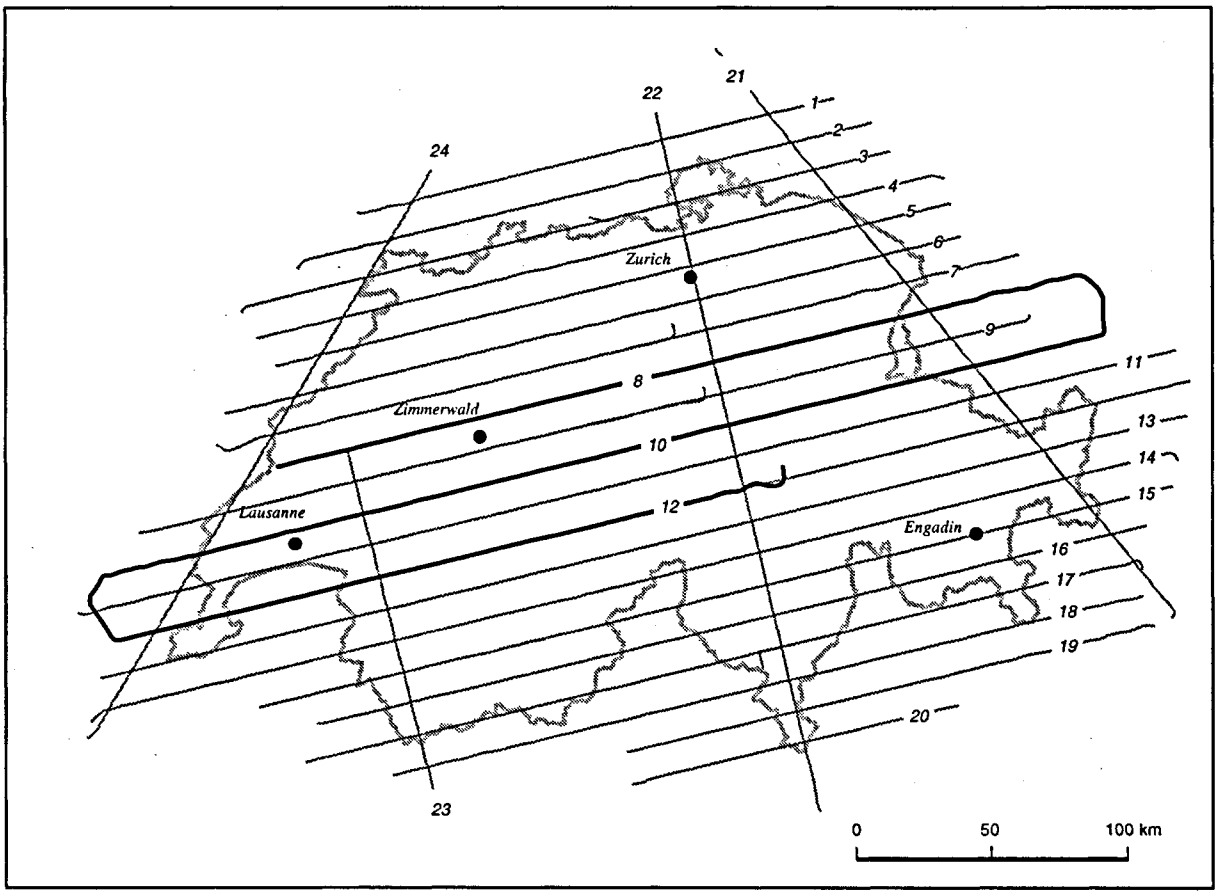

Figure 8.1 : Design of the surveying lines in the 'Aerograv 92' project. The part flown on December 10 (line 8, 10 and part of line 12) is emphasized.

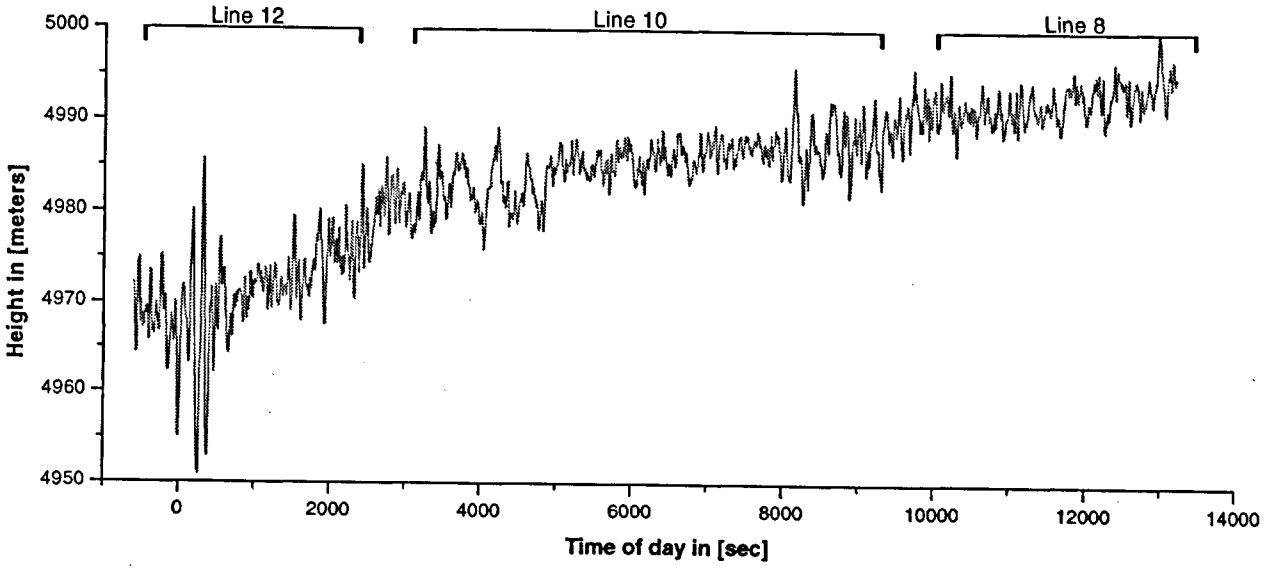

Figure 8.2 : Height as a function of time for the flight on December 10 (recovered from the GPS trajectory).

8.2.2 *Recovery of the trajectory*

Our first objective was to recover the trajectory of the airplane. Four reference stations could be used, allowing comparison.

The measurements from the dual-frequency receiver on board the airplane were combined with the measurements from different reference stations. For every combination (different reference station to the same roving receiver) the coordinates were computed. The same strategy as in section 5.2 ('Laser scanner-flight 94') was used to compare results. First all reference stations were tied to the IGS site at Zimmerwald by means of static baselines. This task was performed using Bernese Software Version 3.4. The entire amount of data over the duration of all 8 flights was used.

Because the constellation was quite poor for this data set, the minimum elevation angle was set to 10° in the computation. This led, however, to different satellite constellations when combining the roving receiver with different reference stations due to individual topographic obstructions at the reference sites. Unfortunately due to a lack of data the trajectory had to be divided into different parts.

The processing scenario is specified in table 8.5 :

Zimmerwald	entire data set	(always at least 4 common satellites with the roving receiver)
Engadin	entire data set	(always at least 4 common satellites with the roving receiver)
Zurich	2 parts	Part 1 (line 12 and line 10) Part 2 (line 8)
Lausanne	2 parts	Part 1 (line 12) Part 2 (line 8) (line 10 could not be processed)

Table 8.5 : Processing scenario for the different combinations of the roving receiver with the four reference stations.

In all data sets discussed so far, e.g. 'Laser Scanner flight 94' (chapter 5.2) or 'Uster 92' (chapter 7.2), the distance between roving and reference receiver was always below 30 km and it was possible to securely retrieve the individual L1- and L2-ambiguities. For the 'Aerograv 92' data set , however, distances up to 300 km did occur. A secure fixing of the individual L1 and L2 ambiguities was impossible. Therefore the following strategy was adopted :

We integrated all code and phase measurements into our NEQ system, and introduced absolute stochastic ionosphere biases as described in chapter 4.4. A value for the absolute ionospheric noise level was based on the following assumptions. During the night activity of the ionosphere is low and a stochastic noise in the total electron content (TEC) of $15 \cdot 10^{16}$ TE-

CUs seemed to be appropriate. This resulted in an assumed stochastic noise of 2.5 m for an absolute ionospheric path delay normalized to the zenith and the L1 frequency.

In a next step the L2 ambiguities are replaced by the corresponding wide-lane ambiguities (wavelength = 86 cm), called L5 ambiguities here after. Instead of a mixed L1/L2-NEQ system we now have a mixed L1/L5 NEQ system.

We then try to fix the L5 ambiguities only and leave the L1-ambiguities as floating point values in the NEQ system. For the fixing of the L5 ambiguities the following strategy was adopted : first a conventional sigma dependent rounding is applied. In the case where it was not possible to resolve the wide lane ambiguities by this method, our search strategy (see chapter 4.2) was used. The search in this case here, however, is only performed over the subset of the wide-lane ambiguities. After a successful fixing of the L5 ambiguities the remaining L1 ambiguities were left as floating point values.

For the final computation of the coordinates these ambiguities (fixed L5 / real valued L1) are used and the same stochastic modeling of the ionospheric path delay is applied.

The strategy described above was applied to all data sets listed in table 8.3. The L5 ambiguities were fixed to integers. Apart from the L3 solutions, L1 solutions were computed. They will also be considered for the computation of the velocity and acceleration of the airplane (see chapter 8.4).

8.2.3 Comparison of the trajectory using different reference stations

For the following comparisons the solutions with respect to Zimmerwald were chosen as reference. The differences between the solutions with respect to the other ground stations (Zurich, Lausanne, Engadin) and the reference solution are given in figures 8.3 and 8.4. Note that for every data set the same data from the roving receiver was used.

As already pointed out, there are slight differences in the constellation of the individual combinations (reference - roving). In figures 8.3 and 8.4 the constellation with respect to Zimmerwald is given.

In figure 8.3 the differences in the L3-solutions show an agreement on the order of 10 cm for the periods with a reasonably good PDOP. There remain, however, systematic discrepancies, which may be due to the tropospheric path delay : Measurements at low elevation angles are included and there are also big height differences between the reference stations (Lausanne at a height of 400 m / Zurich at 550 m / Zimmerwald at 900 m / Engadin at 1720 m).

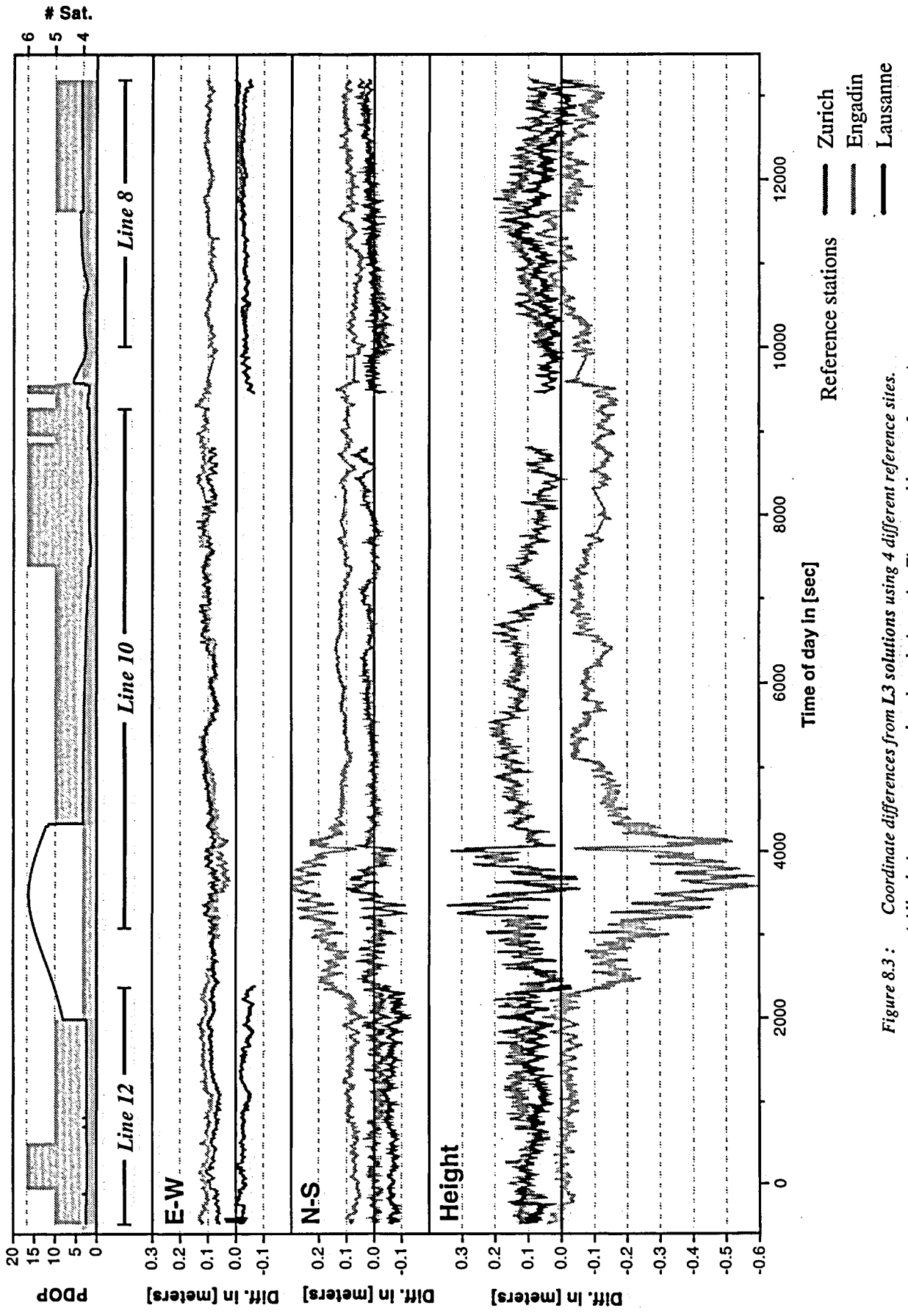

Figure 8.3 : Coordinate differences from L3 solutions using 4 different reference sites.
(All solutions are compared to the solution using Zimmerwald as a reference).

For the computation of the coordinates the Saastamoinen model [Saastamoinen, 1973] for a standard troposphere was used to correct for the tropospheric path delay. [Geiger, 1987] showed that for a homogenous satellite coverage of the sky an error in zenith path delay correction produces an error about three times larger in the height component. This error, however, depending on the actual satellite constellation, may also affect the horizontal components. If we assume a maximum error of 15 cm for the zenith path delay, the resulting error in the coordinates would still be below 50 cm and we are still within the required accuracy limits of 3 m for the height component (see table 8.1).

8.2.4 *Determination of velocity and acceleration*

For the determination of velocity and acceleration the geocentric coordinates may be used. In a first and for our purposes sufficient approximation, this coordinate system rotates with a constant angular velocity with respect to an inertial frame. Therefore by taking the derivation of the rotating coordinates twice with respect to time, the obtained acceleration has to be corrected for the Coriolis and the centrifugal accelerations in order to obtain the 'true' acceleration with respect to an inertial frame (see e.g. [Schneider, 1981]).

$$\vec{a}_{airplane} = \frac{d^2}{dt^2}\vec{x} + 2\vec{\omega} \times \frac{d}{dt}\vec{x} + \vec{\omega} \times (\vec{\omega} \times \vec{x}) \tag{8.1}$$

where

$\vec{a}_{airplane}$ denotes the total acceleration vector acting on the gravimeter due to the motion of the airplane with respect to an inertial frame.

$\vec{x}$ the position vector given in the rotating frame.

$\frac{d}{dt}$ the time derivative of the coordinates given in a rotating frame.

$\vec{\omega} = \omega\vec{e}$ rotation vector of the earth (ω = constant angular velocity of the earth and $\vec{e}$ = unit vector parallel to the earth's rotation axis)

$\vec{a}_{Coriolis} = 2\vec{\omega} \times \frac{d}{dt}\vec{x}$ the Coriolis acceleration

$\vec{a}_{centrifugal} = \vec{\omega} \times (\vec{\omega} \times \vec{x})$ the centrifugal acceleration

By adding the gravitational acceleration of the earth's we obtain the following total acceleration $\vec{a}_{tot}$ (Tidal effects are neglected).

$$\vec{a}_{tot} = \vec{a}_{earth} + \vec{a}_{aircraft} = \left[\vec{a}_{earth} + \vec{\omega} \times (\vec{\omega} \times \vec{x})\right] + \frac{d^2}{dt^2}\vec{x} + \vec{a}_{Coriolis} \tag{8.2}$$

The term $\vec{a}_{earth} + \vec{\omega} \times (\vec{\omega} \times \vec{x})$ is commonly denoted as gravity vector $\vec{g}$ of the earth (see e.g.

[Heiskanen and Moritz, 1967]). By introducing this abbreviation into equation (8.2) we obtain :

$$\vec{a}_{tot} = \vec{g} + \frac{d^2}{dt^2}\vec{x} + \vec{a}_{Coriolis} \tag{8.3}$$

Apart from cross-coupling effects and stabilization problems of the gyro-platform the measured acceleration is the vertical component of $\vec{a}_{tot}$.

$$a_{gravimeter} = \vec{a}_{tot} \cdot \vec{e}_n = g + \left(\frac{d^2}{dt^2}\vec{x}\right) \cdot \vec{e}_n + \vec{a}_{Coriolis} \cdot \vec{e}_n \tag{8.3}$$

where $\vec{e}_n$ denotes the vertical direction, taken as ellipsoidal normal vector.

An equivalent approach consists of first extracting the ellipsoidal height from the geocentric coordinates and performing the time derivatives on the ellipsoidal height. Here the Coriolis term has to be extended to account for the curvature of the reference surface (ellipsoid). The resulting correction term is known as Eotvoes correction. (For the ellipsoidal case the formula for the Eotvoes correction may be found in [Harlan, 1968]).

$$a_{gravimeter} = g + \frac{d^2}{dt^2} h_{ell} + a_{Eotvoes} \tag{8.4}$$

In the following we will directly use the coordinates given in the rotating geocentric Cartesian frame and correct the acceleration for the Coriolis term.

In geodesy collocation methods are often used for the interpolation of the geoid. [Gurtner, 1978]. They may also be applied for the interpolation of a kinematic GPS trajectory and allow integrated determination of the time derivatives. The collocation method is an extension of a least squares estimation, where the residuals of the measurements are split up into a noise and a signal part with an assumed correlation between the signals of the different measurements. An a priori value for the noise of the measurements is necessary and a covariance function for the signals has to be known. For a detailed description of the collocation method see e.g. [Wirth, 1990].

The position vector was assumed to be a polynomial in time of degree 2. The remaining residuals were then interpolated using collocation methods. For the resulting time series (position, velocity, acceleration) a time spacing of 1 sec was adopted. For every epoch we used only the data within a time span of 5 seconds around this central epoch, which correspond to 11 data points in total from the original 2 Hz data set.

We assume the following covariance function of the signal :

$$Covariance\ function = \sigma^2_{signal} \frac{1}{1 + \left(\frac{dt}{T}\right)^2} \tag{8.5}$$

with $\sigma_{signal} = 2\ mm$ and $T = 2\,\text{sec}$ $(\sigma_{noise} = 5\ mm)$

For the GPS trajectories (L1 and L3 solutions), separately for each line, the velocity and acceleration vectors were calculated in a geocentric Cartesian reference frame. The Coriolis acceleration was added to the acceleration vector. Then a transformation in the corresponding horizontal frame was performed. The east and north component of the velocity were combined into a horizontal velocity.

Figure 8.4 shows the horizontal velocity, figure 8.5 the vertical component of the velocity.

The horizontal velocities are on the order of 90 m/s for the lines 12 and 8 (flight direction East-West) and of 60 m/s for the line 10 (flight direction West-East). Many systematic errors are removed by taking the derivatives.

For every epoch a mean value from the results with respect to the different reference stations was computed and the *rms* error of the residuals as a function of time is given in figures 8.4 and 8.5. Note that in the computation of the different versions the same GPS data from the roving receiver is included, therefore this comparison is not an external validation. The agreement of the velocity components obtained with different reference stations is on the order of a few millimeters/sec. Let us keep in mind that the aimed at accuracy for the horizontal velocity is about 7 cm. It is obvious that the recovered horizontal velocity from kinematic GPS easily meets all requirements of aerogravimetry

Figure 8.6 gives the vertical component of the acceleration. Maximum values of 15 cm/s^2 are reached, but in general the accelerations are on the order of 3 to 5 cm/s^2. This corresponds to 3000 to 5000 mgal of 'noise' acceleration acting on the gravity meter. The quality of our derived accelerations is a few mm/s^2 (a few 100 mgal) and it is clear that the required accuracy of 1 mgal is not achievable for an 'instantaneous' acceleration.

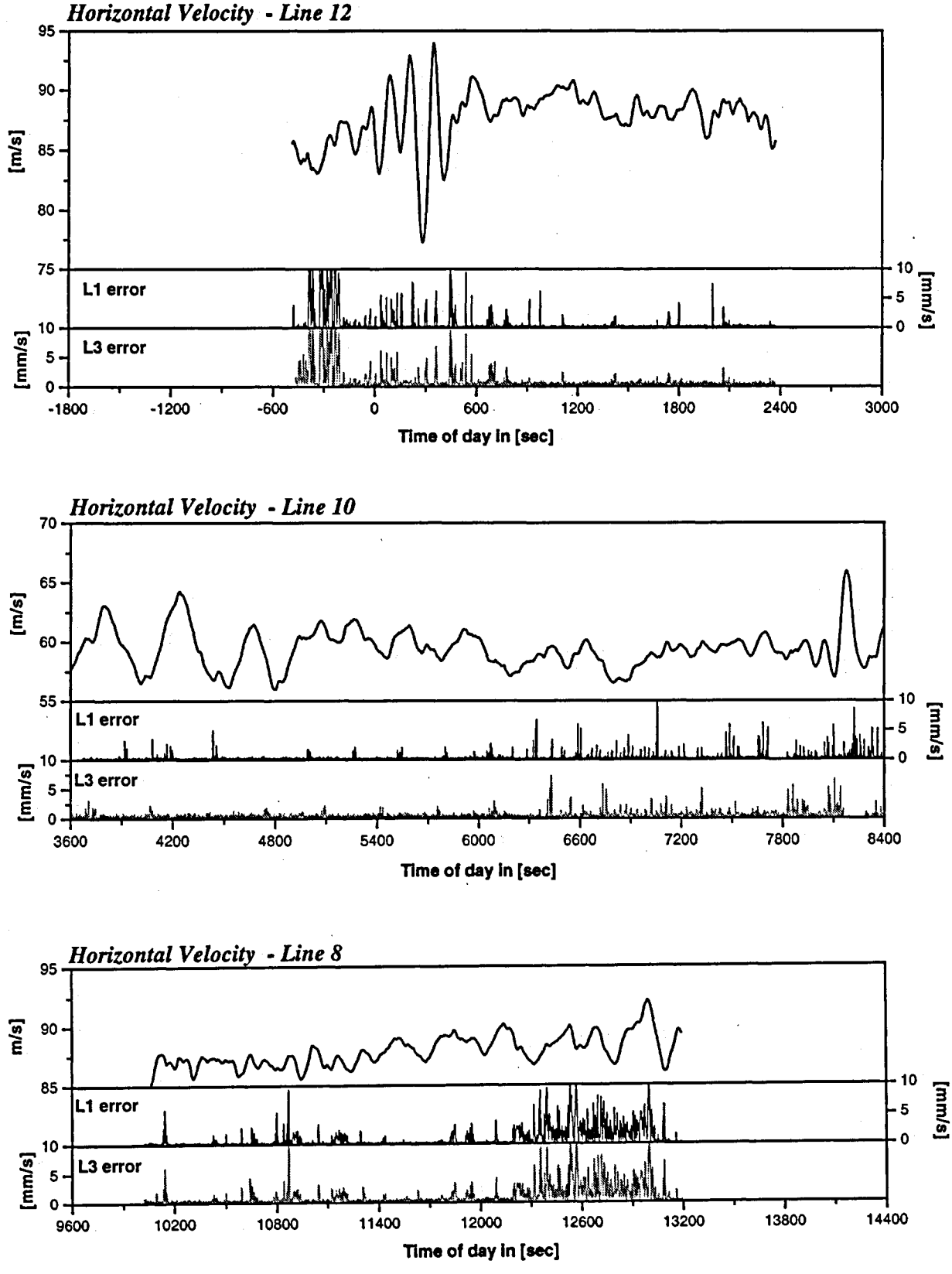

Figure 8.4 : Horizontal velocity derived from the GPS trajectories for lines 12, 10 and 8. The errors represent the standard deviation of the different solutions.(same rover - different reference stations)

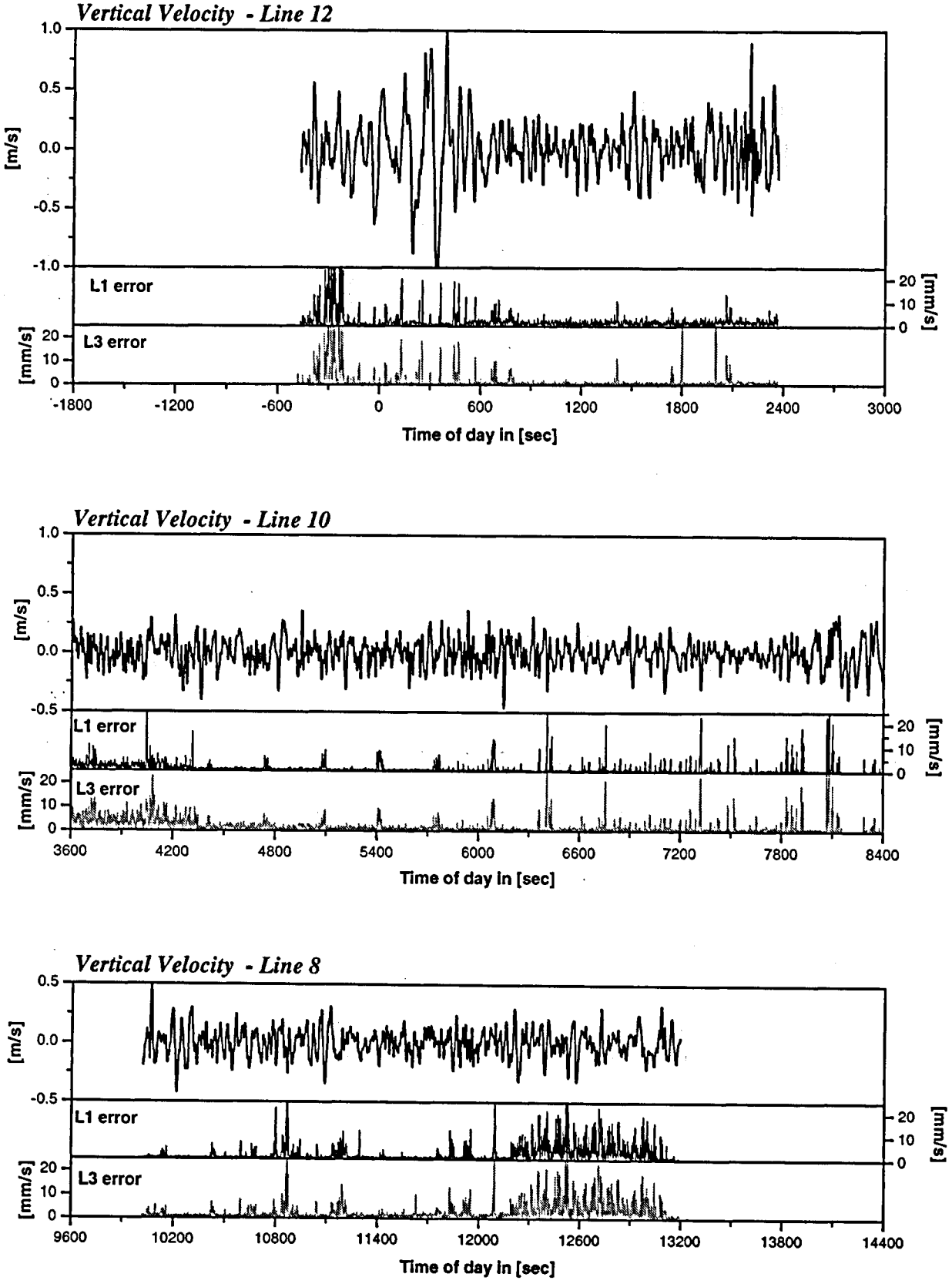

Figure 8.5 : Vertical velocity component from the GPS trajectories for lines 12, 10 and 8. The errors represent the standard deviation of the different solutions. (same rover - different reference stations)

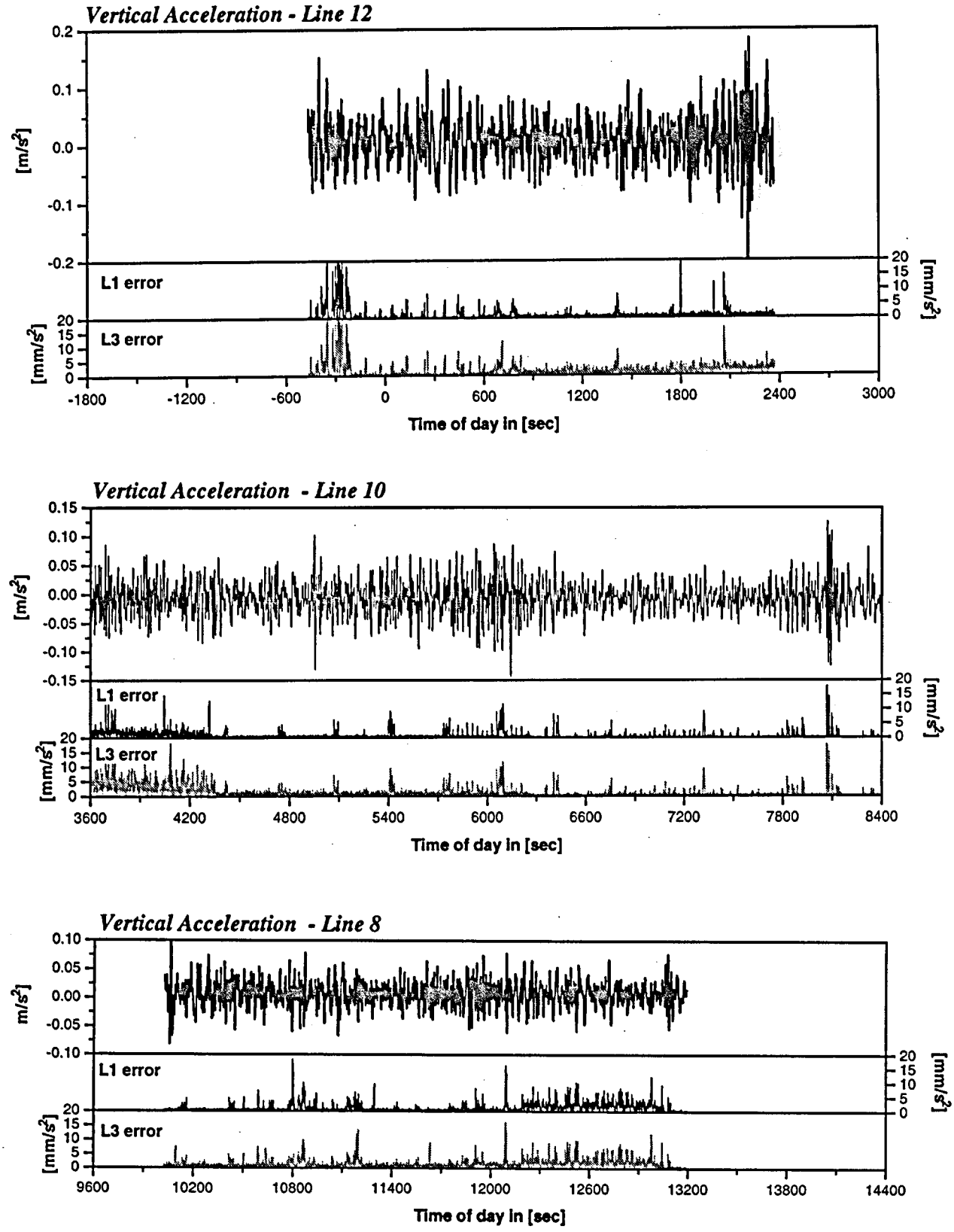

Figure 8.6 : Vertical acceleration component from the GPS trajectories for lines 12, 10, 8. The errors represent the standard deviation of the different solutions. (same rover - different reference stations)

8.2.5 *Comparison with the gravity meter acceleration*

As already pointed out, our goal here is not the filtering of the GPS trajectories in combination with the gravity meter measurements in order to retrieve the gravity. Two approaches for this task, using Kalman filter techniques and RC filters have been applied to this data set and first results have been published by [Klingelé, 1994]. We restrict the discussion to a comparison of the accelerations, derived from GPS as presented in section 8.4, with those of the gravity meter. For the recovery of the latter accelerations the raw data as recorded by the gravity meter was treated in a similar way to the GPS data.

The comparison for the 3 lines 12, 10 and 8 is given in figure 8.8. Note that the LaCoste and Romberg gravity meter measures relative gravity. The non-calibrated values of the measured accelerations were directly used for the comparison and therefore the absolute value of the difference is of no importance.

Lines 12 and 8 were flown from east to west and line 10 from west to east. The resulting Coriolis accelerations are of opposite signs and its influence is clearly seen in figure 8.8. The main level of the gravity meter and GPS accelerations of line 10 compared to lines 8 and 12 is different by about 2 gal.

Figure 8.7 shows a short sequence of 2 minutes from line 8, for which the agreement is best.

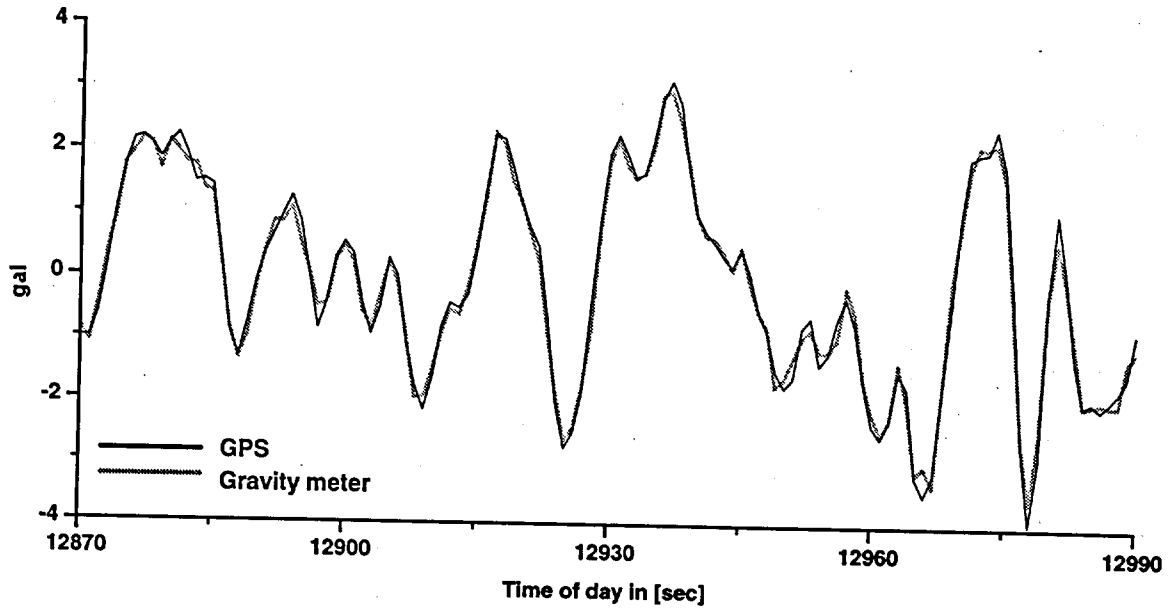

Figure 8.7 : Accelerations from gravity meter and GPS accelerations for a sequence of 2 minutes (line 8).

As expected the differences between the two accelerations are still on the order of a few gals. Figure 8.8 only demonstrates the main problem in aerogravimetry : The recovery of a signal of some tens of mgal with an accuracy of 1 mgal from measurements corrupted by accelerations of some gals.

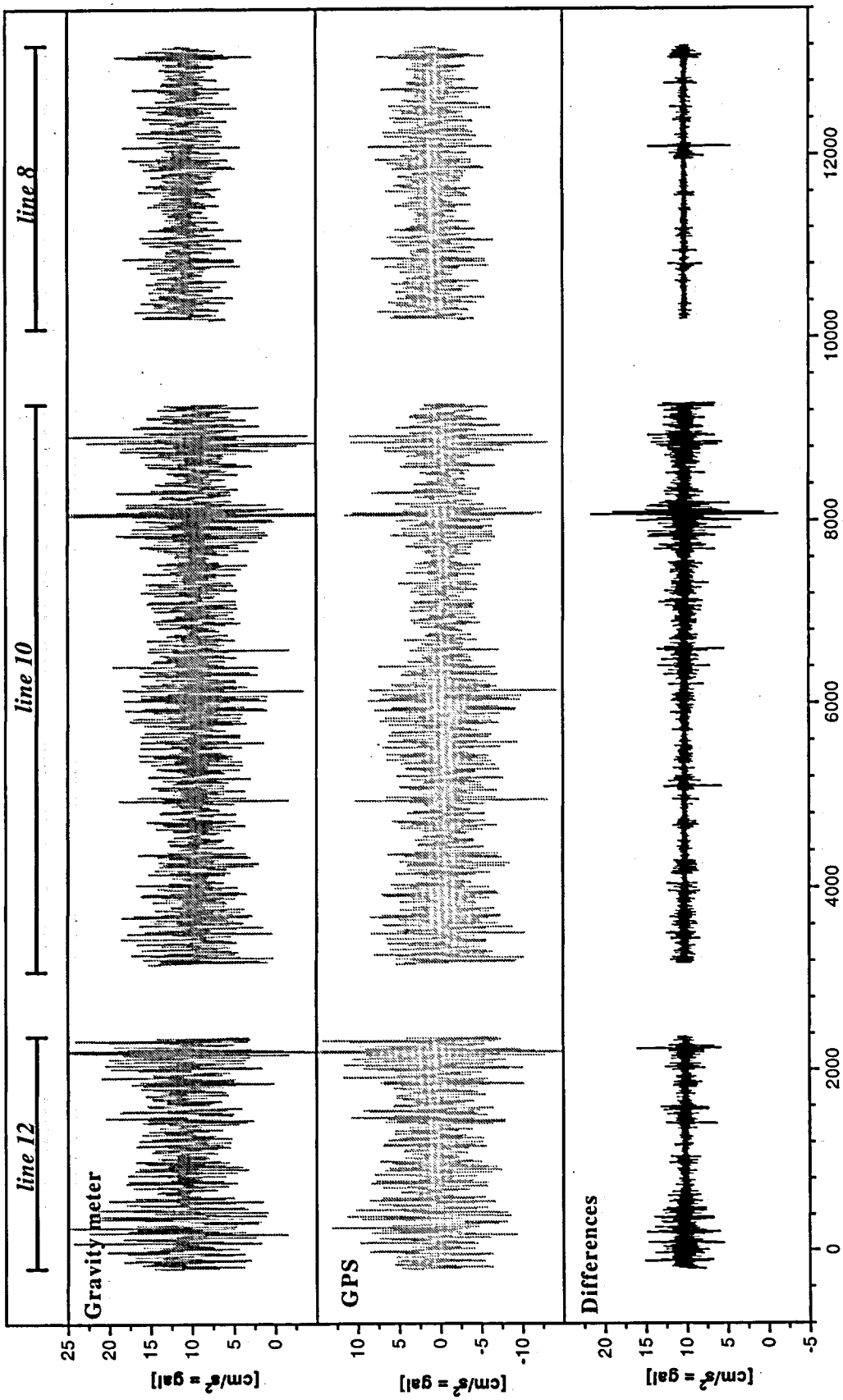

Figure 8.8 : Vertical accelerations derived from the gravity meter and from GPS trajectory for lines 12, 10, 8

8.2.6 Conclusions

When processing kinematic dual frequency data, with distances between roving and reference receiver up to 300 km, fixing L1 and L2 ambiguities becomes critical. However, the fixing of the wide lane combinations is easier to achieve and the introduction of the fixed wide lane ambiguities already significantly improves the quality of the trajectory. The different solutions showed an agreement of within 10-20 cm.

An approach for fixing the wide lane ambiguities on the zero difference level was proposed by [Wuebbena, 1985] and [Melbourne, 1985]. It could not, however, be applied to this data set, because these methods require good P code measurements on both frequencies. Therefore if good and unbiased dual band code measurements are available a pre-fixing of the wide lane ambiguities for every data set separately may and should be considered.

The quality of kinematic GPS meets the requirements of aerogravimetry concerning the determination of position and velocity. For the most critical component, i.e. vertical acceleration, the information from the GPS trajectory is also very useful.

9 Summary and conclusions

Differential GPS is a powerful tool for the determination of highly accurate coordinates in the kinematic mode. It can be used for a variety of applications. In many cases like e.g. airborne surveys (aerophotogrammetry, airborne Laser-Scanning, aerogravimetry etc.) the high precision recovery of the trajectory may be carried out in the off-line mode. Under favorable conditions an accuracy of a few centimeters has been achieved.

The key problem consists of the resolution of the ambiguities of the double difference phase measurements, i.e. the identification of the correct corresponding integer values. With the approach presented here it is possible to solve this problem within a few observation epochs and to yield a precise kinematic position at the cm level for short distances (< 5 km) between roving and reference receiver.

Applications for high-precision GPS positioning in the kinematic mode have increased considerably in the last years. An increasing number of commercial software packages is made available by various GPS receiver manufacturers and also by research institutes. Strategies mainly dealing with kinematic data in the on-line mode are being developed. Such software packages are or will be soon commercially available from different manufacturers and are normally adapted to the peculiarities for their receivers. The main problem in the on-line applications is the transmission of the data. For the high-precision mode the total amount of measurements (code and phase observations on both frequencies) has to be transmitted from the reference station to the roving receiver or vice versa.

The range of these on-line systems initially will be limited to a few kilometers due to the increasing problems in resolving the ambiguities over longer distances and due to the transmission problem. They will be mainly used for static and rapid static surveying applications, but they will also be well suited for specific kinematic applications such as e.g. accurate positioning on lakes or rivers in combination with sonic depth finder etc. In this case the user will always be responsible for the reference station and the transmission of the data to the roving receiver.

The transmission problems over distances of hundreds of kilometers covering a large area are not of technical but of 'political' nature. In different countries DGPS (differential GPS) services are being installed to provide the user with correction information for the code measurements. This leads to a positioning accuracy of about 1-10 m and already meets the requirements of the majority of the users. Such a DGPS service will be established in Switzerland on a national basis and tested over the next two years (1995-1996).

The next logical step would be the transmission of the full phase observations of a network of reference stations, in order to provide the DGPS user with the necessary information for an on-line phase solution on the cm level in the static and on the cm to dm level in the 'pure' kinematic mode. I am personally convinced that in the case of Switzerland installing such a network might be worth considering. With 6 stations the maximum distance to the next reference station of this network would be reduced to 50 - 80 km.

Despite the tremendous developments concerning the integration of the phase measurements in the on-line mode, the processing in the off-line mode will still have a certain importance

in the future. It is not advisable to carry out an aerogravimetric survey as presented in chapter 8 without collecting the raw measurements in order to be able to re-process the data. There are additional options in the off-line mode. Precise epherimides may be used; the ambiguity may be fixed in amore reliable way. The impact of different strategies for accounting with the ionospheric and tropospheric path delay may be studied.

The two-step approach

Our strategy for dealing with kinematic data is a two-step approach. The first step consists of determining the time invariant parameters (i.e. the ambiguities), whereas in the second step the time variant parameters (i.e. the coordinates) are processed (see chapter 2). This two-step approach showed itself to be appropriate and flexible for processing kinematic GPS data in the off-line mode, where the fixing of ambiguities must not be done as rapidly as possible (as it is the case in the on-line mode). This advantage was fully exploited for the design of the processing approach. The entire data set may be used to build up the NEQ system related to the ambiguities. In many cases a conventional sigma dependent rounding strategy could be used. Moreover the approach allowed easy study of different scenarios (single frequency measurements versus dual frequency measurements, different resolution strategies for the ambiguities, etc.).

Ambiguity resolution strategies

It is well known that the key problem of kinematic GPS processing is the fixing of the ambiguities. The first strategy implemented in our software was a conventional sigma dependent rounding method (chapter 4.1), which works well for long observation times. When reducing the observation time span it became obvious, however, that a search strategy was necessary to retrieve the integer ambiguities. The search algorithm adopted proved to be quite efficient. Since the code measurements are also integrated in the NEQ system an explicit definition of limit values for the ambiguities is not required. The best and second best integer ambiguity sets are always found in our approach. Because the search algorithm was only used in the off-line mode the processing time for finding all combinations of interest is not critical and no further attempts to improve the search were made.

The search algorithm (chapter 4.2), designed for small integration times, however, often suffers from a lack of sensitivity when data over longer time spans are used in the NEQ system. The search is performed using only one global value, namely the rms of the unit weight, integrated over the total time span. In our approach we always set up a new ambiguity parameter after a loss of lock to the satellite. Therefore phase measurements related to a particular ambiguity make only a small contribution to this integrated rms value, in particular if this ambiguity is only valid for a short time span. The sensitivity of the discrimination factor is thus weakened. Further investigations into increasing the sensitivity of the discrimination factor over longer integration times (e.g. by combining the conventional sigma dependent rounding strategy with the search strategy) are worth considering in future work.

When processing data sets involving longer distances between moving and reference receivers ionospheric refraction caused problems. The introduction of stochastic parameters for the ionosphere proved to be efficient but longer integration times were required. For a rapid

ambiguity resolution over longer distances, ionospheric refraction is the most important factor.

The impact of the code quality

The quality of code measurements is essential in the processing of kinematic GPS data. Good code measurements lead to good quality in the floating point solution for the ambiguities and they strongly confine the associated search area. They significantly increase the speed of the search algorithm and strengthen the epoch-specific discrimination factor (chapter 4.3.2). In the cases where it was not possible to resolve the ambiguities better code measurements led to smaller drifts in the coordinates derived from the floating point solution. In chapter 7.4 a combined adjustment of phase and C/A code measurements over 5 minutes showed offsets in the coordinates of up to 4 meters. When processing the same phase data with the more accurate P code measurements all offsets were below 1 meter.

The impact of the phase quality

An essential characteristic of the receivers nowadays is their performance under Anti-spoofing (AS). Different receiver types produce either full cycle or half cycle ambiguities in the L2 band. The decrease of the epoch-specific discrimination potential in the 'half-cycle' mode was theoretically derived (chapter 4.3.2) and tested with real data from a static 10 m baseline (chapter 5.1.3). The percentage of epochs with a discrimination factor of 2.5 (corresponding to an error probability of 1 %) decreased from 90% in the 'full-cycle' mode to 63% in the 'half-cycle' mode.

The number of cycle slips in the phase measurements is a good quality indicator for the receiver types. Phase data from receivers of the first generation were frequently corrupted by cycle slips. The new generation of receivers, however, produces only very few cycle slips. As pointed out in chapter 3, however, it is not possible to assume that cycle slips do not exist. An easy way to brush through the data and check for cycle slips is to look at the differences in the L1 and L2 phase measurements (chapter 3.3). Because most of the data used here stem from dual-band receivers this procedure could be applied and cycle slip detection did not pose major problems. There were indeed only very few cycle slips. In the data set 'Thun 94' we found only one cycle slip in the L2 measurements over a period of 24 hours. The screening strategies of chapter 3 are convenient for the screening under 'good' ionospheric conditions and for data sets of a 'good' quality level. The development of the software was always closely related to the processing of individual data sets. It never seemed necessary to develop more sophisticated screening procedures. Therefore our discussion of this topic is rather short. This is also true for the method of screening raw phase measurements of a reference station (chapter 3.4). Further refinements and extensions of the proposed approach are possible; [Goad, 1992] showed e.g. that it is possible to recover the wide-lane ambiguities from zero-difference phase measurements, a topic closely related to data screening.

Accuracy of the recovered trajectories

The best results in the kinematic mode are obtained if it is possible to fix the ambiguities to integers. In this case the actual quality of the coordinates only depends on the PDOP values defined by the satellite constellation. A deterioration in the coordinate quality with increasing distance to the reference receiver is observed as in the static mode.

The distortion introduced by errors in the satellite coordinates depends on the distance between moving and reference receivers. Fortunately precise ephemerides are available today from the International GPS Service for Geodesy (IGS) [Beutler et al, 1994].

A more important source for systematic errors is the tropospheric path delay. When processing airborne GPS data the height difference between the moving and reference receiver is in general at least a few hundred meters and may reach up to 5-10 kilometers. In the extreme case the tropospheric path delay for the moving receiver is close to zero whereas the path delay through the entire troposphere has to be taken into account for the reference station. By applying a tropospheric correction derived from a standard model the remaining systematic errors of the tropospheric path delay may be considerable (up to some decimeters). Mainly the height component is affected, but depending on the satellite constellation distortions in the horizontal components are also possible. A method applied in the processing of static GPS measurements consists of introducing additional troposphere biases as parameters into the adjustment (see e.g. [Rothacher, 1992]). It would be interesting to study whether or not it is possible to implement such tropospheric biases in a kinematic environment, too.

The kinematic positions from GPS data always represent a discretization of a continuous trajectory. Therefore we normally have to interpolate the positions at the epochs of interest (e.g. at the time of exposure of the camera during an aerophotogrammetric survey). To ensure a good interpolability of a few millimeters a high measurement rate of 1 Hz or higher is necessary. Closely related to this problem of interpolability is the derivation of velocity and acceleration. By using. e.g. the collocation method it is possible to retrieve the velocity with an accuracy of 1-5 mm/sec.

Our main conclusion is the following :

For kinematic surveys in small areas (< 5 km) it should always be possible to resolve the ambiguities within very short data spans (over a few epochs of observations), provided excellent code data (< 1 m) are available on L1 and L2 and provided six or more satellites well distributed over the sky may be used. Under these circumstances we expect the recovered trajectory to have a quality well below the 10 cm level. Over longer distances longer integration times improve the ambiguity estimation and an accuracy of 10-20 cm may be achieved.

Acknowledgment

This is to acknowledge all institutes and offices which actively supported us during our kinematic GPS campaigns. The availability of the Twin-Otter of the Cadastral Authority and the flexibility and cooperation of R. Huebscher were essential for the collection of many of our kinematic data sets. Dr. U. Wild and Dipl. Ing. A. Wiget from the Federal Office of Topography actively supported us, providing us with data from the reference receiver in Zimmerwald and on several occasions with their own receivers.

Personally I am indebted to Prof. Dr. H.-G. Kahle for giving me the opportunity to work in this interesting field of geodesy. His support and energy were a necessary driving force for the accomplishment of this work. I thank Prof. Dr. G. Beutler for his precious advice and suggestions during the elaboration of the work. A particular thanks to Dr. A. Geiger for his support and humor. I am grateful to Mrs. K. Hahn for her help in editing the English.

References

Ackermann F. (1992) : Operational rules and accuracy models for GPS-aerotriangulation. *International Archives of Photogrammetry and Remote Sensing, 29(B3), pp 691-700.*

Bagnaschi L. (1993) : Application of an Adaptive Kalman Filter for the Estimation of Position, Velocity and Acceleration of a Moving Body from GPS Measurements. *IGP Bericht Nr 226, ETH-Zurich.*

Bauersima I. (1983) : NAVSTAR/Global Positioning System (GPS) Band II: Radiointerferometrische Satellitenbeobachtungen. *Mitteilungen der Satelliten-Beobachtungsstation Zimmerwald Nr 10.*

Beutler G., D.A. Davidson, R. Langley, R. Santerre, P. Vanicek, D.E. Wells (1984) : Some Theoretical and Practical Aspects of Geodetic Positioning Using Carrier Phase Difference Observations of GPS Satellites. *Mitteilungen der Satelliten-Beobachtungsstation Zimmerwald Nr 14.*

Beutler G., W. Gurtner, U. Hugentobler, M. Rothacher, T. Schildknecht, U. Wild (1988) : Ionosphere and GPS Processing Techniques. *Paper presented at the 1988 Chapman Conference on The Use of GPS for Geodynamics, Ft Lauderdale, U.S.A.*

Beutler G. (1992) : The Impact of 'The International GPS Geodynamics Service (IGS) on the Surveying and Mapping Community, *XVII ISPRS Congress Washington.*

Blewitt G. W.G. Melbourne, W.I. Bertiger, T.H. Dixon, P.M. Kroger, S.M. Lichten, T.K. Meehan, R.E. Neilan , L.L. Skumeda, C.L. Thornton, S.C.Wu, L.E. Young (1988) : GPS Geodesy with Centimeter Accuracy, *Lectures Notes in Earth Sciences, 19, 30-40, Springer 1988.*

Blewitt G. (1989) : Carrier Phase Ambiguity Resolution for the Global Positioning System Applied to Geodetic Baselines up to 2000 km. *Journal of Geophysical Research. Vol. 94. No.B8.*

Bock Y., S.A. Gourevitch, C.C. Counselman III, R.W. King, R.I. Abbot (1986) : Interferometric analysis of GPS-Phase Observations. *Manuscripta Geodaetica, Vol. 11, No. 4, pp. 282-288.*

Brozena J.M. (1991) : The Greenland Aerogeophysics Project : Airborne Gravity, Topographic and Magnetic Mapping of an Entire Continent. *From Mars to Greenland: Charting Gravity with Space and Airborne Instruments. IAG Symposium Nr 110 Vienna, Austria, August 1991, pp 203-215, Springer Verlag.*

Cocard M. (1990) : Kinematic Experiences with GPS and Laser-Tracker. *Cahiers du Centre Européen de Géodynamique et de Séismologie : GPS for Geodesy and Geodynamics, pp 19-25.*

Colomina I. (1989) : Combined adjustment of photogrammetric and GPS-data. *Schriftenreihe des Institutes für Photogrammetrie, Universität Stuttgart, Nr 13, pp 313-328.*

Counselman C.C. S.A. Gourevitch (1981) : Miniature interferometric terminals for earh surveying : ambiguity and multipath with Global Positioning System, *IEEE Trans. Geosciences and Remote Sensing, GE-19-4, pp 244-252.*

Euler H.J., B. Schaffrin (1990) : On the Discernibility between Different Ambiguity Solutions in the Static-kinematic GPS-mode. *Kinematic Systems in Geodesy, Surveying and Remote Sensing, IAG Symposium No 107, Banff, Canada, September 1990, pp 285-292, Springer Verlag.*

Euler H.J., C.C. Goad (1991) : On Optimal Filtering of GPS Dual Frequency Observations without Using Orbit Information, *Bulletin géodésique 65, pp 130-143.*

Euler H.J. (1992) : Fast GPS Ambiguity Resolution On-the-fly for Real Time Applications. *in proceedings of the 6th International Symposium on Satellite Positioning , March 1992, Columbus, Ohio. pp 650-659.*

Frei E., G. Beutler (1990) Rapid static positioning based on the fast ambiguity resolution approach 'FARA': theory and first results. *Manuscripta geodaetica, Vol. 15, Nr. 6, pp 325-356.*

Frei E. (1991) : Rapid Differential Positioning with the Global Positioning System (GPS). *Geodätisch-geophysikalische Arbeiten in der Schweiz, SGK-Publikation Band 44.*

Friess P. (1990) : Kinematische Positionsbestimmung für die Aerotriangulation mit dem NAVSTAR Global Positioning System. *DGK, Verlag der Bayerischen Akademie der Wissenschaften, Beck'sche Verlagsbuchhandlung.*

Geiger A. (1987) : Einfluss richtungsabhängiger Fehler bei Satellitenmessungen. *IGP-Bericht Nr 130, ETH-Zürich.*

Geiger A. (1988) : Einfluss und Bestimmung der Variabilität des Phasenzentrums von GPS-Antennen. *ETH-Mitteilung 43, Institut für Geodäsie und Photogrammetrie, ETH Zürich.*

Geiger A., M. Cocard (1990) : Comparison of Heterogeneous Unsynchronized Data By Transforming Coordinate Independent Functionals. *International Symposium on Kinematic Systems in Geodesy, Surveying and Remote Sensing. Banff, Alberta, Canada.*

Gelb A. (1974) : Apllied Optimal Estimation, *The M.I.T. Press, Cambridge, 1974.*

Gurtner W. (1978) : Das Geoid der Schweiz. *IGP-Bericht Nr. 20, ETH-Zurich.*

Goad C. (1992) : Robust Techniques for Determining GPS Phase Ambiguities, *in proceedings of the 6th International Symposium on Satellite Positioning , March 1992, Columbus, Ohio. pp 245-254.*

Grün A., A. Runge (1988) : The accuracy potential of self-calibrating aerial trangulation without control. *International Archives of Photogrammetry and Remote Sensing. Vol. 27, Part B3. Kyoto.*

Grün A., B. Moser, H.G. Kahle, M. Cocard, A. Geiger (1993a) : GPS-gestützte photogrammetrische Triangulation, *Schlussbericht des ETH-Forschungsprojektes.*

Grün A., M. Cocard, H.G. Kahle (1993b) : Photogrammetry and Kinematic GPS: Results of a High Accuracy Test, *in Photogrammetric Engineering & Remote Sensing PE&RS, Vol 59, November 1993, pp 1643-1650.*

Harlan R.B. (1968) : Eotvoes-Corrections for Airborne Gravimetry. *Journal of Geophysical Research, Vol. 73, Nr. 14, pp. 4675-4679.*

Hatch R.R. (1989) : Ambiguity Resolution in the Fast Lane, *in proceedings of the 2nd International Technical Meeting of the Satellite Division of The Institute of Navigation, Colorado Springs, pp 45-50.*

Hatch R.R. (1990) : Instantaneous Ambiguity Resolution, *Kinematic Systems in Geodesy, Surveying and Remote Sensing, IAG Symposium No 107, Banff, Canada, September 1990, pp 299-308, Springer Verlag.*

Hehl, K. (1992) : Bestimmung von Beschleunigungen auf einem bewegten Träger durch GPS und digitale Filterung. *Schriftenreihe des Studienganges Vermessungswesen Universität der Bundeswehr München Heft 43.*

Heiskanen W.A, H. Moritz (1967) : Physical Geodesy, *Reprint by the Institute of Geodesy TU-Graz, Austria, 1987.*

Høgholen A. (1993) : Kinematic GPS in Aerotriangulation in Finland, *Report of the Finnish Geodetic Institute 93:5.*

King R.W., E.G. Masters, C. Rizos, A. Stolz, J.Collins (1985) : Surveying with GPS. *Monograph 9. School of Surveying, University of New South Wales, Australia.*

Klingele E.E, L. Bagnaschi, M. Halliday, M. Cocard, H.G. Kahle (1993) : Airborne Gravimetric Survey of Switzerland (First Results). *IGP Bericht Nr. 239, ETH-Zurich.*

Mader G. (1986) : Dynamic Positioning using GPS Carrier Phase Measurements. *Manuscripta geodetica, 11(4), 272-277.*

Mader G. (1992) : Kinematic GPS Phase Initialization using the Ambiguity Function *in proceedings of the 6th International Symposium on Satellite Positioning , March 1992, Columbus, Ohio. pp 712-719.*

Melbourne W.G. (1985): The case for ranging in GPS based geodetic system. *First International Symposium on Precise Positioning with GPS, Rockville.*

Mervart L., G. Beutler, M. Rothacher, U. Wild (1994) : Ambiguity resolution strategies using the results of the International GPS Geodynamics Service (IGS), *published in Bulletin géodésique Nr 68, pp. 29-38.*

Pelzer H. (1985) : Kontaktstudium 1985 : Geodätische Netze in Landes- und Ingenieurvermessung II. *Vermessungswesen bei Konrad Wittwer Stuttgart. Band 13.*

Remondi B.W. (1984) : Using the Global Positioning System (GPS) Phase Observable for Relative Geodesy : Modeling, Processing and Results. *Ph.D. Thesis, University of Texas Austin.*

Remondi B.W. (1985) : Global Positioning System Carrier Phase : Description and Use. *Bulletin géodésique , Vol. 59, pp. 361-377.*

Remondi B.W. (1992) : Real-time Centimeter-Accuracy GPS without Static Initialization, *in proceedings of the 6th International Symposium on Satellite Positioning , March 1992, Columbus, Ohio. pp 691-701.*

Rothacher M. (1992) : Orbits of Satellite Systems in Space Geodesy. *Geodätisch-geophysikalische Arbeiten in der Schweiz, SGK-Publikation Band 46.*

Rothacher M. G. Beutler, W. Gurtner, E. Brockmann, L. Mervart (1993) : Bernese Software Version 3.4, *Documentation published by the Astronomical Institute of the University of Berne.*

Saastamoinen J. (1973) : Contributions to the Theory of Atmospheric Refraction / Introduction to Practical Computation of Astronomical Refraction. *Bulletin géodésique Nrs 105, 106, 107, pp 50.*

Schneider M. (1981) : Himmelsmechanik. *Bibliographisches Institut Mannheim/Wien/Zurich BI Wissenschaftsverlag.*

Schwarz H, H. Rutishauser, E.Stiefel (1968) : Numerik symmetrischer Matrizen. *B.G. Teubner Verlag Stuttgart.*

Spilker J.J. (1978) : GPS-Signal Structure and Performance Characteristics. *Navigation : The Journal of the Institute of Navigation , Washington, Vol. 25, Nr. 2. pp. 121-146.*

Valliant H.D. (1991) : The LaCoste and Romberg Air/Sea Gravity Meter : An Overview. *Geophysical Exploration at Sea, 2nd Edition, Vol. 1, pp 141-176. December 1991.*

Van Dierendonck A., S. Russell, E. Kopitzke, M. Birnbaum (1978) : The GPS Navigation Message. *Navigation : The Journal of the Institute of Navigation , Washington, Vol. 25, Nr. 2. pp. 147-165.*

Wei M., S. Ferguson, K.P. Schwarz (1991) : Accuracy of GPS-derived Acceleration from Moving Platform Tests. . *From Mars to Greenland: Charting Gravity with Space and Airborne Instruments. IAG Symposium Nr 110 Vienna, Austria, August 1991, pp 235-250, Springer Verlag.*

Wild U., G. Beutler, W.Gurtner, M. Rotacher (1989) : Estimating the Ionosphere Using One or More Dual Frequency Receivers. *Paper presented at the 5th International Geodetic Symposium on Satellite Positioning, March 13-17, 1989, Las Cruces, New Mexico.*

Wild U. (1993) : Ionosphere and Geodetic Satellite Systems : Permanent GPS Tracking Data for Modeling and Monitoring, *Geodätisch-geophysikalische Arbeiten in der Schweiz, SGK-Publikation Band 49.*

Wirth B. (1990) : Höhensysteme, Schwerepotentiale und Niveauflächen : Systematische Untersuchungen zur zukünftigen terrestrischen und GPS-gestützten Höhenbestimmung in der Schweiz. *Geodätisch-geophysikalische Arbeiten in der Schweiz, SGK-Publikation Band 42.*

Wübbena G. (1985) : Software Developments for Geodetic Positioning with GPS Using TI 4100 Code and Carrier Phase Measurements. *First International Symposium on Precise Positioning with GPS, Rockville.*

"Geodätisch-geophysikalische Arbeiten in der Schweiz"

(Fortsetzung der Publikationsreihe "Astronomisch-geodätische Arbeiten in der Schweiz") der Schweizerischen Geodätischen Kommission (ab Bd. 36):

36 1984 Ein gravimetrisches Krusten-Mantel-Modell für ein Profil im nördlichen Alpenvorland bis an die Ligurische Küste. H. Schwendener. 160 Seiten.

37 1986 Les levés aéromagnetiques de la Suisse. E. Klingelé. 69 Seiten.

38 1986 Lokale Schwerefeldbestimmung und gravimetrische Modellrechnungen im Satelliten (GPS)- Testnetz "Turtmann" (Wallis). I. Bernauer, A. Geiger. 106 Seiten.

39 1989 125 Jahre Schweizerische Geodätische Kommission
- I. Bedeutung geodätischer Raumverfahren für Landesvermessung und Geodynamik. (R. Sigl)
- II. Beitrag der Geodäsie zur Geodynamik. (H.-G. Kahle)
- III. L'état actuel de la recherche sur les movements de l'écorce terrestre en Suisse. (F. Jeanrichard)
- IV. Die Satellitengeodäsie im Dienste der globalen Geodynamik. (I. Bauersima)
- V. Die Veranstaltungen zum 125 Jahr-Jubiläum der Schweizerischen Geodätischen Kommission. (W. Fischer). 62 Seiten.

40 1989 Integrale Schwerefeldbestimmung in der Ivrea- Zone und deren geophysikalische Interpretation. B. Bürki. 186 Seiten.

41 1990 ALGESTAR satellitengestützte Geoidbestimmung in der Schweiz. U. Marti. 61 Seiten plus Punktprotokolle.

42 1990 Höhensysteme, Schwerepotentiale und Niveauflächen: Systematische Untersuchungen zur zukünftigen terrestrischen und GPS-gestützten Höhenbestimmung in der Schweiz. B. Wirth. 204 Seiten.

43 1990 Gravimetrisches Geoid der Schweiz: Potentialtheoretische Untersuchungen zum Schwerefeld im Alpenraum. A. Geiger. 231 Seiten.

44 1991 Rapid Differential Positioning with the Global Positioning System (GPS). E. Frei. 178 Seiten.

45 1992 Dreidimensionales Testnetz Turtmann 1985-1990 Teil I. F. Jeanrichard (Hrsg.) Autoren: A.Geiger, H.-G. Kahle, R. Köchle, D. Meier, B. Neininger, D. Schneider, B. Wirth. 183 Seiten.

46 1993 Orbits of Satellite Systems in Space Geodesy. M. Rothacher. 243 Seiten.

47 1993 NFP 20. Beitrag der Geodäsie zur geologischen Tiefenstruktur und Alpendynamik. H.-G. Kahle (Hrsg.) Autoren: I. Bauersima, G. Beutler, B. Bürki, M. Cocard, A. Geiger, E. Gubler, W. Gurtner, H.-G. Kahle, U. Marti, B. Mattli, M. Rothacher, Th. Schildknecht, D. Schneider, A. Wiget, B. Wirth. 153 Seiten plus 90 Seiten Anhang.

48 1994 Ionosphere and Geodetic Satellite Systems: Permanent GPS Tracking Data for Modelling and Monitoring: Urs Wild, 155 Seiten.

49 1994 Optical Astrometry of Fast Moving Objects using CCD Detectors: Thomas Schildknecht, 200 Seiten.

50 1995 Geodätische Alpentraverse Gotthard: A. Elmiger, R. Köchle, A. Ryf und F. Chaperon. 214 Seiten.

51 1995 Dreidimensionales Testnetz Turtmann 1985-1993, Teil II (GPS-Netz). F. Jeanrichard (Hrsg.) Autoren: G. Beutler, A. Geiger, M. Rothacher, Stefan Schaer, D.. Schneider, A. Wiget, 173 Seiten.

52 1995 High Precision GPS Processing in Kinematic Mode. Marc Cocard, 139 Seiten.